TECHNICAL MEMORANDUM 1516

JUNE 1971

CONCEPTS AND APPLICATIONS OF PHOTOCHEMICAL SMOG MODELS

A. Q. Eschenroeder
J. R. Martinez

GENERAL RESEARCH CORPORATION
P.O. BOX 3587, SANTA BARBARA, CALIFORNIA 93105

Portions of this work were performed pursuant to Contracts CPA 22-69-127, National Air Pollution Control Administration, Dept. of Health, Education, and Welfare, CRC-APRAC Project No. CAPA-7-68, Coordinating Research Council, and EHSD 71-22, Air Pollution Control Office, Environmental Protection Agency.

ABSTRACT

Following an overview of mathematical methods of analyzing air pollution, detailed developments of inputs, techniques, and validations are presented for photochemical smog modeling. Finite difference formulations are employed to compute concentration histories. The chemical kinetics are expressed as lumped parameter reaction mechanisms derived from laboratory data in the literature. Turbulent diffusion coefficients, which depend on height and time, come from atmospheric measurements. Inputs consist of source inventories for the Los Angeles basin and solar irradiation curves for the appropriate days. Predicted time histories of reactive hydrocarbons, oxides of nitrogen, and ozone are consistent with the variations observed at air monitoring stations. With refined descriptions of advection, the mathematical model will serve as a tool in planning legislation and guiding urban planning in the future.

CONTENTS

SECTION		PAGE
	ABSTRACT	i
I	INTRODUCTION	1
	A. Background Discussion	1
	B. Dispersion Models Based on Inert Pollutants	4
	C. Related Work on Photochemical Smog Modeling	8
	D. Overview of the Combined Photochemical/Diffusion Model	10
II	SOME SIMPLIFIED KINETIC MECHANISMS	14
	A. The Original Scheme	14
	B. Addition of More Realistic Oxidation Chains	23
	C. Influence of Initial Composition	31
	D. Atmospheric Adaptation Based on Reactivity Data Analysis	39
III	THE ATMOSPHERIC MODEL AND ITS NUMERICAL SOLUTION	49
	A. The Governing Equations	49
	B. Application of Padé Approximants to Smog Chamber Calculations	52
	C. Application of Padé Approximants to the Atmospheric Model Equation	57
	D. Meteorological Reformulation of Model	62
IV	THE EXERCISE AND VALIDATION OF THE MODEL	65
	A. Objectives of the Tests	65
	B. Sources of Data	65
	C. Validation Tests of An Early Version of the Model	82
	D. Sensitivity Studies on 1969 Trajectories with the Expanded Model	97
	E. History Analysis of the 1030 El Monte Trajectory	101
V	CONCLUDING REMARKS	110
	LITERATURE CITED	116

ILLUSTRATIONS

NO.		PAGE
1	Schematic of Diffusion Model for Air Pollution Simulation	12
2	Original Reaction Mechanism	15
3	Computed and Observed Reactant Histories for the Trans-2-Butene/Nitric Oxide System	16
4	Computed and Observed Product Histories for the Trans-2-Butene/Nitric Oxide System	17
5	Expanded Kinetic Mechanism	26
6	Computed Curves Compared with Experimental Points for the Propylene/Nitrogen Oxides System	29
7	Hydrocarbon Decay with Two Reactivities	32
8	Ozone Buildup with Two Reactivities	34
9	Influence of NO_x: HC-Ratio on Oxidant Production	36
10	Average Reactivity History for Commerce, 1969: Hydrocarbon Consumption Scale from Altshuller	43
11	Average Reactivity History for El Monte, 1969: Hydrocarbon Consumption Scale from Altshuller	44
12	Average Reactivity History for Commerce, 1969: Biological Effects and Product Formation Scale from Altshuller	46
13	Average Reactivity History for El Monte, 1969: Biological Effects and Product Formation Scale from Altshuller	47
14	Variations of Diffusivity with Height for Different Average Wind Speeds	67
15	Estimated Trajectory of Air Mass Arriving at El Monte, 1030 hours, 29 Sept. 1969	70
16	Estimated Trajectory of Air Mass Arriving at El Monte, 1130 hours, 29 Sept. 1969	71
17	Estimated Trajectory of Air Mass Arriving at El Monte, 1230 hours, 29 Sept. 1969	72
18	Estimated Trajectory of Air Mass Arriving at El Monte, 1330 hours, 29 Sept. 1969	73
19	Geographical Traffic Distribution in Los Angeles County, ca. 1951	77
20	Los Angeles Traffic/Time Distributions ca. 1951	78

ILLUSTRATIONS (cont'd)

NO.		PAGE
21	Geographical Distribution of Freeway Traffic in the Los Angeles Basin Area ca. 1970	79
22	Los Angeles Traffic/Time Distributions ca. 1970	80
23	Carbon Monoxide Concentration at Huntington Park on Type 3 Day	84
24	C_2H_2/NO_x Ratios for High Oxidant Days	86
25	CO/NO_x Ratios for Huntington Park 1968	87
26	CO/NO_x Ratios for Commerce 1969	88
27	$(NO + NO_2)$ - Concentration Ground Level Huntington Park on Type 3 Day	90
28	High-Reactivity Hydrocarbons Concentration on the Type 3 Day	91
29	Ozone Concentration at Huntington Park on Type 3 Day	92
30	Nitric Oxide Concentration at Huntington Park on Type 2 Day 1968. f = 1/4; r = 1/2	94
31	High Reactivity Hydrocarbon Concentration at Huntington Park on Type 2 Days 1968. f = 1/4; r = 1/2	95
32	Ozone Concentration at Huntington Park on Type 2 Days 1968. f = 1/4; r = 1/2	96
33	Reactive Hydrocarbon History Along the 1030 Trajectory. f = 1/4; r = 1/2	103
34	Nitric Oxide History Along the 1030 Trajectory. f = 1/4; r = 1/2	104
35	Nitrogen Dioxide History Along the 1030 Trajectory. f = 1/4; r = 1/2	105
36	Oxides of Nitrogen $(NO + NO_2)$ History Along the 1030 Trajectory. f = 1/4; r = 1/2	107
37	Ozone History Along the 1030 Trajectory. f = 1/4; r = 1/2	108

TABLES

NO.		PAGE
1	Rate Coefficients for Trans-2-Butene/Nitric Oxide System	20
2	Rate Coefficients for Expanded Model of the Hydrocarbon/ Nitric Oxide Mechanism	30
3	Influence of 100 ppm Carbon Monoxide on the System Shown in Fig. 6 with Various Values of the Ratio of (OH + HC)/ (OH + CO) Reaction Rate Coefficients Reaction Time in Minutes	39
4	Hydrocarbon Reactivity Scales	41
5	CDC 6400 Central Processor Time to Run C_3H_6 + NO + hν Chamber Experiment Simulation	56
6	Contaminants in Tons Per Day from Major Sources Within Los Angeles County in 1968	75
7	Results of Model Sensitivity Study Using 1969 El Monte Data	100

I. INTRODUCTION

A. BACKGROUND DISCUSSION

Atmospheric simulation models will play a central role in our efforts to improve the quality of the urban air environment because decision-makers must anticipate the outcomes of available courses of action. Although air pollution models are still under development, their validation will provide the link needed to establish the source emission limits required to achieve desired air quality standards. This approach can be broadened to answer questions of social and economic significance for different ameliorative strategies.

The anticipated evolution of modeling methods leads ever closer to a direct contact with our immediate problems. Whereas we are presently seeking a technical understanding of chemical interactions with transport processes, the next step is integration of this understanding in cost-benefit analyses. (In view of the difficulties arising, probably a more realistic goal is a cost-of-restoration study.) Successive improvement and confirmation of modeling techniques will offer quantitative criteria for Federal and State legislation to improve air quality by controlling mobile sources of emissions. Addressing more specific problems, local government needs criteria for urban planning to prescribe population patterns and industrial land uses that tend to preserve air quality. Hence the local application of predictive modeling influences the dispositions of both fixed and mobile emitters. At the finest level of detail, a predictive model could provide the logic for the data

processor in a real-time tactical system to guide decisions for temporary source shutdowns that would avoid calling alerts after dangerous pollutant buildups.

Although we would hope that preventive policies would preclude the need for this kind of alarm system, it is possible that some communities may be moving toward unacceptable limits faster than controls can be imposed.

Implementation plans for abating air pollution problems require a quantitative cause-and-effect relationship to estimate future air quality in terms of source controls proposed for the region. Mathematical models, which are most likely to provide this needed connection, must ultimately describe chemical transformations as well as meteorological transport. Air quality criteria documents now exist for particulate matter, sulfur oxides, carbon monoxide, photochemical oxidants, and hydrocarbons. Each of these materials is involved in chemical changes in urban atmospheres. All except possibly CO (carbon monoxide) and some particulates are either transformed or decay within a short enough time scale so that their concentrations in the urban domain are substantially affected by chemical reactions. (Even both CO and particulates are now suspected of direct involvement in the chemistry.) Although our understanding of the detailed mechanisms is far from complete, we do possess at this time a workable mathematical framework for modeling atmospheric dispersion of multicomponent pollutant systems undergoing coupled chemical reactions.

Having recognized these modeling requirements imposed by implementation planning, how best can we exploit our available methods to meet the immediate needs? For a limited number of regions, we can test some of the simplistic linear relationships connecting pollution with emissions (1, 2). For those areas that have had many sensors in the field measuring air contaminants over the years, the relationships are assumed to be derivable from plots of pollution levels versus emission tonnages. Global background concentration has been suggested as an initial intercept point for the straight-line formulas.

For most regions, however, not even a simple quantitative rationale can be used for implementation planning because neither time nor money is available for deploying a network of sensors and collecting a significant sample of monitoring data. This dilemma suggests another approach: the requirements that have been imposed can be met by instituting a deliberate effort to adapt second-generation mathematical models to the implementation-planning problem. Admittedly, unresolved conflicts in present experimental results may seem to indicate that this approach is premature, but the urgency of the situation likely justifies parallel activities. The adaptation of the mathematical framework can proceed simultaneously with laboratory investigations and field programs. As fundamental knowledge expands, the blanks in the framework can be filled. In the meantime, the preliminary framework will already be in operation examining atmospheric pollution relationships. In addition, early attempts to solve planning problems with models will highlight specific deficiencies and will provide valuable feedback to the research community.

The two-way interaction between modeling and data-gathering can be considered as mutual support between research activities and enforcement activities. The efforts put forth in abatement are thereby more directly related to research efforts put forth on meteorology, chemistry, and physics. With the emerging complexities of economic factors, the decision-maker must employ techniques more subtle than massive rollback. The legislative approach based on flat prohibitions can be pressed to some extent, but it ultimately meets some very stout barriers in the real world. A powerful combination of quantitative justification and technological innovation will be needed to penetrate these barriers. Optimization will be the key word; concern for computer expenditures will wane as the dollar costs of damage caused by air pollution and of resources needed to control it are generally realized.

B. DISPERSION MODELS BASED ON INERT POLLUTANTS

Atmospheric spreading of inert gaseous contaminant that is not absorbed at the ground has been described by the various Gaussian plume formulas. Many of the equations for concentration estimates originated with the work of Sutton (3). Subsequent applications of the formulas for point and line sources state the Gaussian plume as an assumption, but it has indeed been rigorously shown to be an approximate solution to the transport equation with a constant diffusion coefficient and with certain boundary conditions (4). The restrictive conditions just recited occur only for certain special situations in the atmosphere. Hence, these approximate solutions must be applied with great care.

Prior to extensive application of these plume models, Frenkiel employed a puff model to study photochemical smog in Los Angeles (5). A point source was assumed to be centered within each four-mile-square in the grid pattern extending over the basin. Nashville, Tennessee was the subject of some later papers by Pooler and Turner, who used Gaussian formulations (6, 7). Point sources were assumed in Ref. 6, but cross-wind line sources were assumed in Ref. 7 to approximate the emission emanating from each area element. Checks against field measurements of SO_2 were made in each case. Turner allowed for a first-order reaction in the gas phase to remove SO_2 from the air.

Extending the work to include NO_x (oxides of nitrogen), Clarke divided Cincinnati into sixteen angular sectors, each having four radial zones (8). This grid was centered on a monitoring station. Reactions were allowed to deplete SO_2, but not NO_x. Koogler later added allowance for changing wind direction by periodically treating old plumes as new line sources (9). Also, the vertical confinement of an elevated inversion layer was approximated along with height variation of wind speed. Evidently the SO_2 was not allowed to react. Miller and Holzworth also considered a limited mixing layer by assuming a uniform vertical profile when the "effluent reaches the top of the mixing layer" (10). The method was applied to Los Angeles, Washington, and Nashville for SO_2 and NO_x. A seasonal or monthly average model was reported by Martin and Tikvart, to be applied to CO and SO_2

concentrations (11). Following Turner's equations (7), a program was developed for the IBM 1130 computer.

Analysis and tabulations of data to be used in Gaussian plume formulas are also available. The report for the St. Louis Dispersion Study (12) gives further insights into tracer-spreading over urban areas in contradistinction to open areas where many measurements have been made. Detailed working charts and numerous examples in Turner's workbook (13) offer a real aid for practical estimation of atmospheric dispersions under the conditions outlined above.

For very approximate calculations of either peak or average pollutant levels, a simple slab model can be employed for the air overlying the urban area. The ground is the lower boundary and the uppermost extent of mixing (e.g., an elevated inversion base) is the upper boundary of the slab. Uniform vertical profiles are assumed, and horizontal flow carries the polluted air away. This concept was suggested by Smith for order-of-magnitude estimates (14). It was also discussed in Wanta's review article (15) along with most of the Gaussian plume models referred to above.

In an effort to overcome the limitations of the Gaussian plume assumptions, Lamb presented a Green's function approach to the solution of the transport equation, with both area sources at the ground and volumetric sources due to reactions (16). Two further features included in the model were time dependence and absorption at the ground. (The latter generalization of boundary conditions might be especially

important for pollutants such as NO_x , SO_2 , and O_3 , which combine with surfaces or with moisture on surfaces.)

Recent work at Stanford Research Institute has been directed toward a simple and practical urban diffusion model for carbon monoxide (17). Its objectives include not only hour-to-hour predictions, but also long-term climatological effects. Traffic distributions in time and space are inputs to the model and concentration history at some receptor point is an output. This approach is still in the developmental stage and will be improved with the aid of validation tests against field data to account for peculiarities of sampling sites and their microclimates. Combination of the philosophy of this approach with our methods of treating photochemical reactions may provide an urban modeling technique that could be used for planning and abatement.

Puff models such as that in Ref. 5 employ Gaussian spread parameters, but by subdividing the effluent into discrete contributions, they avoid the restrictions of steady-state assumptions that limit the plume models just described. A recently documented application of a puff model for urban diffusion is that of Roberts, et. al. (18). It is capable of accounting for transient conditions in wind, stability, and mixing height. Continuous emissions are approximated by a series of instantaneous releases to form the puffs. The model, which has the capability of describing multiple area sources, has been validated for the City of Chicago by comparison with over 10,000 hourly averages of sulfur dioxide concentration.

C. RELATED WORK ON PHOTOCHEMICAL SMOG MODELING

Models for photochemical air pollution require extensions of earlier methods. Coupled chemical reactions and radiation attenuation in the ultraviolet introduce nonlinearities into the analysis. As a consequence, the superposition of linear solutions from collections of point, line, or finite-area sources may inaccurately describe the chemical interactions with meteorological conditions in the air basin. Chemical evolution of pollutants, therefore, demands a step-by-step description to reflect the cumulative effects of the processes occurring.

Efforts aimed at overcoming the limitations have resulted in methods that range from modified classical treatments to entirely new formulations. Because detailed chemical descriptions were not yet available, the previously referenced work of Frenkiel (5) on the Los Angeles basin stresses diffusive aspects of the problem by treating plume trajectories from a collection of puff sources. Other early work (19) made use of simplified chemistry in an analogue computer solution for composition histories in a network of homogeneously mixed cells. The horizontal faces of each cell were assumed to be the inversion base and the ground respectively. This approach somewhat resembles that of Ref. 14. Suggestions have been made that chemical changes be superimposed on a dispersion model like that of Frenkiel's (5), but only inert gases have been treated.

Friedlander and Seinfeld, recognizing that the generality needed could be provided by finite difference numerical solutions to the diffusion equations, developed their dynamic model of photochemical smog (20).

This model allowed for nonlinear chemical interactions, but the Lagrangian profile similarity required by the diffusion scheme still may be too restrictive to allow full freedom in specifying ground boundary conditions. Tests of the technique for photochemical smog with actual emission inventory data (in the form of distributed ground boundary conditions) have not been reported.

The models developed by Calvert (21) and by Wayne, et al. (22) stress chemical kinetic mechanism. In the former, the photochemical smog mechanism is reduced to 17 steps and in the latter to 31 steps. In the larger mechanism, care is taken to describe plausible reactions for the $C_3H_6/NO_x/$ air system, but it is ultimately applied to the atmospheric case where dozens of smog-forming hydrocarbons are involved. To preserve a consistent level of detail, the number of reactions must be increased by a large factor; however, this is avoided by adjusting the rate constants to obtain observed results. Homogeneously stirred air parcels following wind trajectories are assumed in order to retain first-order, ordinary differential equations. Chemical kinetic studies have been carried out by numerical integrations of the coupled rate equations for conditions appropriate to laboratory chamber experiments in the absence of diffusion. Other computer investigations of this general nature include the work of the group headed by Dr. Bernard Weinstock of Ford Motor Company, and of Dr. Karl Westberg at the Aerospace Corporation (23). These approaches follow the philosophy of studying a proposed chemical scheme by modeling laboratory data. Modifications are usually necessary for applications to the atmosphere.

Three-dimensional, time-dependent methods (24, 25) have been proposed recently, but results for reactive atmospheres have not been reported at this writing. Simplified chemistry must be employed in each of these approaches because of the emphasis on details of advection and diffusion. Unfortunately, the body of data for most air basins falls short of the input requirements for any transport formulation of this complexity. In some cases, it may be difficult to avoid the problem of allowing too many unspecified parameters to obscure the physically based portions of the calculation. One of the new methods employs an Eulerian coordinate frame* which introduces the chronic problem of artificial (or numerical) diffusion. Small time and space steps are the only means suggested heretofore to remedy this problem. The other method uses a discretized representation of species concentrations in a Lagrangian frame.* For multicomponent systems, the latter type of approach has previously been limited because of the large quantity of rapid access memory storage needed for each species. Both of these problems have been recognized for some time with three-dimensional, time-dependent calculations. More powerful computers and novel algorithms may well be required for their solutions.

D. OVERVIEW OF THE COMBINED PHOTOCHEMICAL/DIFFUSION MODEL

Following a desire to incorporate the best aspects of some previous work, we have endeavored to balance the detail between the chemical

---

* Lagrangian coordinates refer to a fluid mass which is followed in time and space in contrast with an Eulerian frame which has fluid moving relative to a fixed coordinate system.

and meteorological formulations in our model. The development methodology begins with pure chemical kinetics validations using laboratory data from irradiation chamber experiments. This development has evolved through two stages--one involving only seven reactions and another employing twelve reactions. Both are based on a lumped-parameter approach that includes groups of parallel reactions that perform a common function into a single effective kinetic step. Another aspect of the lumping is the collapse of a reaction chain into a rate-controlling step. Non-stoichiometric product yields sometimes occur with these simplifications.

The application of the chemical schemes to atmospheric phenomena requires a diffusion formulation that reflects time-dependence and spatial variability of meteorological conditions. An attempt has been made to keep the mathematical description near the level of detail and precision of the observational data. This has resulted in a Lagrangian air parcel formulation with finite-rate vertical diffusion. The approach avoids the artificial numerical diffusion because it uses natural (or so-called "intrinsic") coordinates that are aligned with fluid motion. This permits us to include upward dispersion and chemical change simultaneously. Figure 1 schematically illustrates the main features of the formulation. High-speed memory requirements are limited by allowing sequential point-by-point output of the history of the air parcel.

Some insights into model requirements are gained by examining some length and time scales characteristic of the Los Angeles basin, the region chosen as a prototype for validation. The horizontal scale of the air region is tens of kilometers, but the distance from ground to inversion

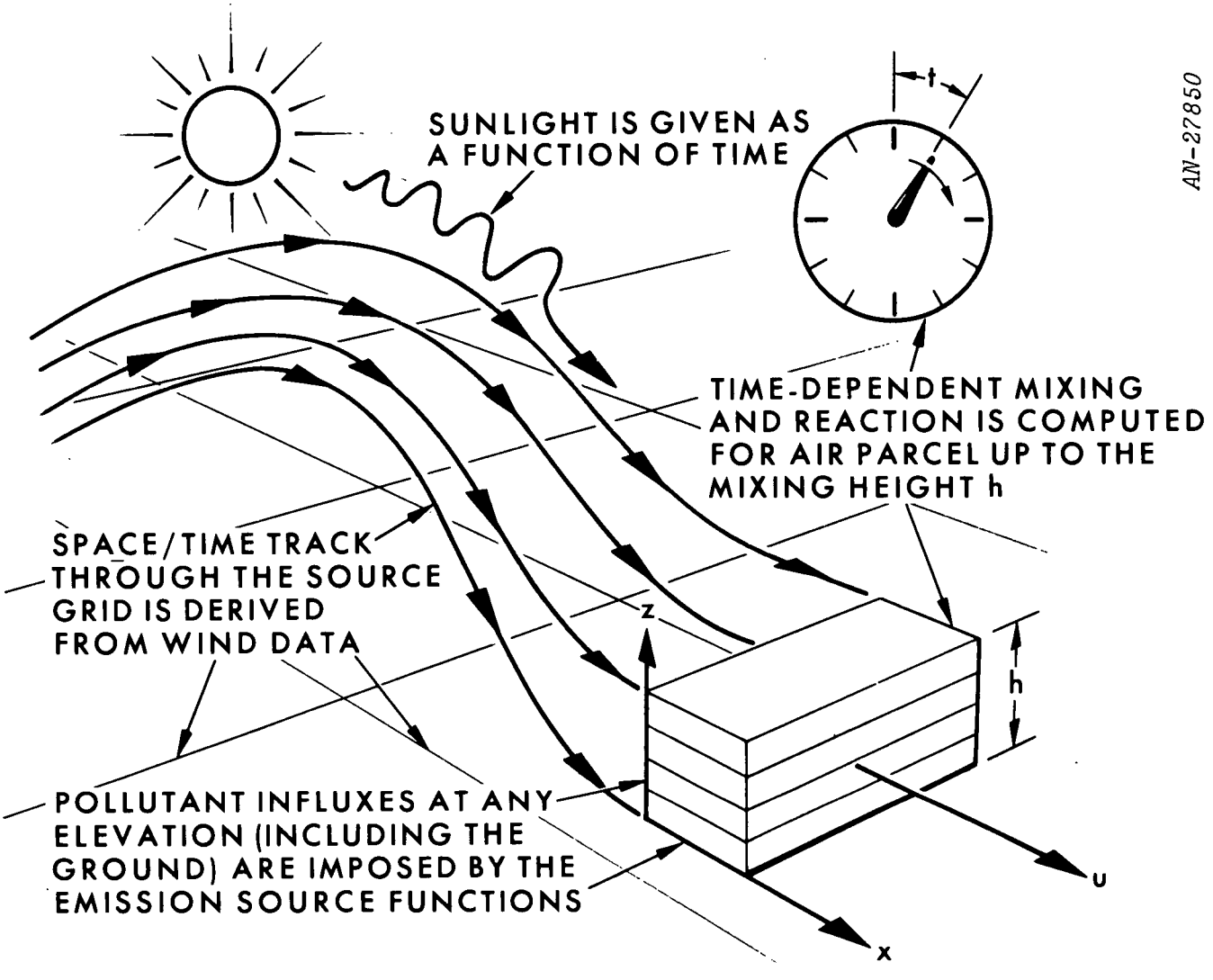

Figure 1. Schematic of Diffusion Model for Air Pollution Simulation

base is usually less than one-half kilometer during smog episodes. During late morning buildup of secondary pollutants, winds are only three or four kilometers per hour and the vertical diffusion coefficient averages approximately 10^{-2} km^2/hr or less. High reactivity hydrocarbons are halfway photo-oxidized about two or three hours after their appearance in the morning. If vertical diffusion approximates a random walk, the characteristic diffusion time from the ground to the inversion base can be one to four hours. A ten-kilometer downwind drift also occurs within this interval. Consequently, we conclude that a smog event must be modeled by treating simultaneously the processes of vertical diffusion, horizontal advection, and finite rate photochemistry.

This paper describes the evolution and validation of our mathematical model for photochemical smog. The methodology stresses flexibility of input specifications, efficiency in computation, and conformity with observable phenomena. The central sections of the paper deal successively with simplified chemical kinetic schemes, finite-difference formulation, and atmospheric validation tests. In the chemical kinetic discussions, the two versions of mechanisms are developed. Novel applications of Padé approximants are covered in the mathematical section in some detail. 1968 and 1969 Los Angeles basin data form the bases of numerical tests described in the validation section. Tests are outlined using a simple slab model for stagnant conditions and the moving parcel model for wind conditions. The concluding section establishes some future directions of research and application that are suggested by the previous course of development.

II. SOME SIMPLIFIED KINETIC MECHANISMS

A. THE ORIGINAL SCHEME

The photochemical reactions lead to most of the uniquely new requirements placed on this model. Before treating atmospheric studies, we must understand the action of the chemistry and describe it simply enough to keep the ultimate computer requirements within reasonable bounds. First, an extremely simple version of a kinetic mechanism (26) will be explained and examined.

Experimental chamber results have been computer analyzed to provide a kinetic model for the Los Angeles basin studies. In developing the model scheme, we began by trying combinations of elementary reaction steps that have been suggested previously (27-32). After many successive simplifications, we obtained the seven species by seven reaction model mechanism which is the version to be discussed first. Simultaneous solutions of the coupled rate equations guided the evolution of the representation. We retained only those classes of rate-controlling steps needed to replicate observed concentration histories. On the other hand, enough generality is included to validate the assumptions over a range of composition and light intensity conditions representative of photochemical air pollution. Hence, no claim is made that the scheme is a complete, mechanistic embodiment of the available chemical kinetic hypotheses.

Figure 2 illustrates the lumped-parameter kinetics by means of a block diagram and Figs. 3 and 4 show concentration histories in a trans-2-Butene/nitric oxide system which illustrate the action. Symbolically,

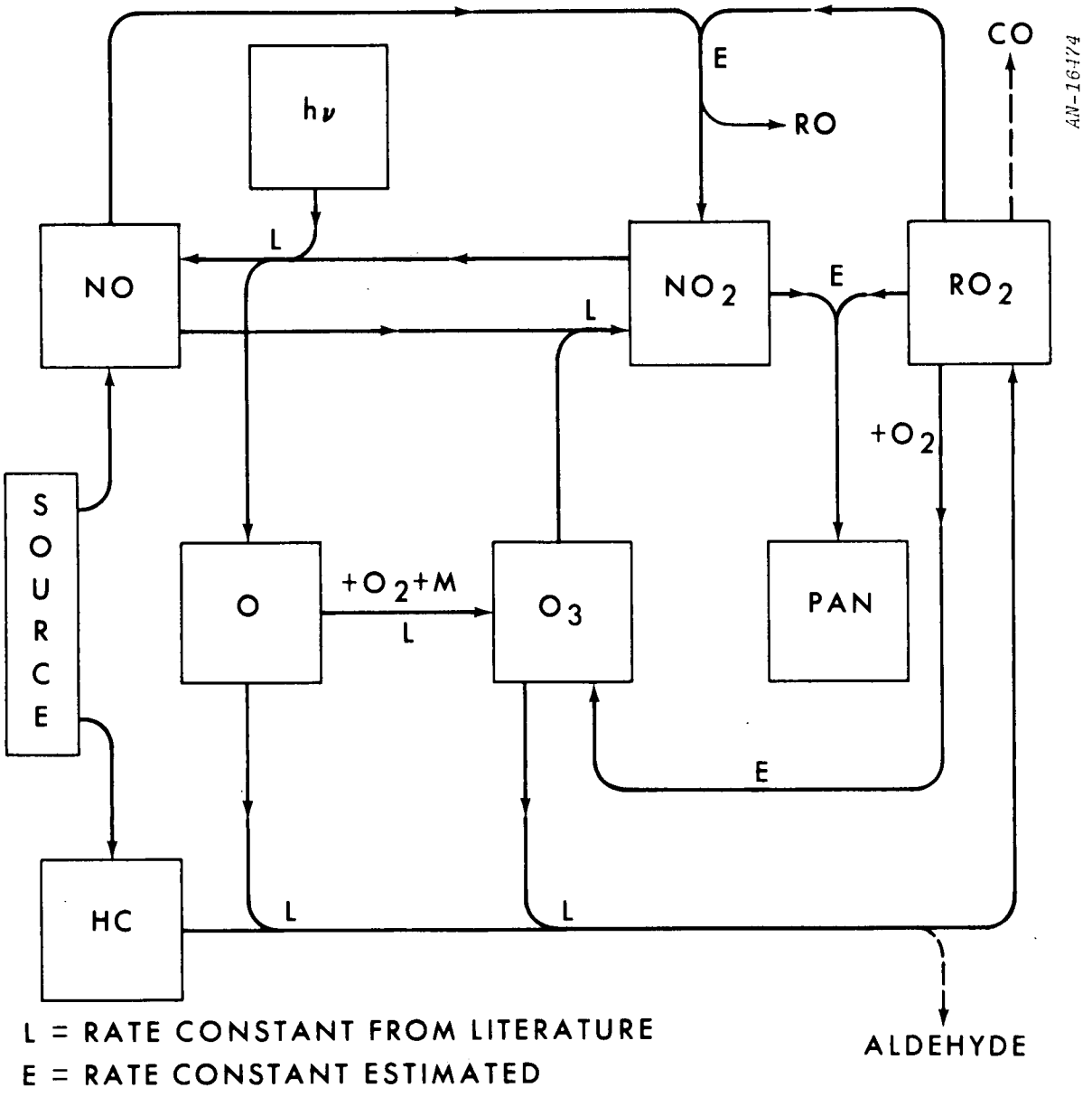

Figure 2. Original Reaction Mechanism*

---

* Stoichiometry imbalances may occur because of lumped parameter assumptions in the schematic diagram.

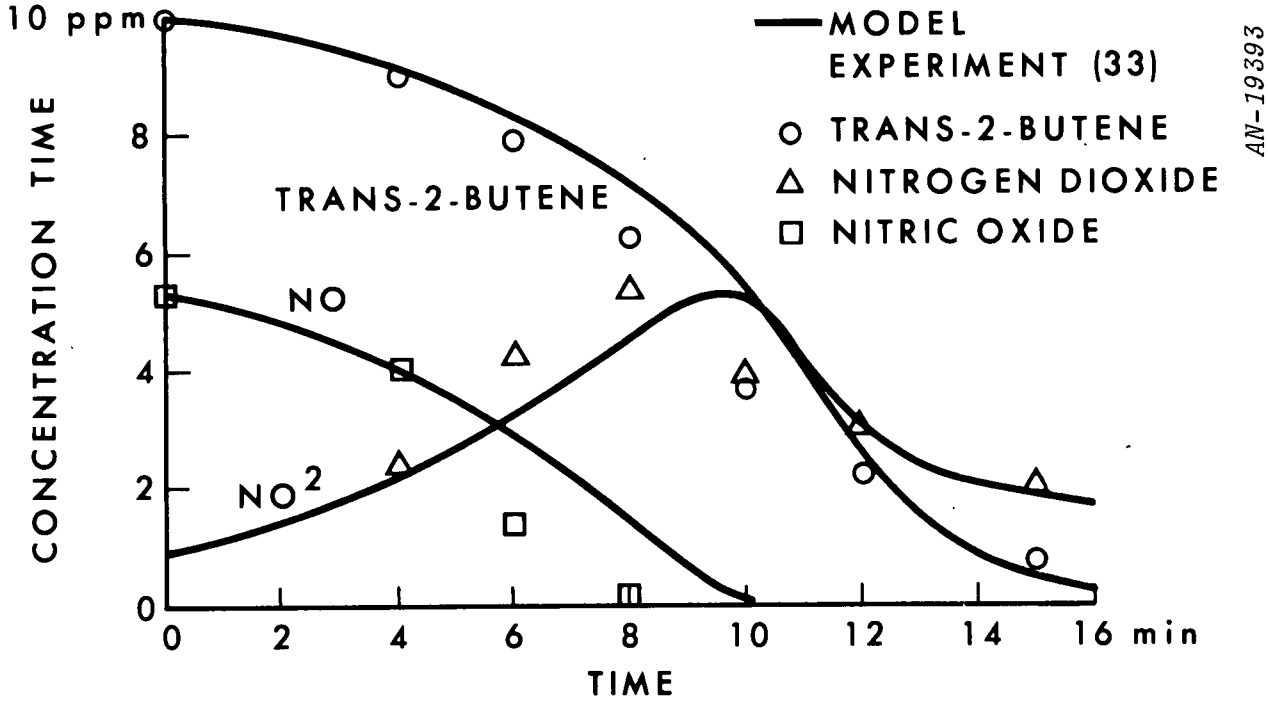

Figure 3. Computed and Observed Reactant Histories for the Trans-2-Butene/Nitric Oxide System (Rate Coefficients in Table 1)

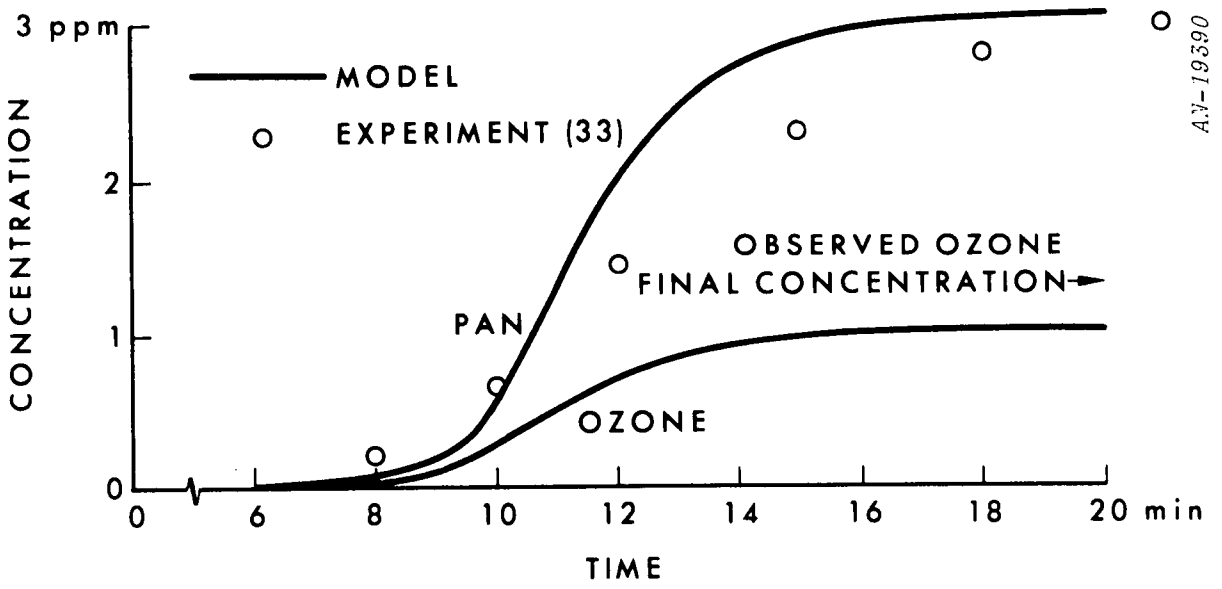

Figure 4. Computed and Observed Product Histories for the Trans-2-Butene/Nitric Oxide System (Same Conditions as Those for Figure 3)

the diagram shows species as boxes and reactions as path intersections. In Fig. 2, the emitter is labeled "SOURCE" and sunlight is denoted by "$h\nu$." The experiment (33) illustrated in Figs. 3 and 4 replaces the source with a premixed charge of HC and NO and employs simulated sunlight.

Examination of Fig. 2 shows that the NO_2 photodissociates to contribute O-atoms and NO . The O-atoms attack the hydrocarbon and produce free radicals represented here by RO_2 . In turn, the RO_2 provides an oxygen source for reconversion of NO to NO_2 . This path augments the already rapid reaction of ozone with NO to form NO_2 . Three-body association of O with O_2 contributes most of the ozone; however, an abstraction reaction of O_2 with RO_2 also provides ozone.* Nitrate formation removes NO_2 in chain termination reactions. One minor branch of the chain is included in Fig. 2 as the production of peroxyacetyl nitrate (PAN). This is included in the model because PAN has been established to be a phytotoxicant.

Following the concentration histories in Figs. 3 and 4, we note that the hydrocarbon disappearance contributes RO_2 which oxidizes NO up to NO_2 . When this induction phase is complete, ozone concentration rises because there is no longer any NO to compete for the ozone. Nitrate formation and photodissociation then take over to reverse the

---

* In the more advanced version of the model, this abstraction reaction is dropped because it is energetically unfavorable. It is needed here to provide ozone buildup at late time.

rising trend in NO_2. In the later stages, ozone becomes a serious competitor with oxygen atoms in the attack on hydrocarbons.

Before we assess the validity of the calculations, we shall enumerate some of the processes which are absorbed in certain overall steps so that the simplicity of the scheme is preserved for ultimate economy in computation. First, free radicals like RO_2 or OH also attack hydrocarbons so that the O + HC and O_3 + HC rates must be artificially elevated. Second, aldehyde photolysis (34) is an additional branch of the mechanism that must be absorbed in the rates and stoichiometry of a lumped parameter scheme. Third, inorganic particulate nitrate products would be added if it were necessary to complete the material balance to account for nitrogen (35). Fourth, radical regeneration involving CO may be implicitly absorbed in the chain branching factor applied to RO_2 (36).

Curves in Figs. 3 and 4 illustrate calculated results* for the conditions of one of Tuesday's experiments. Table 1 details the reaction stoichiometry and rate constants for the calculation. The calculated photo-oxidation rates for the main reactants are somewhat slow around 8 minutes time and the appearance rate of PAN is too fast between 12 and 16 minutes time. This results from a compromise needed because of a certain inflexibility in the schematic kinetics. The calculation employs

---

* Quasi-stationarity is assumed for O-atom and RO_2-radicals to facilitate calculations. Numerical tests confirm the validity of these approximations.

TABLE 1

RATE COEFFICIENTS FOR TRANS-2-BUTENE/NITRIC OXIDE SYSTEM

(Stoichiometry imbalances occur in some reaction steps because of lumped parameter kinetic assumptions.)

Reaction	Nominal Values*	Validation Values**
$h\nu + NO_2 \rightarrow NO + O$	0.072 to 0.55 min^{-1}	0.072 to 0.55 min^{-1}
$O + O_2 + M \rightarrow O_3 + M$	1.32×10^{-5} $ppm^{-2}min^{-1}$	1.32×10^{-5} $ppm^{-2}min^{-1}$
$O_3 + NO \rightarrow NO_2 + O_2$	21.8 $ppm^{-1}min^{-1}$	21.8 $ppm^{-1}min^{-1}$
$O + C_4H_8 \rightarrow 2.5\ RO_2 + 0.12$ Ald.	3.34×10^{4} $ppm^{-1}min^{-1}$	1.11×10^{5} $ppm^{-1}min^{-1}$
$O_3 + C_4H_8 \rightarrow 2.5\ RO_2 + 0.12$ Ald.	4.2×10^{-2} to 6.4×10^{-1} $ppm^{-1}min^{-1}$	6×10^{-1} $ppm^{-1}min^{-1}$
$RO_2 + NO \rightarrow NO_2 + RO$	$\leq$ 50 $ppm^{-1}min^{-1}$	50 $ppm^{-1}min^{-1}$
$RO_2 + O_2 \rightarrow 0.5\ O_3$	$\leq$ 50 $ppm^{-1}min^{-1}$	3×10^{-5} $ppm^{-1}min^{-1}$
$RO_2 + NO_2 \rightarrow 0.67$ PAN	$\leq$ 50 $ppm^{-1}min^{-1}$	1 $ppm^{-1}min^{-1}$

* See Sec. II for sources.

** Values consistent with experimental measurement (33).

established values of rates from the literature for the three inorganic reactions. The NO_2 photolysis was calibrated (33) according to the light intensity at 0.37 min^{-1} and the other two reaction rate constants were obtained from Ref. 37, assuming an ambient temperature of 27°C. In order to obtain observed oxidation rates, the O-atom plus C_4H_8 rate was increased nearly fourfold to absorb the competing radical reactions and the ozone on C_4H_8 rate fell near the upper end of measured range. Nominal values for these reactions are obtained from the literature (30). Collision theory estimates yield upper limit nominal values for the last three reactions listed in Table 1.

The discussion has centered on a single experiment to illustrate the validation of the simple scheme. Other experiments bring out special features. For example, the ozone reaction with a hydrocarbon is actually far more complex than a single step because somewhat lower rate values for $O_3 + C_4H_8$ (still in the nominal range shown in Table 1) are observed in experiments involving C_4H_8/NO_2 systems under irradiation. Apart from this complication, the set of rates in Table 1 exhibit good modeling results near the value of initial C_4H_8/NO-ratio employed in the prototype experiment. These rates also give excellent agreement for experimental light intensities both below and above that used for Fig. 3 (see Table 1 for range).

Several features of this particular system, however, are atypical of photochemical air pollution. Such features include the reactivity, the concentration levels, the time scales, and the organic nitrate

production. Trans-2-Butene is far more reactive than the average of atmospheric hydrocarbons. Even omitting low reactivity components (methane, ethane, and acetylene) from automotive exhaust compositions, we find that the remaining fraction of hydrocarbons has a weighted average reactivity index (38) many times less than that of the butenes. Regarding concentration levels, the experiment (33) cited begins with 10 ppm reactive hydrocarbon whereas atmospheric values are ten times less. As a result of these two differences, smog reaction times are close to 20 times longer than those of the experiment. Finally the PAN yields from butene oxidation exceed those of the atmospheric reactants. Despite these limitations, Ref. 33 covers a broader scope of parametric variables than most experiments reported in the literature. Therefore, it gives many validation benchmarks for various compositions and light intensities. Since the propylene-nitric oxide system is more nearly like reactive systems in air pollution, validation tests were conducted on that system also. Again, measured composition behavior from chamber irradiation tests (39, 40) serves as a basis for modifying some of the rate constants to absorb the additional effects. Lower oxidation rates and lower PAN yields occur with propylene compared with trans-2-butene. Lumped rate constants for $O + C_3H_6$ and $O_3 + C_3H_6$ were found to be 4.97×10^4 and 1.8×10^{-1} ppm^{-1} min^{-1}, respectively, for use with this simple mechanism. In the more complex mechanism to follow the literature values are adhered to.

In viewing the transition from the simple to the complex mechanisms, one should realize what the limitations and objectives are for

the simple mechanism. It provides a description of pure hydrocarbon photooxidation with nitric oxide within a rather restricted range of initial mixtures typical of polluted air; however, it describes well the overall rate dependence on light intensity. The rate constants for organic reaction steps must be changed for different hydrocarbons as evidenced by the changes cited above needed to fit the propylene results. Major objectives of the more complex treatment discussed in the following sections are to relax the restrictions on initial mixture composition and to describe the chain initiating steps individually (instead of lumping them in the O + HC-rate).

B. ADDITION OF MORE REALISTIC OXIDATION CHAINS

As alluded to above, it has been known for some time that hydrocarbon consumption rates observed in chamber experiments cannot be explained by ozone and oxygen atom attack alone. This is discussed in the review by Altshuller and Bufalini (30) where it is noted that Schuck and Doyle (41) termed the disparity an "excess rate." Our previous modeling work treated this by increasing both the O_3 and O-atom rates of reaction with hydrocarbon.

To use known rate constants to a maximum extent in the present work, we have added a hydrocarbon oxidation chain to reflect the attack of RO upon the hydrocarbon. Because of its suspected dominance (42, 43), hydroxyl radical (OH) was assumed to be the only RO reacting with the hydrocarbon.

Following the inorganic cycle formed by

$$\left.\begin{array}{l} h\nu + NO_2 \rightarrow NO + O \\ O + O_2 + M \rightarrow O_3 + M \end{array}\right\} \qquad (1)^*$$

$$NO + O_3 \rightarrow NO_2 + O_2 \qquad (2)$$

we have allowed each hydrocarbon oxidation to generate multiple RO_2 radicals as expressed by the b-factors in the steps

$$O + HC \rightarrow b_1(RO_2) \qquad (3)$$

$$OH + HC \rightarrow b_2(RO_2) \qquad (4)$$

$$O_3 + HC \rightarrow b_3(RO_2) \qquad (5)$$

Subsequent conversion of NO to NO_2 was assumed to occur via

$$RO_2 + NO \rightarrow NO_2 + d(OH) \qquad (6)$$

where d expresses that fraction of the conversion responsible for returning hydroxyl to the system.

Note that reactions (4) and (6) form something of a closed loop and that a stability requirement like $b_2 d < 1$ may be needed to prevent RO_2-runaway. This is not a precise requirement because of the variety of external factors that influence the flow rate of free radicals around

---

* The two reaction steps bracketed by (1) are combined by assuming O-atom stationarity internal to the logic of the computer program. Hence reaction (1) nets the system $h\nu + O_2 + NO_2 \rightarrow NO + O_3$.

the loop. Some of the RO_2 is formed by the other two reactions, and there are radical removal processes in the chain termination steps we discuss in the following paragraph.

Both RO_2 and OH are held in check by removal steps that terminate the chains. We continue to use some lumped parameter reactions such as

$$RO_2 + NO_2 \rightarrow c(PAN) \tag{7}$$

and some elementary reactions like

$$OH + NO + M \rightarrow HONO + M \tag{8}$$

$$OH + NO_2 + M \rightarrow HNO_3 + M \tag{9}$$

This rounds out the expanded mechanism. Figure 5 shows it in the form of a schematic diagram.

In summary, the main changes from the scheme described in Sec. II A are: addition of radical species RO (treated as OH), the provision for a multiplicity of hydrocarbons (not shown in equations), and the elimination of ozone production from an RO_2 reaction. The multiplicity of hydrocarbons is done by adding parallel reactions to (3), (4), and (5). The omission of the ozone production reaction is justified on the basis of its suspected endothermicity (23).

For our initial validation tests, we tried the rate constants compiled and estimated by Westberg and Cohen (23). Stoichiometric coefficients b_1, b_2, b_3, and d were determined by hand-calculation analysis

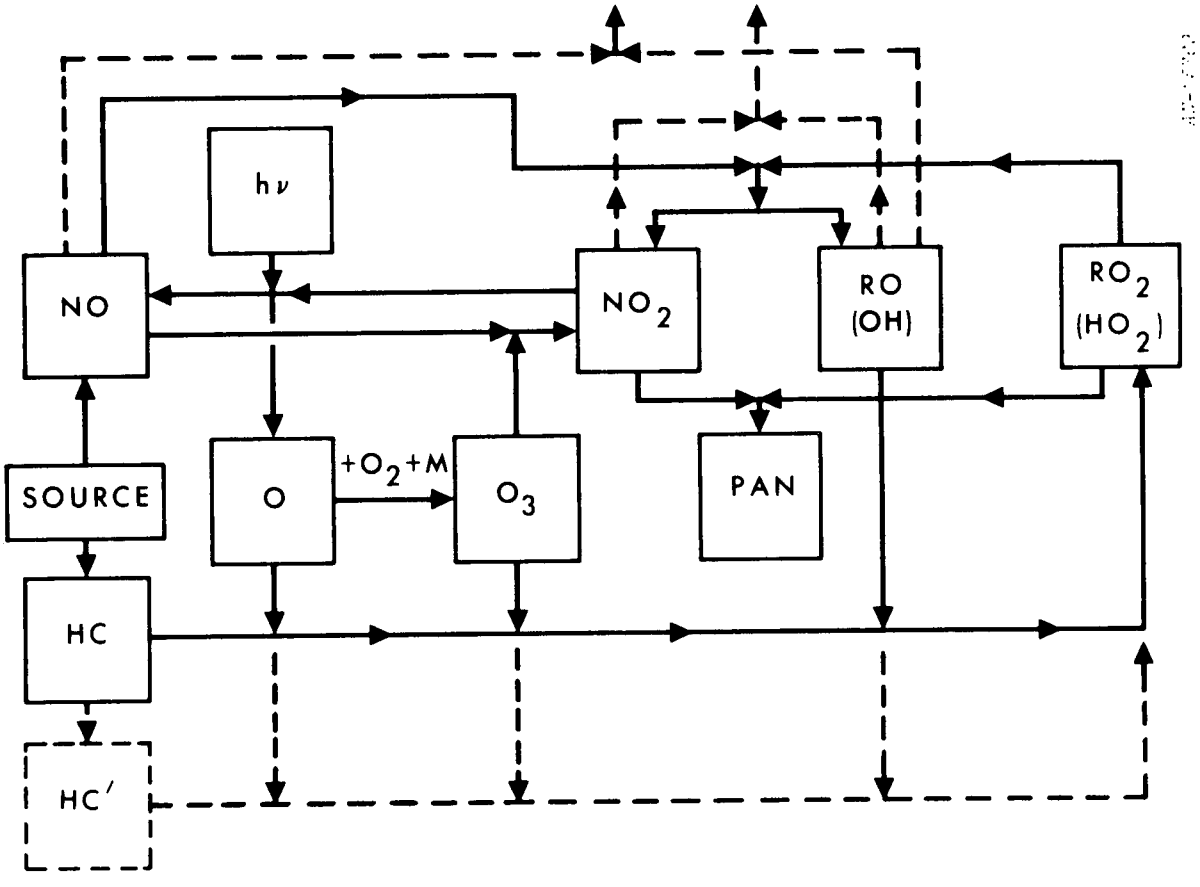

Figure 5. Expanded Kinetic Mechanism

of some of the propylene data represented by Ref. 39. We found that $bd \simeq 1$, where b is a composite branching factor, and $b \simeq 2$ in order to explain the decay rate of NO compared with that of propylene.

Explosions of RO_2-concentration characterized some early choices of bd-combinations because of the positive feedback loop involving radical reactions shown in Fig. 5. Since these occurred in the first few seconds of real time, they were difficult to detect. This is unexpected because of the longer time scales usually associated with the system. Sudden drops of NO and HC (to some nonzero levels) occurred during the first minute followed by the dynamic equilibrium between NO, NO_2, and O_3 with a slow decay of hydrocarbon. The underlying pathology was discovered by rerunning with special diagnostic outputs.

Nominal rate constants were adjusted to reconcile computed results with measured values. For example, the (OH + HC)-rate was cut to about one-third the estimated value and the (NO + RO_2)-rate was increased eightfold. Reaction rates which have been reported individually in the literature were held at their nominal values including the (O + HC)-rate which we had to increase many-fold in Sec. II A. Also, the retention of reaction (5) was still necessary to describe the continued C_3H_6-decay after the near disappearance of NO .

In order to reproduce the late-time behavior of NO_2 and propylene, we included chain termination reactions in addition to those indicated in Fig. 5. In their more recent review (44), Altshuller and Bufalini

point out that HONO might be formed by the reaction with water vapor

$$NO + NO_2 + H_2O \rightarrow 2HONO \tag{10}$$

which is likely to proceed in the two steps

$$NO + NO_2 \rightarrow N_2O_3 \tag{11}$$

$$N_2O_3 + H_2O \rightarrow 2HONO \tag{12}$$

A possible source of OH-radical (42, 43) is the photodissociation of HONO

$$h\nu + HONO \rightarrow OH + NO \tag{13}$$

Figure 6 shows the computed concentration history using this scheme to describe the experimental observations of Altshuller, et al. (39) and Table 2 summarizes the reaction rate constants that were used. The column in Table 2 labeled "nominal" gives the values we started from on the basis of tabulations in Ref. 23. Following an empirical procedure, our calculations effectively combined H_2O-concentrations with the rate constant for reaction (10) as indicated; therefore no comparable nominal value is shown. Higher levels of precision than that shown in Fig. 6 were not among our objectives, since a detailed investigation of propylene is not justified for describing the potpourri of hydrocarbons in the urban atmosphere. Orders of magnitude for conversion times and levels are sufficiently good to proceed from here. The objective that we have fulfilled is to represent the so-called "excess rate"

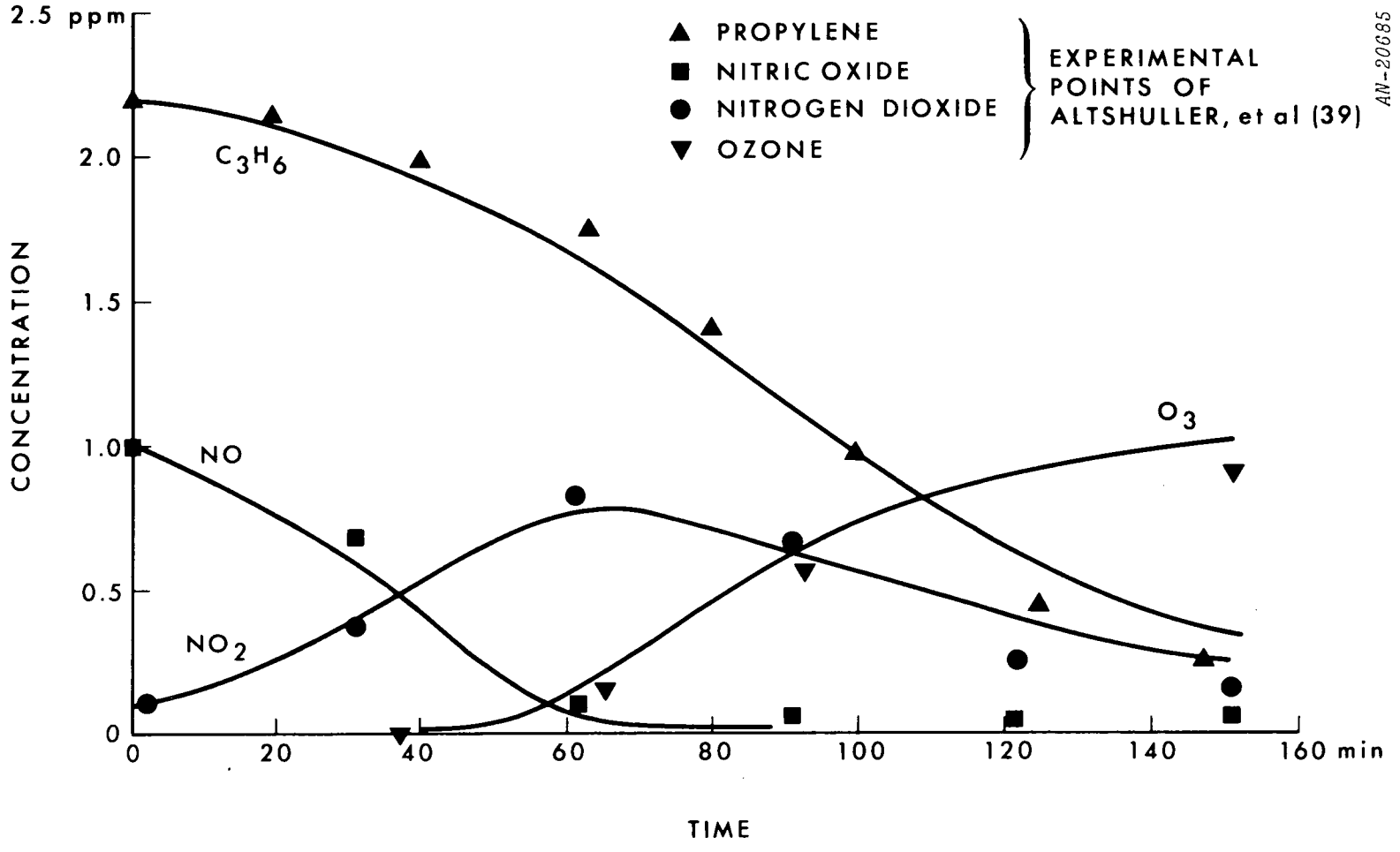

Figure 6. Computed Curves Compared With Experimental Points for the Propylene/Nitrogen Oxides System

TABLE 2

RATE COEFFICIENTS FOR EXPANDED MODEL OF THE HYDROCARBON/NITRIC OXIDE MECHANISM

(Stoichiometry imbalances may occur because of lumped parameter assumptions.)

Reaction	Model Values from Validation	Nominal Values for Propylene System (23)
$h\nu + NO_2 \rightarrow NO + O$	$0.4\ min^{-1}$	$0.4\ min^{-1}$
$O\ (+\ O_2) + M \rightarrow O_3 + M$	$1.32 \times 10^{-5}\ ppm^{-2} min^{-1}$	$1.32 \times 10^{-5}\ ppm^{-2} min^{-1}$
$O_3 + NO \rightarrow NO_2\ (+\ O_2)$	$40\ ppm^{-1} min^{-1}$	$22\text{-}44\ ppm^{-1} min^{-1}$
$O + HC \rightarrow 2RO_2$	$6100\ ppm^{-1} min^{-1}$	$6100\ ppm^{-1} min^{-1}$
$OH + HC \rightarrow 2RO_2$	$80\ ppm^{-1} min^{-1}$	$244\ ppm^{-1} min^{-1}$
$RO_2 + NO \rightarrow NO_2 + 0.5\ OH$	$1500\ ppm^{-1} min^{-1}$	$122\ ppm^{-1} min^{-1}$
$RO_2 + NO_2 \rightarrow PAN$	$6\ ppm^{-1} min^{-1}$	$122\ ppm^{-1} min^{-1}$
$OH + NO \rightarrow HNO_2$*	$10\ ppm^{-1} min^{-1}$	$99\ ppm^{-1} min^{-1}$
$OH + NO_2 \rightarrow HNO_3$*	$30\ ppm^{-1} min^{-1}$	$300\ ppm^{-1} min^{-1}$
$O_3 + HC \rightarrow RO_2$	$0.0125\ ppm^{-1} min^{-1}$	$0.00927 - 0.0125\ ppm^{-1} min^{-1}$
$(H_2O +)\ NO + NO_2 \rightarrow 2HNO_2$**	$0.01\ ppm^{-1} min^{-1}$	
$h\nu + HNO_2 \rightarrow NO + OH$	$0.001\ min^{-1}$	

* Rate constant lumps third body concentration

** Water vapor lumped into rate coefficient

of hydrocarbon oxidation with added reactions instead of artificially increasing the O-atom rate with hydrocarbon.

C. INFLUENCE OF INITIAL COMPOSITION

1. Synergism Between Hydrocarbons

The fact that free radicals produced in the photooxidation of one hydrocarbon can accelerate the attack on a coexistent hydrocarbon has been illustrated with experimental findings by Altshuller and Bufalini (44). Because of the limited understanding of detailed interactive mechanisms, we limited our multiple hydrocarbon investigation to a simple parametric study. Using a truncated version of the mechanism in Table 1, we added a parallel series of oxidation steps. This scheme is shown in the flow chart of Fig. 5 with dashed lines along the bottom portion of the diagram.

In the parametric study, the same initial values of total hydrocarbon and nitric oxide as those in Fig. 6 were employed. The hydrocarbon, however, was partitioned into two hypothetical compounds, one having triple the (OH + HC) rate constant and the other having one-third the (OH + HC) rate constant as propylene. The compound with the tripled rate is called species "B" and the one with the decreased rate is called species "A." All other reactions in the scheme are the same in all respects as their counterparts in the (C_3H_6 + NO_x)-system.

Figure 7 shows the hydrocarbon decay curves from the parametric study. On the same coordinates, we plot curves for model calculations

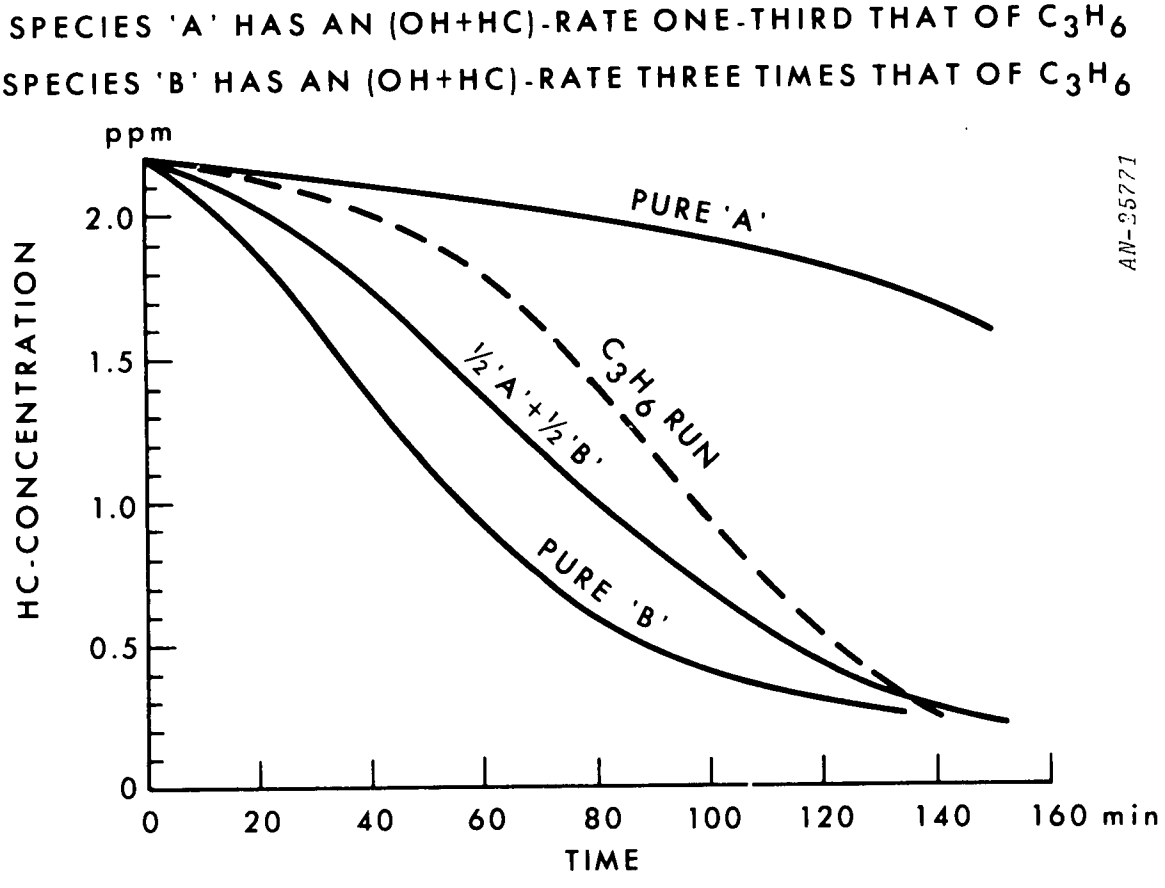

Figure 7. Hydrocarbon Decay With Two Reactivities

of pure hydrocarbon "A", pure hydrocarbon "B", and pure propylene for comparative purposes with the half-and-half mixture of hypothetical compounds. The most interesting aspect of Fig. 7 is that the mixture decays faster than propylene even though it contains equal quantities of "A" and "B" which bracket propylene symmetrically. The coupling between the two hydrocarbons occurs via the RO_2 conversion of NO to NO_2 and the production of OH . Evidently the combination of the rapid incubation (afforded by the reactive hydrocarbon) with the twofold chain-branching is sufficient to increase the decay rate over that of pure propylene.

Figure 8 shows corresponding curves for ozone buildups predicted in the computer experiment. Again the combination seems to exceed the pure propylene in its rapidity to produce ozone. This occurs because of the enhanced conversion rate of nitric oxide to nitrogen dioxide stimulated by the early abundance of RO_2 generated by the high-reactivity fraction.

These findings illustrate a plausible mechanism for the interaction of multiple hydrocarbons. In future applications of our photochemical/diffusion model, this type of representation is likely to be more realistic than a super-detailed single hydrocarbon mechanism with many adjustable constants. Also, other radical interactions like RO_2 + HC and RCO_3 + HC might provide plausible coupling paths (44) in addition to the hydroxyl attack on the hydrocarbon. Indeed, other forms of coupling may favor the slower reacting hydrocarbon in a similar numerical experiment with a half-and-half mixture.

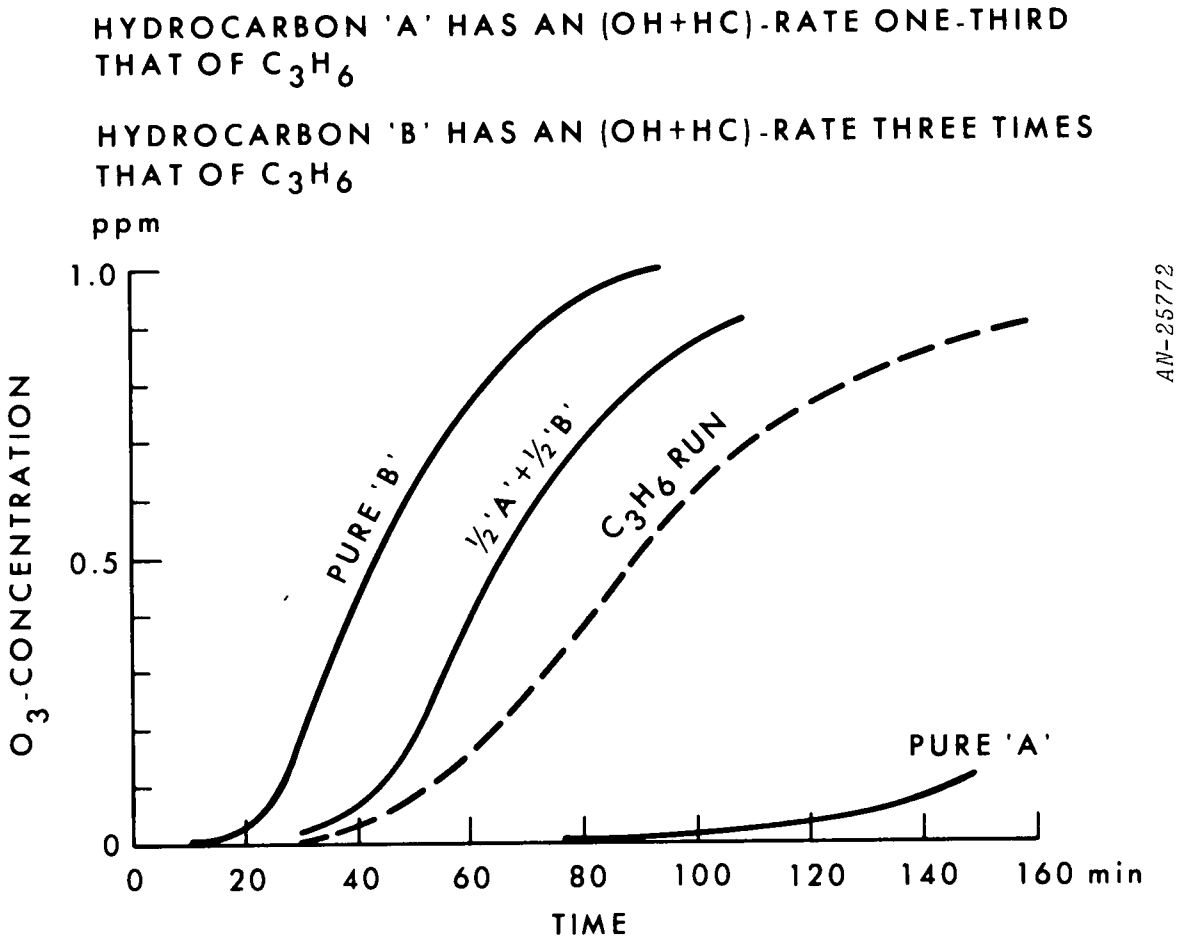

Figure 8. Ozone Buildup With Two Reactivities

2. Modeling the Influence of NO_x/HC-ratio on Oxidant Production

Our main purpose in including the chain termination results for nitrogen oxides in the previous subsection was to improve the modeling of initial mixture effects. It will be recalled that in Sec. II A we issued a caveat restricting the seven-step mechanism to a narrow range of NO_x/HC ratios. Seinfeld (45) pointed out that the slope of the curve of peak oxidant versus NO_x/HC-ratio did not even have the correct sign. If modeling is to be used to evaluate hypothetical abatement strategies, it is clear that this deficiency must be remedied.

Figure 9 shows the results from the twelve-step* mechanism given in Table 2. Experimental results for pure and mixed hydrocarbons are shown on this plot of peak oxidant versus NO_x/HC-ratio. The model mechanism displays a monotonically declining trend of oxidant production as the oxides of nitrogen increase. Both of the pure hydrocarbons measured by Altshuller, et al., show peaks at widely separated values of the mixture ratio. It seems plausible then that the typical mixture of atmospheric pollutant hydrocarbons should show a decrease of oxidant with increasing NO_x/HC-ratio. This is supported by the fact that the relative abundance of hydrocarbon species decreases with increasing reactivity. Now since the low reactivity species peak at lower NO_x/HC-ratios the combined effect should give a negative slope.

The two plots on Fig. 9 of oxidant production from diluted and irradiated automobile exhaust (47, 48) both have negative slopes comparable to that of the model. As stated earlier, our purpose in using

*Stationary state treatment of O-atoms reduces this to eleven.

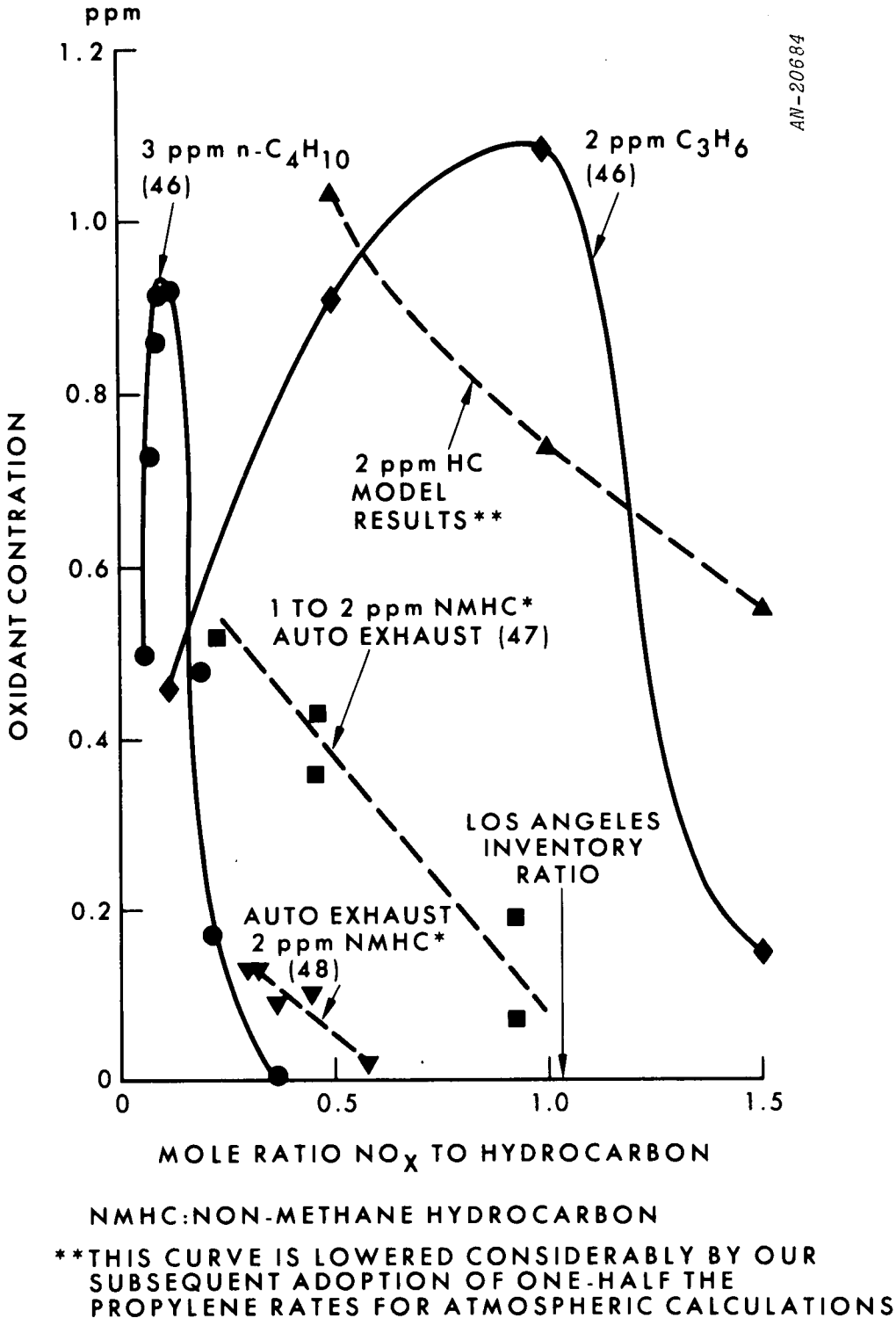

Figure 9. Influence of NO_x:HC-Ratio on Oxidant Production

chamber data for propylene to validate the mechanism is to capture the main features of the experiments that apply to the atmosphere. If, on the other hand, propylene were the subject of our study, we would proceed to expand on the mechanism to get the proper curve shape shown in Fig. 9.

Having subjected the 12-step mechanism to these laboratory tests, we use it in its present form for atmospheric validation studies described in a later section.

3. Examination of Carbon Monoxide Effects

Recent work (43, 49, 50) of photochemistry of smog has suggested that carbon monoxide may play a role in accelerating the photooxidation of hydrocarbon/nitric oxide mixtures. The mechanism suggested is

$$OH + CO \rightarrow CO_2 + H \tag{14}$$

$$H + O_2 + M \rightarrow HO_2 + M \tag{15}$$

$$HO_2 + NO \rightarrow OH + NO_2 \tag{16}$$

$$(H_2O +)\ HO_2 + NO_2 \rightarrow 2HNO_2 \tag{17}$$

Reaction (15) is postulated to contribute HO_2 rapidly as it responds to the presence of H-atom, and reaction (16) enhances the NO-to-NO_2 conversion already occurring in reaction (6). Likewise, the hydroxyl radical supplied by reaction (16) goes on to react with the hydrocarbon in reaction (4), producing RO_2-radicals in a branched chain already described. Reaction (17) is a chain termination step suggested for HO_2 .

The key feature we wish to examine in this alternate path is the competition of CO with hydrocarbon for the hydroxyl radicals. The rate constant for $OH + C_3H_6$ suggested in Ref. 23 is approximately equal to that suggested in Ref. 49 for $OH + CO$. We tried a wide range of (OH + CO)-rates holding the basic system at the values in Table 1. Since reaction (15) is fast, reactions (14) and (15) were added to give the overall reaction

$$O_2 + OH + CO \rightarrow CO_2 + HO_2 \tag{18}$$

The rate constant for reaction (16) was taken to be the same as its RO_2-analogue, reaction (6), and the rate constant for reaction (17) was assigned the value of 1.2 $ppm^{-1}min^{-1}$ based on the estimate in Ref. 23. The species O_2 is carried implicitly in the calculation, and the rate constant for reaction (18) is varied parametrically for this study.

Beginning with (CO + OH)-values at the level suggested in Ref. 49, ($k_{18} \simeq 200$ $ppm^{-1}min^{-1}$) we found very rapid NO-to-NO_2 conversion and HC disappearance with 100 ppm added CO. Only when k_{18} was lowered to 1 or 2 $ppm^{-1}min^{-1}$ did we obtain only small effects. Since much experimental verification is yet to be done, only a limited effort was devoted to this aspect of the study. Table 3 summarizes the main findings. It indicates that the half disappearance time of NO is the strongest effect of k_{18} on the system, and the half-disappearance time of hydrocarbon is least affected. Both the peaking time for NO_2 and the half-rise time of ozone are moderately sensitive to the rate constant.

TABLE 3

INFLUENCE OF 100 ppm CARBON MONOXIDE ON THE SYSTEM SHOWN IN FIG. 6 WITH VARIOUS VALUES OF THE RATIO OF (OH + HC)/(OH + CO) REACTION RATE COEFFICIENTS REACTION TIME IN MINUTES

k_4/k_{18}	$t_{1/2}$ - NO	t_{pk} - NO_2	$t_{1/2}$ - HC	$t_{1/2}$ - O_3
0.4*	<1	4	40	10
4	6	13	48	22
40	25	43	73	62
80	29	52	81	73
System in Fig. 6 (No CO)	36	66	92	83

*This is with k_{18} set at the estimated value from Ref. 49.

In any event, whether we use the estimated rate of (OH + CO)-reaction or even only preserve its ratio to that of the (OH + HC)-reaction suggested in Ref. 23, we get very large effects. Other work (42) suggests a much larger (OH + HC)-rate constant for propylene. In view of our findings and of the wide disagreements on some of the rates, a very real need exists for definitive experimentation to achieve a deeper understanding of the kinetics.

D. ATMOSPHERIC ADAPTATION BASED ON REACTIVITY DATA ANALYSIS

In order to apply the reaction mechanisms developed above to cases of realistic photochemical air pollution, some means must be devised to

convert the laboratory-derived rate constants to those suitable for atmospheric processes. Although the atmosphere over a city contains a wide variety of hydrocarbon species, we will attempt to characterize it by a single "averaged" species. The averaging will be in the sense of reactivity; that is, the hydrocarbon's susceptibility to oxidative attack, its ability to produce oxidants, or its likelihood to lead to undesirable biological effects. To do this we will relate the reactivity of pollutant species to the pure species observed in the laboratory.

When a deeper understanding of hydrocarbon synergism is attained, we can model the interactions by including the key reactions; however, an interim approach has been adopted for scaling hydrocarbon rate constants according to observed reactivities. Gas chromatographic measurements made by Scott Research Laboratories (51, 52) provide the input information employed in the analysis. Air samples were analyzed at a central basin station and at a northeastern basin station for two smog seasons.

Prior to interpreting the results of the analysis it is useful to examine the reactivity scales and their application. For some time reactivity ratings have been assigned to the individual hydrocarbon compounds occurring in photochemical air pollution (38, 53, 54, 55). Various classification criteria have evolved on the basis of different observable effects. Reactivity response numbers represent the relative extent to which each effect occurs. Some of the effects are hydrocarbon consumption rate, nitric oxide consumption rate, nitrogen dioxide peaking

time, product yields, and biological responses. Also, a number of experimental studies on distributions of specific hydrocarbons in polluted atmospheres are reported in the literature (e.g., Refs. 56 through 60). Each of these studies analyzed data that are limited either in number of samples or number of compounds when compared with the body of data presented for analysis in the present program. Consequently our data base permits us to go further in drawing general conclusions. Table 4 shows the two reactivity scales used for this analysis.

TABLE 4

HYDROCARBON REACTIVITY SCALES (54)

		Reactivity Response	
Group No.	Class of Compounds	Hydrocarbon Consumption	Product Formation and Biological Effects
1	C_1-C_5 paraffins, acetylene, benzene	0	0
2	C_6 + paraffins	1	1
3	Toluene and other monoalkylbenzenes	3	3
4	Ethylene	4	4
5	Dialkyl- and trialkyl-benzenes, diolefins	8	6
6	1-alkenes	17	7
7	Internally double-bonded olefins	100	8

We use the reactivity groupings as a method of classifying compounds to provide some insights into the processes occurring. Means and standard deviations for the values at each time of day are derived using the whole sample of days available. For the level of detail in the present work, this approach gives more breadth to the results than one of focusing attention on a limited number of compounds or on a limited number of days.

Figures 10 and 11 show reactivity histories averaged over all 1969 data days in the Scott program (52) using the hydrocarbon consumption scale (54). Our interest in this scale is directed mainly to the modeling problem. In these graphs, and in succeeding ones, we have aggregated the hydrocarbons of non-zero reactivity response and have determined the mole fraction within each group number. The reactivity for any particular time is found by summing the products of the reactivity response of each group and the mole fraction in the group. Although summation of these products may not be a precise way of characterizing the mixture, we have used it for our analysis because generalized algorithms are not yet available for computing overall reactivity.

Examining the results in Figs. 10 and 11, we note that the reactivity at Commerce picks up in the hours following the morning traffic but decreases in the early afternoon hours as the photochemical fractionation overtakes the input of new hydrocarbons. All changes are small with a mean reactivity value of about 6. Because of its remoteness from

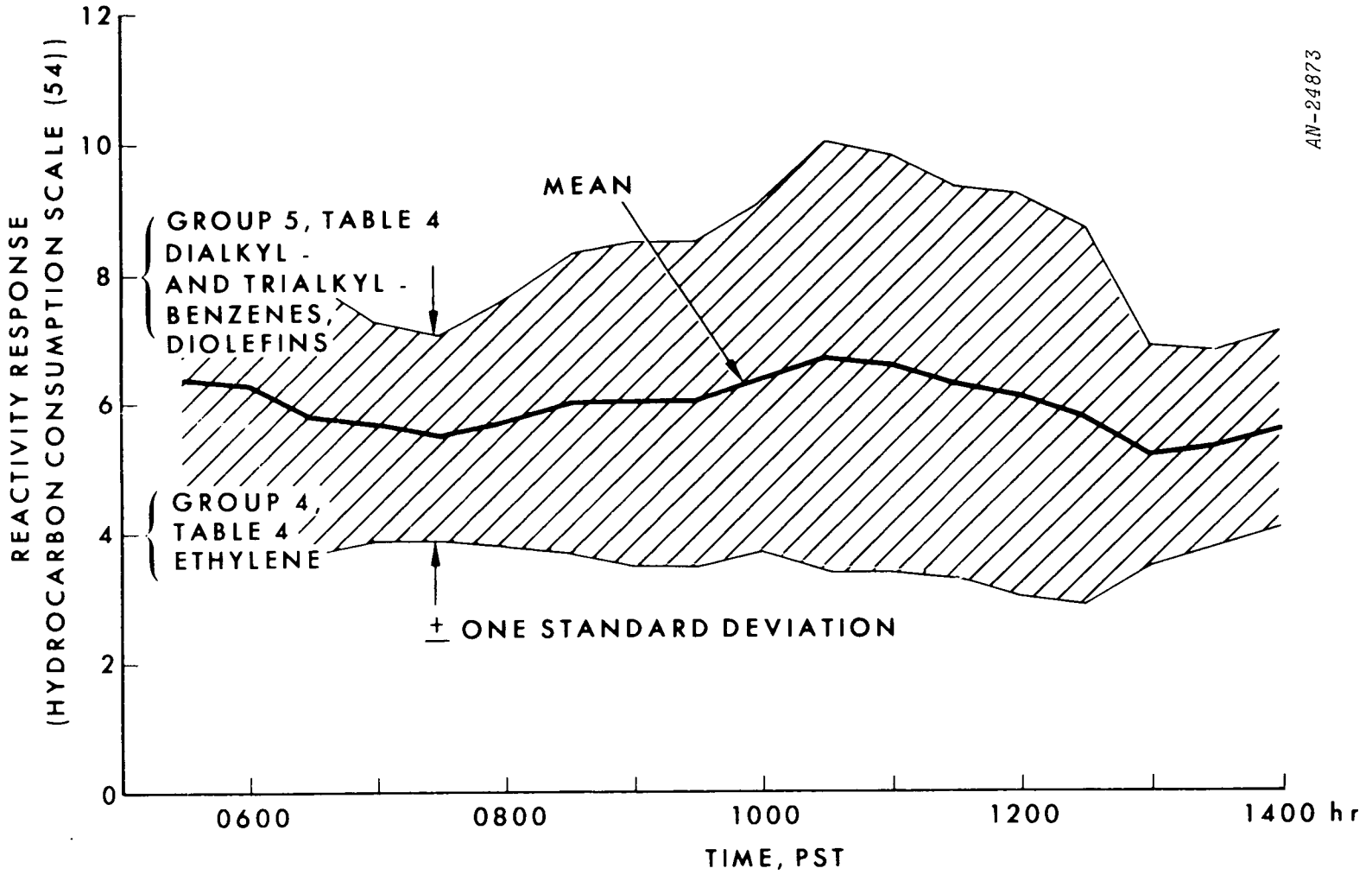

Figure 10. Average Reactivity History for Commerce, 1969: Hydrocarbon Consumption Scale from Altshuller (54)

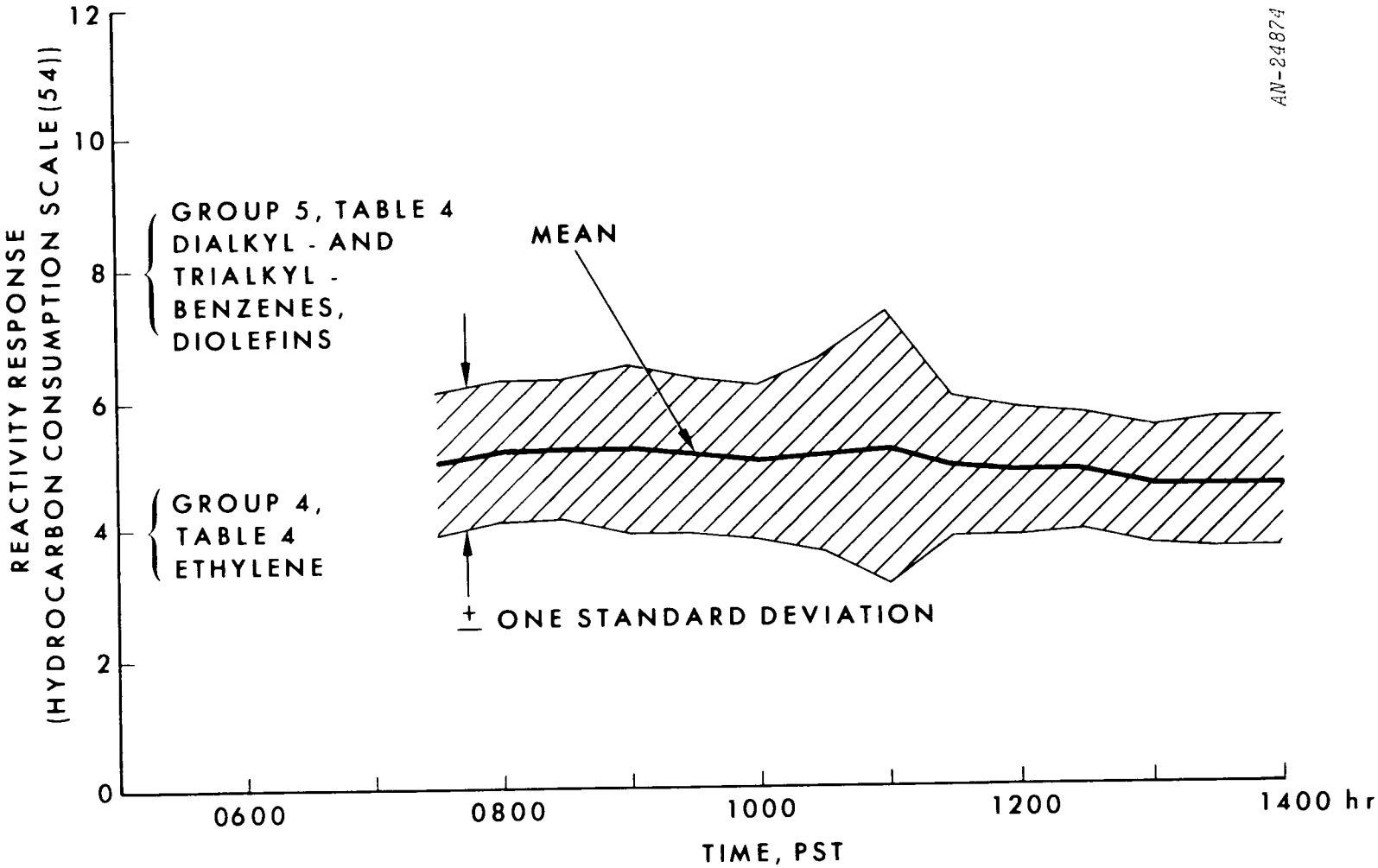

Figure 11. Average Reactivity History for El Monte, 1969: Hydrocarbon Consumption Scale from Altshuller (54)

the strong sources, El Monte has a lower and flatter reactivity mean of about 5. The scatter at El Monte is far less than that at Commerce.

From the standpoint of adapting a simple kinetic model to the atmosphere, the behavior of the average reactivity is indeed fortuitous. The flatness of the histories and the modest scatters about the mean suggest that our propylene validation cases be scaled down by factors of two or three in the hydrocarbon rate constants. This adjustment arises because propylene is in Group No. 6 on Table 4 showing a hydrocarbon consumption response of 17.

Beside kinetic parameters, we should check the influences of various hydrocarbons on receptors to see if they display the same type of averaged behavior. Indeed, more significant from an abatement point of view are reactivity scales based on biological effects and on product formation; Figs. 12 and 13 show reactivity histories using such scales due to Altshuller (54); the reactivity responses of exhaust hydrocarbons and evaporative gasoline emissions are indicated in the figures for purposes of comparison. Only slight variations are noted throughout the daytime hours. Commerce begins at its highest point at 0600 hours PST and decreases only slightly thereafter. As might be expected from windborne transport from the west, El Monte experiences its peak at about 0900 hours PST after which time it decreases slightly to approximately the same values as those at Commerce in the early afternoon. Both curves move only narrowly between reactivity responses of 3.4 and 3.9. Slightly higher peak reactivities are observed at El Monte than at Commerce

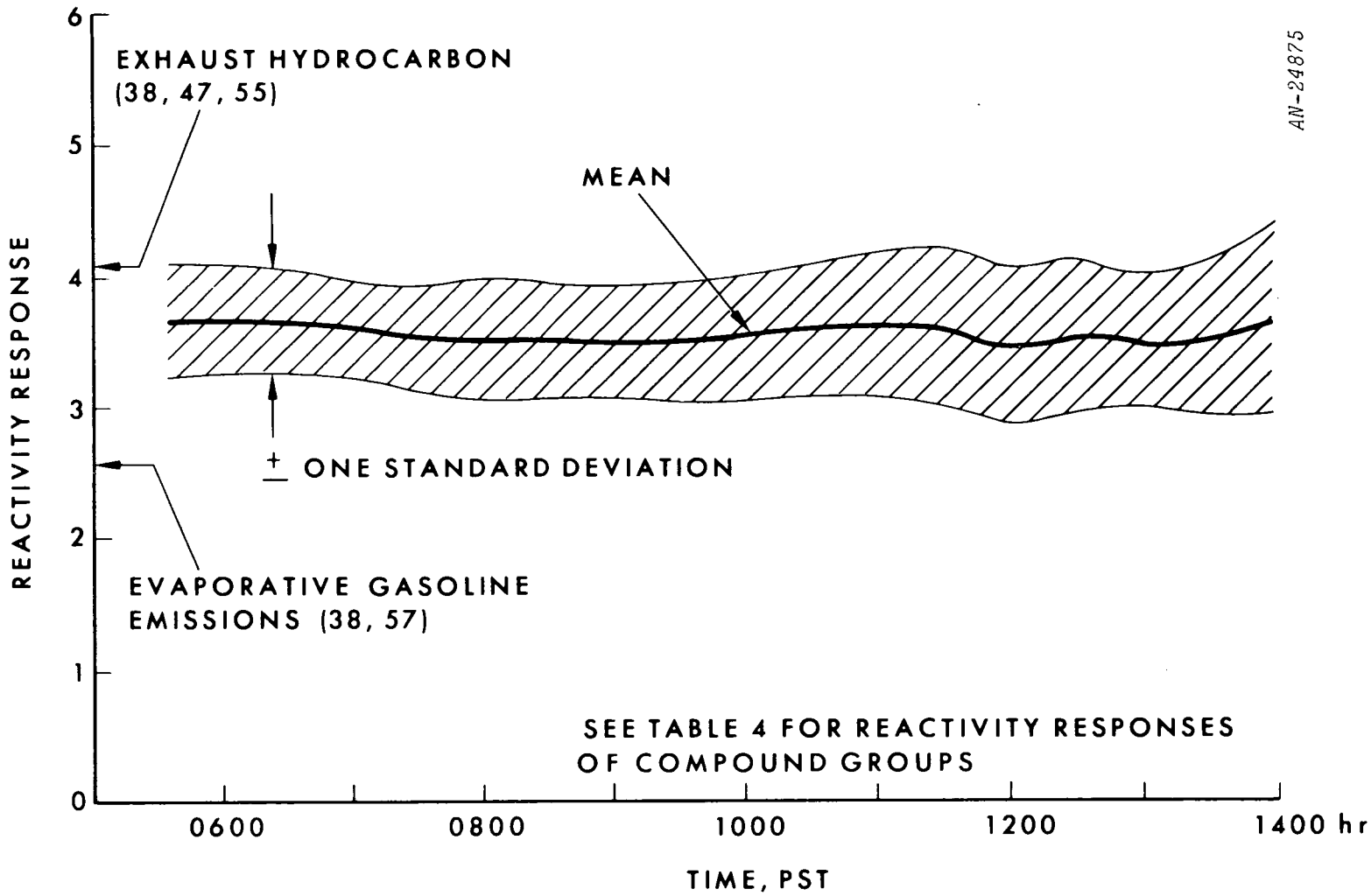

Figure 12. Average Reactivity History for Commerce, 1969: Biological Effects and Product Formation Scale from Altshuller (54)

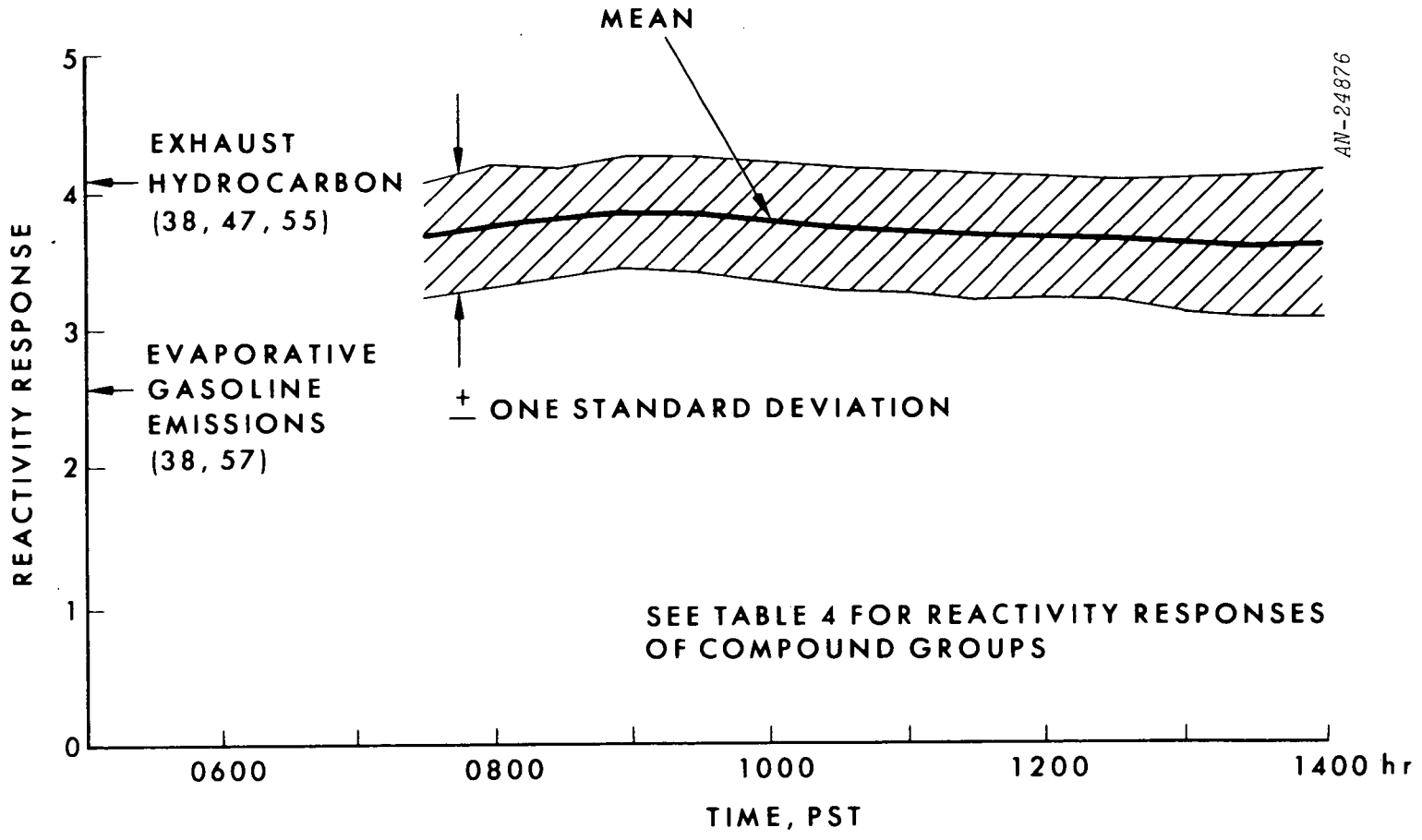

Figure 13. Average Reactivity History for El Monte, 1969: Biological Effects and Product Formation Scale from Altshuller (54)

(in contrast with the hydrocarbon consumption scale results); however, the relative flatness in the average curves and the tightly grouped data that generate the curves still prevail. Consequently, both on the basis of hydrocarbon consumption and of biological effects, we can begin to approach the atmospheric kinetics problem with a single lumped hydrocarbon. Prior to incorporating this in the diffusion model, the properties of the governing equations will be examined and an efficient numerical solution method will be described in the next section.

III. THE ATMOSPHERIC MODEL AND ITS NUMERICAL SOLUTION

A. THE GOVERNING EQUATIONS

Having a simplified chemical scheme, we now turn our attention to incorporating it in an atmospheric transport model. We have sought approximations appropriate to air basins subject to photochemical pollution. Because of the severity of the problem and the availability of data, the Los Angeles basin area serves as the object of validation studies.

Probably the most characteristic causative factor in Los Angeles smog is the lid created by the stagnation of warm air subsiding on the cool marine layer. Late in the summer, air flows from an anticyclone over the Pacific Ocean and compresses as it loses altitude in its outward course. Onshore movement of marine air under this outflow maintains a buoyantly stable interface at the base of the elevated inversion which is marked by a temperature increase with height. Sometimes this inversion base starts out at ground level in the morning. This condition, which is chronic and of large scale, should not be confused with the transient inversions due to nocturnal radiative cooling.

The regularity exhibited by this phenomenon holds the key to extensive reduction in atmospheric model detail. As mentioned in the introduction, the relatively thin (marine) layer between the ground and the inversion base contains the bulk of the pollutants. The diurnal horizontal flow patterns within the marine layer are almost reproducible from day to day of the smog season. Periodic variations in height (above land) are experienced by the elevated inversion base over any given day.

Some of the best detailed data illustrating these points are found in a report by Neiburger and Edinger (61). A subsequent report (62) in the same series has some graphs which associate smog events with the meteorological conditions.

The entire picture described above strongly suggests that we make a marine layer model with a prescribed internal flow field. The top of the layer is nearly as wall-like as the bottom because vertical disturbances are strongly resisted by buoyant forces. Therefore, very little Reynolds stress momentum transfer occurs across the interface just as there is almost no normal transport of species (a property with which Angelenos are very familiar).

For the species budget along a streamtube in the marine layer, we assume a channel-like flow with zero flux through the top "wall" and some specified flux from the ground. In choosing boundary conditions for the balance equations governing free radicals, we are confronted with the usual uncertainties regarding wall catalycity. Computational tests ranging from infinite to zero catalytic efficiency for removal of oxygen atoms and RO_2 result in unimportant differences at instrument elevations of several meters because the radicals achieve steady state much faster than they diffuse over several meters.

The governing species equation is taken to be

$$\frac{\partial c}{\partial t} + u \frac{\partial c}{\partial x} = \frac{\partial}{\partial z} \left(D \frac{\partial c}{\partial z} \right) + R \tag{19}$$

where c = mass concentration

t = time

u = wind speed

x = downwind distance

z = height above ground

D = vertical turbulent diffusion coefficient

R = production rate

Mean vertical advection is suppressed by the channel-like character of the marine layer and horizontal diffusion is relatively unimportant because of a nearly uniform distribution of emission sources. Hence these terms do not appear in Eq. 19. The chemical source term is calculated from the usual rate expressions.

Since a significant period following sunrise on a high smog day has little wind, much is to be learned by omitting the second term and studying slab solutions of the heat-equation-with-sources form. As will be summarized in a later section, this was the first approach that we followed (63) to extend laboratory data on kinetics to the atmosphere. The problem without advection (second term, Eq. 19) was solved using the Crank-Nicolson technique (64). To test advection and diffusion without chemistry, we modeled carbon monoxide only using Eq. 19 with $R = 0$. Using Eulerian (ground-fixed) coordinates, the complete equation with the simple chemistry ran a minute of CDC 6400 time for each minute of real time that was simulated. This was considered to be unacceptable.*

*Slow computation resulted for the ten-cell test case because of the chemistry. It also had artificial diffusion which is an error from numerical differencing of the equation. It produces effects that resemble physical diffusion in the x-direction.

We also use a restricted form of Eq. 19 for the kinetics studies described in the previous section. Smog chamber analyses use just the first and last terms so that they depend on ordinary differential equations. These are solutions which describe the time-dependent behavior of a homogeneous gas mixture. We used standard Runge-Kutta techniques to solve them at the outset of the work, but as will be shown here, adaptations of Padé approximants have been employed to improve computational efficiency.

The combined needs for computing efficiency and meteorological realism have been met by improvements described in this section. The first two subsections describe the incorporation of a classical approximation method into our numerical integration. The implementation of these computing techniques strengthen the study by allowing numerous modeling trials on both laboratory and atmospheric cases. The final subsection outlines the change from Eulerian to semi-Lagrangian coordinates in the meteorological formulation. By following air masses, we use a natural coordinate system thereby eliminating the artificial diffusion errors.

B. APPLICATION OF PADÉ APPROXIMANTS TO SMOG CHAMBER CALCULATIONS

The chemical model previously described is implemented in rate equations which must be integrated numerically. Because of the widely varying reaction rates, the equations possess a characteristic known as "stiffness" which makes their integration difficult. In the interest of economy and accuracy, special techniques must be employed in obtaining

a solution. Below we describe a method which utilizes Padé approximants (65, 66). For these ordinary differential equations, the procedure has yielded significant speed improvements over the Runge-Kutta method previously used.

For this class of problem, the implicit approach is the basic advantage of the new method, thus guaranteeing stability. Consequently, accuracy controls step size. This provides the principal gain in computing time.

The rudiments of the integration method are twofold. One involves a linearization of the nonlinear chemical term at every step; the other an approximation of the exponential term that appears as a result of the linearization operation. Thus, consider the following system of equations that describe the changes in species concentration due to chemical reaction:

$$\frac{dc}{dt} = R(c) \tag{20}$$

where c = vector of species concentrations

$R(c)$ = vector of chemical reaction rate functions

$$c = \begin{bmatrix} c_1 \\ c_2 \\ \cdot \\ \cdot \\ \cdot \\ c_s \end{bmatrix} \qquad R(c) = \begin{bmatrix} R_1(c) \\ R_2(c) \\ \cdot \\ \cdot \\ \cdot \\ R_s(c) \end{bmatrix}$$

s = number of chemical species

To linearize the rate vector $R(c)$, we expand it about c_o in a Taylor series. The subscript "o" denotes evaluation at some time $t = t_o$. Thus

$$R(c) = R(c_o) + J(c - c_o) + O(\Delta c)^2 \tag{21}$$

where

$$J = \left[\frac{\partial R_i}{\partial c_j}\right] \qquad i,j = 1, 2, \ldots, s$$

is the matrix of order $(s \times s)$ of first derivatives (the Jacobian matrix) of the rate function. Substituting Eq. 21 into Eq. 20 yields

$$\frac{dc}{dt} = Jc + B \tag{22}$$

where $B = R(c_o) - Jc_o$. It should be noted that at time $t = t_o$, the quantities c_o, $R(c_o)$, and J are known. Hence, the matrix differential equation (Eq. 22) is a linear equation with constant coefficients and a constant forcing function. Its formal solution is, therefore,

$$c(t) = e^{J\Delta t}\left[c_o + J^{-1}B\right] - J^{-1}B \tag{23}$$

where J^{-1} denotes the inverse (or reciprocal) of the matrix J.

An approximate solution of Eq. 22 is obtained from Eq. 23 by suitably approximating the matrix exponential $e^{J\Delta t}$. This is accomplished by means of the Padé approximants of the exponential function. These Padé approximants are rational function of the form

$$e^{J\Delta t} \simeq \frac{P(J\Delta t)}{Q(J\Delta t)} = Q^{-1}P \tag{24}$$

where $P(J\Delta t)$ and $Q(J\Delta t)$ are matrix polynomials of degree p and q, respectively. They are defined by

$$P = \sum_{k=0}^{p} \frac{(p + q - k)!p!}{(p + q)!k!(p - k)!} (J\Delta t)^k \tag{25a}$$

$$Q = \sum_{k=0}^{q} \frac{(p + q - k)!q!}{(p + q)!k!(q - k)!} (-J\Delta t)^k \tag{25b}$$

Thus, substituting Eq. 24 into Eq. 23, we obtain

$$c(t) = Q^{-1}P \left[c_o + J^{-1}B \right] - J^{-1}B \tag{26}$$

The choices $p = q = 1$ and $p = q = 2$ are especially useful. The former yields a third-order integration formula, the latter a fifth-order formula. As an example, for $p = q = 1$ we obtain from Eq. 25:

$$P = I + 1/2\ J\Delta t \quad \text{and} \quad Q = I - 1/2\ J\Delta t \tag{27}$$

where I is the identify matrix. Substituting Eq. 27 into Eq. 26 yields, after the appropriate manipulations,

$$c(t) = c_o + [I - 1/2\ J\Delta t]^{-1}\Delta t R(c_o) \tag{28}$$

Equation 28 has a form that is especially well-suited for digital computation. Note that the process requires at every time step: (1) the evaluation of $R(c)$ and J, and (2) the inversion of the matrix Q.

The latter is by far the more computationally costly of the two requirements. In our case, the number of species determines the size of the matrix to be inverted. Since this number is not large in our model, the matrix inversion poses no special problems. Fortunately, the number of species is usually smaller than the number of reactions.

Table 5 shows examples of the gains obtained using the new computational scheme. The typical real-time/computer-time ratio was increased from 36/1 to 180/1. Perhaps more significant is the fact that the Padé method has allowed us to obtain acceptable solutions in situations where Runge-Kutta either failed to converge or produced spurious solutions. One such instance is the integration of full differential equations for the free-radical species: the Padé method successfully computed solutions without algebraic substitution of stationary-state assumptions, whereas Runge-Kutta failed to produce any solution.

TABLE 5

CDC 6400 CENTRAL PROCESSOR TIMES TO RUN
C_3H_6 + NO + $h\nu$ CHAMBER EXPERIMENT SIMULATION

Type of Run	Runge-Kutta	Padé Approximant
Rapidly changing free radical concentration	2400 seconds	122 seconds
Typical run for 150 minutes real time	250 seconds	50 seconds
Run which diverged for Runge-Kutta	267 seconds (diverged at 80 minutes, real time)	50 seconds (ran to completion, 150 minutes real time)

As mentioned previously, the step size must still be controlled in order to preserve accuracy. Referring to Eq. 21 we can see that the difference $\Delta c = c - c_o$ determines the order of the truncation error of the linearization operation. The step size must be constrained so that Δc will remain within some bound specified by the user. Our codes contain a variable-step-size feature which ensures that Δc will stay within the prescribed bounds.

It should also be noted that the nature of our chemical model is such that it leads to a very good first-order approximation as indicated in Eq. 21. This occurs because the full expansion of our particular rate function, $R(c)$, contains only three terms. Hence in the first-order approximation only one term has been dropped from the expansion.

C. APPLICATION OF PADÉ APPROXIMANTS TO THE ATMOSPHERIC MODEL EQUATION

We now describe the use of Padé techniques to solve the diffusion equation with chemical reactions. The equation in question is referred to a moving air mass. Use of the Lagrangian approach* eliminates the second term in Eq. 19 which is reduced to

$$\frac{\partial c}{\partial t} = \frac{\partial}{\partial z}\left(D \frac{\partial c}{\partial z}\right) + R(c) \tag{29}$$

where D is the vertical diffusion coefficient and c and $R(c)$ have been defined previously. Applying the "method of lines" to Eq. 29, the

---

* The Lagrangian approach we use is a moving air parcel with vertical nonuniformity due to finite rate diffusion. It is introduced by schematic description in Sec. I D.

partial differential equation is transformed into an ordinary differential equation for a line describes the concentration changes for a fluid mass moving along the line. The equation for the ith line is derived from Eq. 29 to give

$$\frac{dc_i}{dt} = \frac{D}{(\Delta z)^2} \left[c_{i-1} - 2c_i + c_{i+1}\right] + R_i \tag{30}$$

where $R_i = R(c_i)$, $i = 1, 2, \ldots, M$, where M is the number of mesh points from the ground up to the mixing depth. The symbol c_i defines a vector of s species at the ith point in space. Similarly, R_i defines a vector of s rate functions at the ith mesh point. Thus,

$$c_i = \begin{bmatrix} c_{1i} \\ c_{2i} \\ \cdot \\ \cdot \\ \cdot \\ c_{si} \end{bmatrix} , \qquad R_i = \begin{bmatrix} R_{1i} \\ R_{2i} \\ \cdot \\ \cdot \\ \cdot \\ R_{si} \end{bmatrix}$$

In order to solve Eq. 30 by the Padé method, R_i is linearized as in Eq. 21 to yield

$$R_i = R_{io} + J_i(c_i - c_{io}) + O(\Delta c_i)^2 \tag{31}$$

where the zero subscript again denotes evaluation at time $t = t_o$, and J_i is the Jacobian matrix of the rate function at the ith spatial mesh point. Substituting Eq. 31 into Eq. 30 yields

$$\frac{dc_i}{dt} = \lambda[c_{i-1} - 2c_i + c_{i+1}] + J_i(c_i - c_{io}) + R_{io} \tag{32}$$

where $\lambda = D/(\Delta z)^2$. Writing Eq. 32 more compactly we obtain, after collecting terms,

$$\frac{dC}{dt} = (\lambda A + J)C + R_o - JC_o$$

$$\frac{dC}{dt} = HC + B \tag{33}$$

where $H = \lambda A + J$, $B = R_o - JC_o$, and

$$C = \begin{bmatrix} c_1 \\ c_2 \\ \cdot \\ \cdot \\ \cdot \\ \cdot \\ c_M \end{bmatrix} \qquad A = \begin{bmatrix} -2I & I & 0 & \cdot & \cdot & \cdot & 0 \\ I & -2I & I & \cdot & \cdot & \cdot & 0 \\ 0 & I & -2I & I & \cdot & \cdot & 0 \\ \cdot & & & & & & \cdot \\ \cdot & & & & & & \cdot \\ \cdot & & & & & & \cdot \\ \cdot & \cdot & \cdot & \cdot & \cdot & I & -2I \end{bmatrix}$$

$$J = \begin{bmatrix} J_1 & & & & \\ & J_2 & & \bigcirc & \\ & & \cdot & & \\ & & & \cdot & \\ & \bigcirc & & & \cdot \\ & & & & J_M \end{bmatrix} \qquad R_o = \begin{bmatrix} R_{1o} \\ R_{2o} \\ \cdot \\ \cdot \\ \cdot \\ \cdot \\ R_{Mo} \end{bmatrix}$$

Equation 33 now has the same form as Eq. 22 and its formal solution is thus analogous to Eq. 23. Hence

$$C(t) = e^{H\Delta t}\left[C_o + H^{-1}B\right] - H^{-1}B \tag{34}$$

Approximating the exponential by

$$e^{H\Delta t} \simeq \frac{I + 1/2\ H\Delta t}{I - 1/2\ H\Delta t} = \frac{P}{Q} = Q^{-1}P$$

and substituting in Eq. 34 and simplifying we obtain

$$C = C_o + Q^{-1}G_o\Delta t \tag{35}$$

where

$$G_o = \lambda AC_o + R_o$$

It should be noted that any boundary conditions are implicitly contained in Eq. 35.

Equation 35, which is the analog of Eq. 28, may appear to be simple, but the inversion of Q poses some problems arising from its dimensions. H is an $(M \times M)$ matrix each one of whose entries is an $(s \times s)$ matrix. Hence Q is an $(sM \times sM)$ matrix, and its storage as well as its inversion may be difficult. For example, if we have 10 species ($s = 10$) and 10 space grid points ($M = 10$) then Q is (100×100) and requires rather long computing times as well as large amounts of core storage. However,

we take advantage of the structure of Q to develop an algorithm that reduces the problem to the inversion of M matrices of size $(s \times s)$.

It is noted that since J is a diagonal matrix and A is tridiagonal, then H is tridiagonal. Moreover, the off-diagonal entries of H are identity matrices. Forming Q we have

$$Q = I - 1/2\, H\Delta t$$

and it is apparent that Q is tridiagonal, its off-diagonal entries being identity matrices also. Thus only the M diagonal entries of Q need be stored, thereby reducing memory requirements to Ms^2 cells compared to the maximum of M^2s^2. Writing Eq. 35 in the form,

$$QC = QC_o = G_o\Delta t$$

we note that the tridiagonal property of Q allows us to solve for C without explicitly inverting Q. This simplification is afforded by an extended form of Gaussian elimination (64) which requires the inversion of M matrices of size $(s \times s)$. This is preferable to inverting the full $(sM \times sM)$ matrix.

Note that we can also take advantage of the fact that the off-diagonal elements of Q are identity matrices to reduce the amount of computation.

Because series are truncated in these approximations, some remarks about the resultant errors are necessary. The order of the

truncation error of the solution is $O(\Delta t)^3$. This occurs because the approximation of the exponential is

$$e^{H\Delta t} \simeq \frac{I + 1/2\ H\Delta t}{I - 1/2\ H\Delta t}$$

Also, as in the solution of the chemical rate equations, a linearization error of order $O(\Delta C)^2$ appears in the approximate solution. Thus, the same precautions that were taken to preserve accuracy in solving the ordinary chemical rate equations are required in the solution of the atmospheric model equation.

The new scheme has yielded a better than fourfold increase in the real-time/computer-time ratio, i.e., from 7/1 to 30/1. A more detailed description is given in a separate report by Martinez (67).

D. METEOROLOGICAL REFORMULATION OF MODEL

Long computer runs and unacceptable error propagation hampered the operation of the earlier time-dependent advection and kinetics (TADKIN) code (63). Its application was limited to an analysis of carbon monoxide to examine the influence of advection added to that of vertical diffusion. At the inception of the present work, these severe limitations dictated a reformulation of the advective description before any atmospheric runs were attempted. Combined with the mathematical advances just described, the semi-Lagrangian embodiment of the diffusion with kinetics (DIFKIN) code extends the application of photochemical diffusion modeling to a great many more cases than previously thought practicable.

Following a center-of-mass fixed coordinate system tied to an air mass, we make use of intrinsic coordinates to avoid artificial diffusion in the horizontal direction. Physical diffusion, therefore, is distinct and identifiable because the moving control volume can be allowed to undergo mass exchange with a neighboring air mass in a prescribed fashion. The question of horizontal spatial resolution is answered by a selection of source grid size and the vertical resolution is set by the choice of the interval size in the z-direction.

Mixing depth or vertical extent of the pollution layer can be handled in one of two ways. In the first, the vertical diffusion coefficient is assigned spatially and temporally dependent values according to the combined effects of shear and buoyancy as turbulent energy sources. The vertical extent of the grid is chosen far above the conventional mixing depth so that the pollutants are automatically confined vertically to a degree which depends on the diffusion coefficient profile. In the second way of specifying the vertical behavior, however, the vertical grid either continuously adjusts to the input values of mixing depth or assumes an average value for the inversion base altitude. We have favored the use of this second approach because it limits the field of computation to the polluted region and thereby conserves computer time. A zero-flux boundary condition is imposed at the top of the net.

The next section summaries both the early validations and the results in testing the improvements we attempted in the chemical, mathematical, and meteorological aspects of the problem. Indeed, many times

it appeared that the earlier simple concepts gave better results, but working with better data and more demanding theoretical descriptions than before, we uncovered some significant areas for further investigations.

IV. THE EXERCISE AND VALIDATION OF THE MODEL

A. OBJECTIVES OF THE TESTS

With the development of a more complete chemical model than the previous one, the mathematical and meteorological improvements offset the potential computing slowdowns due to added reactions. Having described these advances in technique, we turn now to the task of subjecting the model to validation tests. Huntington Park is the site of the earlier validation, but El Monte is the station of interest in the recent work. El Monte is closer to the edge of the urbanized areas than Huntington Park or Commerce, and is, therefore, likely to show larger random fluctuations of pollutant concentrations. In view of the variability of wind directions, this is expected because the air over El Monte may have originated from either high or low pollution areas (see Figs. 15-18). Hence the accuracy of the initial conditions for the test calculation may be as important as the accuracy of the flux boundary conditions. In this section we will examine sources of data, validation tests with simple chemistry and stagnant conditions, and validation tests with complex chemistry and advection from one station to another.

B. SOURCES OF DATA

1. Input Information

Except for initial profiles, the input data for the model are the meteorological conditions and the source emission conditions. Wind speed and diffusion coefficients depend on both position and time. Source

inventories include the flux of each primary pollutant as it depends upon location in the basin and time of day.

Empirical parameters governing atmospheric dispersal pervade the literature on this subject. Like most cases of turbulent transport, elimination of a disposable coefficient in one place leads to a reappearance of one somewhere else. The present work uses an experimentally determined turbulent diffusion coefficient, D, in Eq. 19. Near the ground and near the inversion base we must assign a height (z) dependence to the diffusion coefficient.

Going up from the ground, the functional dependence assumed for D upon z allows a linear increase to some constant value. At intermediate levels, D is held constant, but approaching the inversion base a linear decrease with height is assumed. A variation on the lower part of the profile has been to maintain the ground value up to some point prior to initiating the linear increase. This variation causes little change from the original trapezoidal profile. The elevation where constancy is achieved varies from 40 to 100 meters depending upon meteorological conditions.

Figure 14 shows typical values of the turbulent diffusion coefficient we assumed for our model compared with the values either derived or observed by other investigators. At a wind speed of 1 m/s, a surface value of 30 m^2/min is high compared with Pasquill's (68) values at 200 centimeters elevation, but we use it because effective roughness in an

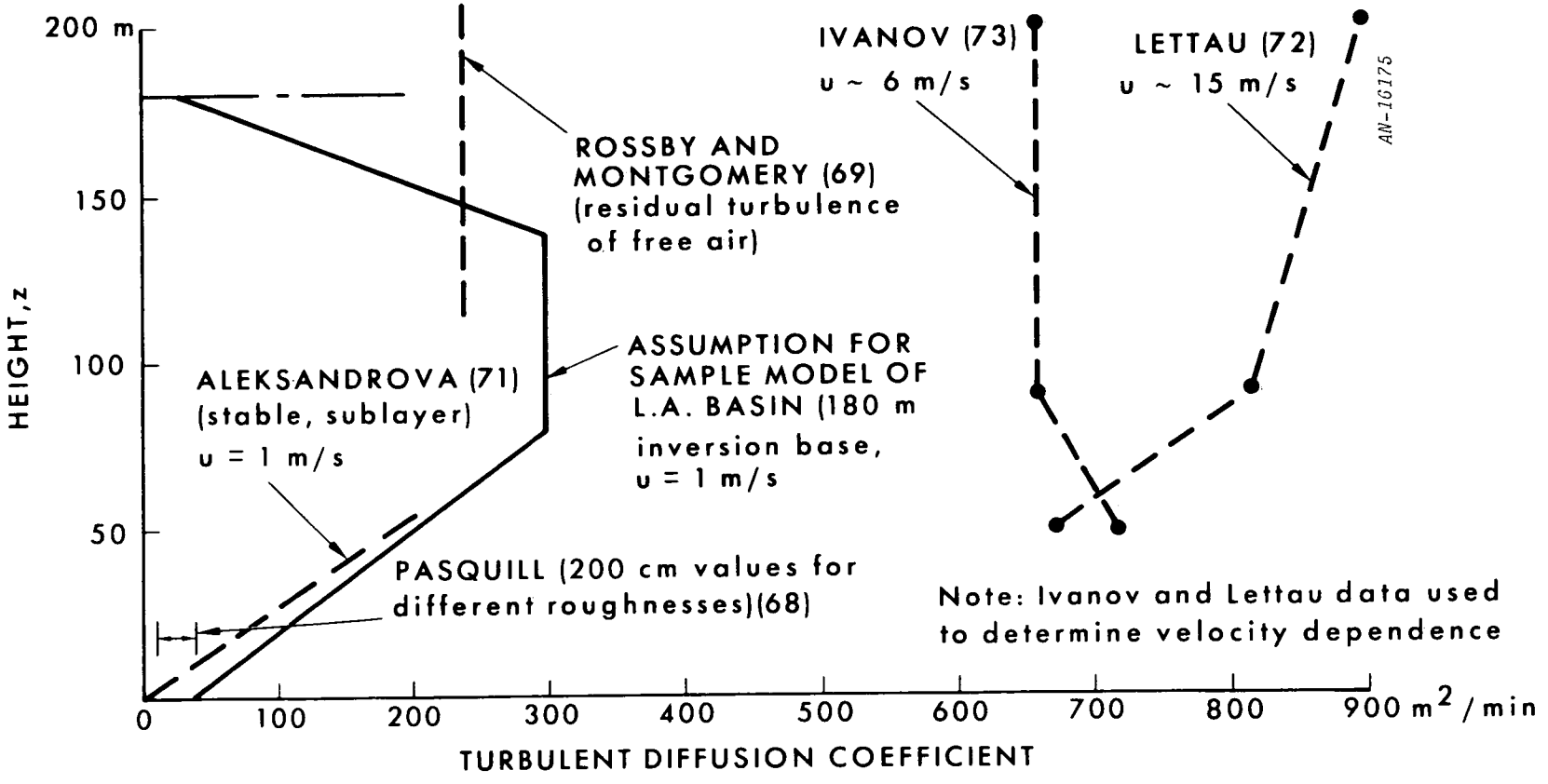

Figure 14. Variations of Diffusivity with Height for Different Average Wind Speeds

urban area far exceed those of "mud flats" or "high grass." The assigned plateau value is slightly higher than that for the residual turbulence of free air attributed to Rossby and Montgomery (69) in Priestley's monograph (70). The decrease approaching the inversion base is introduced to reflect the wall-like inhibition of vertical turbulent motion by buoyant stability.

Note on Fig. 14 that the sublayer region corresponds closely to the values deduced from Aleksandrova's formulas and mast measurements for the precipitation of a puff released from a point source (71). The values reported by Lettau (72) (as "Austausch" coefficients) were obtained from Leipzig wind profile measurements. The data of Ivanov (73) for mean square velocity and dissipation rate were used in Hanna's (74) empirical formula to obtain the 6 m/s values. Neither the Ivanov nor the Lettau results were obtained for stable lapse conditions. The assumed values for the coefficient correspond closely to the turbulent transport observed by Craig (75), who measured water vapor profiles 30 miles offshore as warm air moved seaward across Massachusetts Bay. For light winds, values of 6 to 12 m^2/min were observed at elevations of 1 to 2 meters. At 60 to 80 meters elevation, diffusion coefficients up to 300 m^2/min were found with 6-m/s wind speeds with reduced stability. The plateau value in our profile, therefore, may be expected to vary with wind speed approximately like $50(u+5)$ m^2/min where u is in m/s . This simple relationship has been employed based on the cited findings. Other sources of diffusion coefficient data (76, 77, 78) that are not plotted on Fig. 14 give values which are consistent with those shown.

Wind speed, wind direction and inversion base height are the principal meteorological inputs. Wind data are obtained from Scott Research Laboratories (SRL) measurements (51, 52) and from other observation stations in the area. Inversion data are deduced from airborne temperature measurements (51, 52) where possible and from morning soundings reported (79) by the Los Angeles County Air Pollution Control District (LAAPCD). Some wind data from the district's files have also been employed.

As an example of the preparation of windfield inputs from the station data, let us examine the results for one morning in the Los Angeles basin. The advection patterns are obtained by taking a weighted average of wind-station readings surrounding the point in question. This is truly a receptor-oriented modeling approach, since the trajectories are constructed in hourly upwind segments from the measuring station. Reciprocal distance weighting is employed because of the dominant plane flow pattern which is governed by combinations of sources, sinks, or vortices.* In most cases the three nearest neighbor stations are included in the stepwise upwind tracing or air movement, but occasionally conditions of proximity suggest including only the nearest one or two stations where coastal crossings are involved in the analysis.

Figures 15, 16, 17 and 18 show examples of the paths of air masses estimated in the manner just described. The times of arrival in El Monte are used to identify each trajectory in any subsequent references in this report. The date of September 29, 1969, is chosen because of the rich

*See Sec. I D for a discussion of characteristic scale sizes.

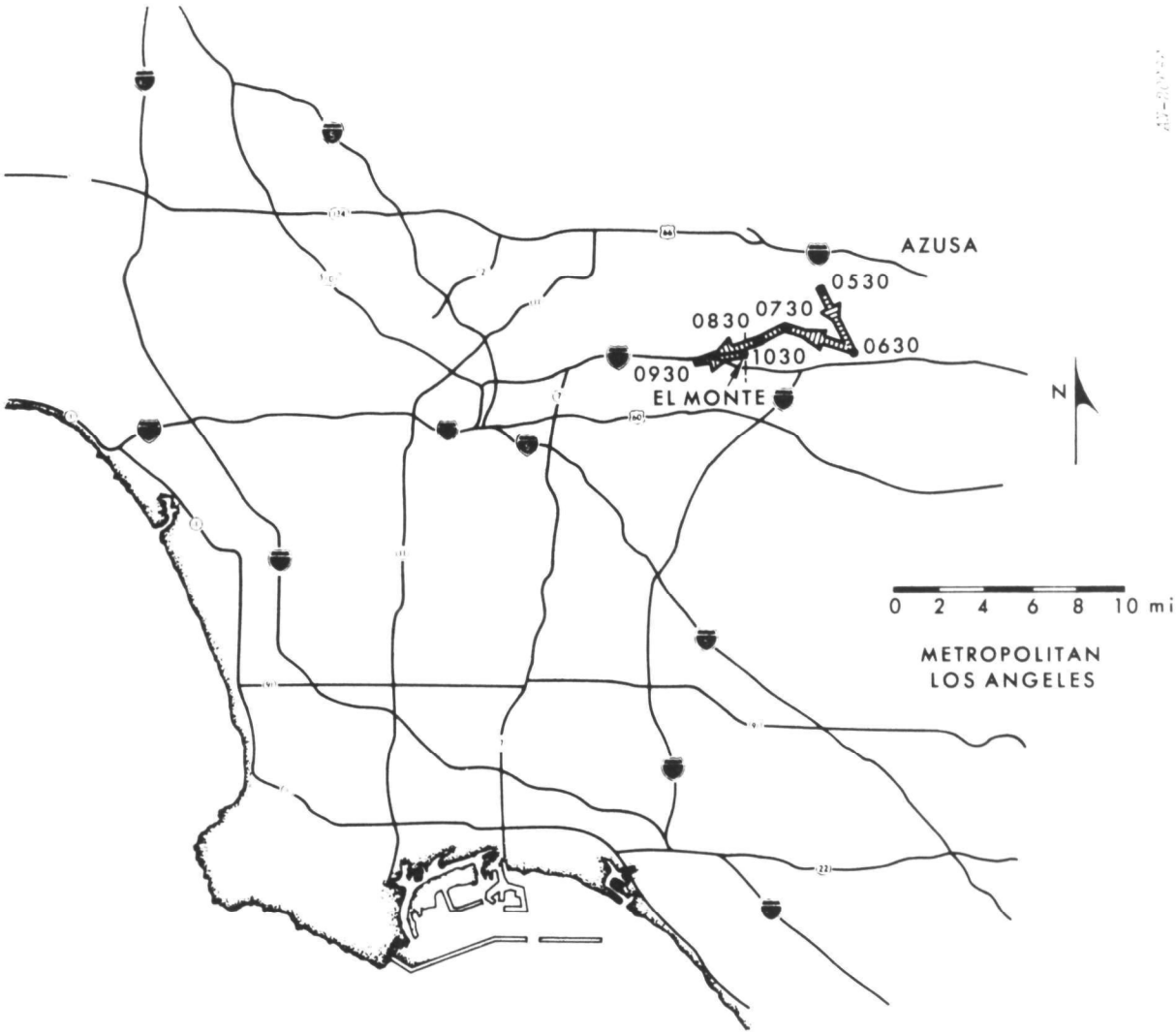

Figure 15. Estimated Trajectory of Air Mass Arriving at El Monte, 1030 hours, 29 Sept. 1969

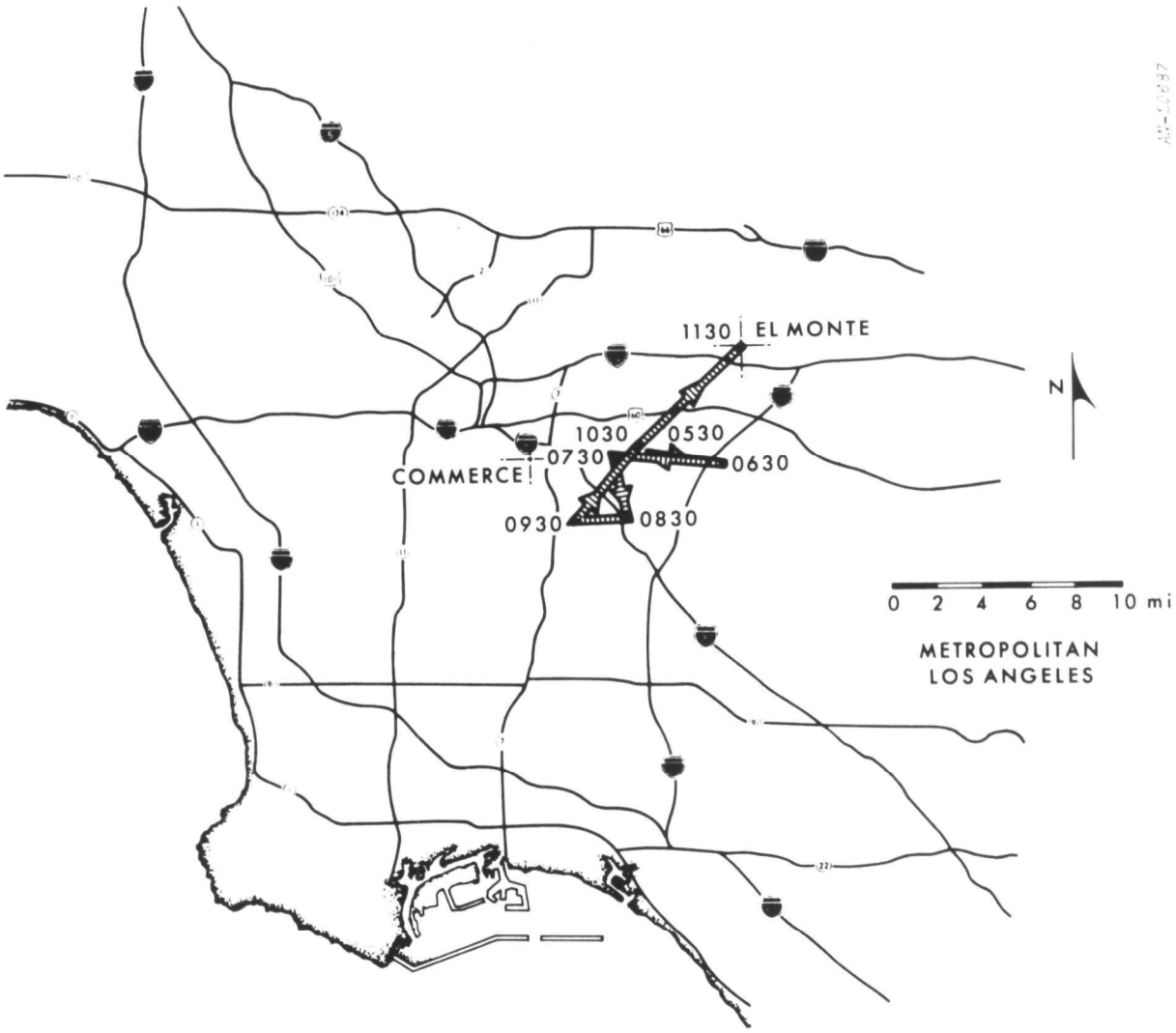

Figure 16. Estimated Trajectory of Air Mass Arriving at El Monte, 1130 hours, 29 Sept. 1969

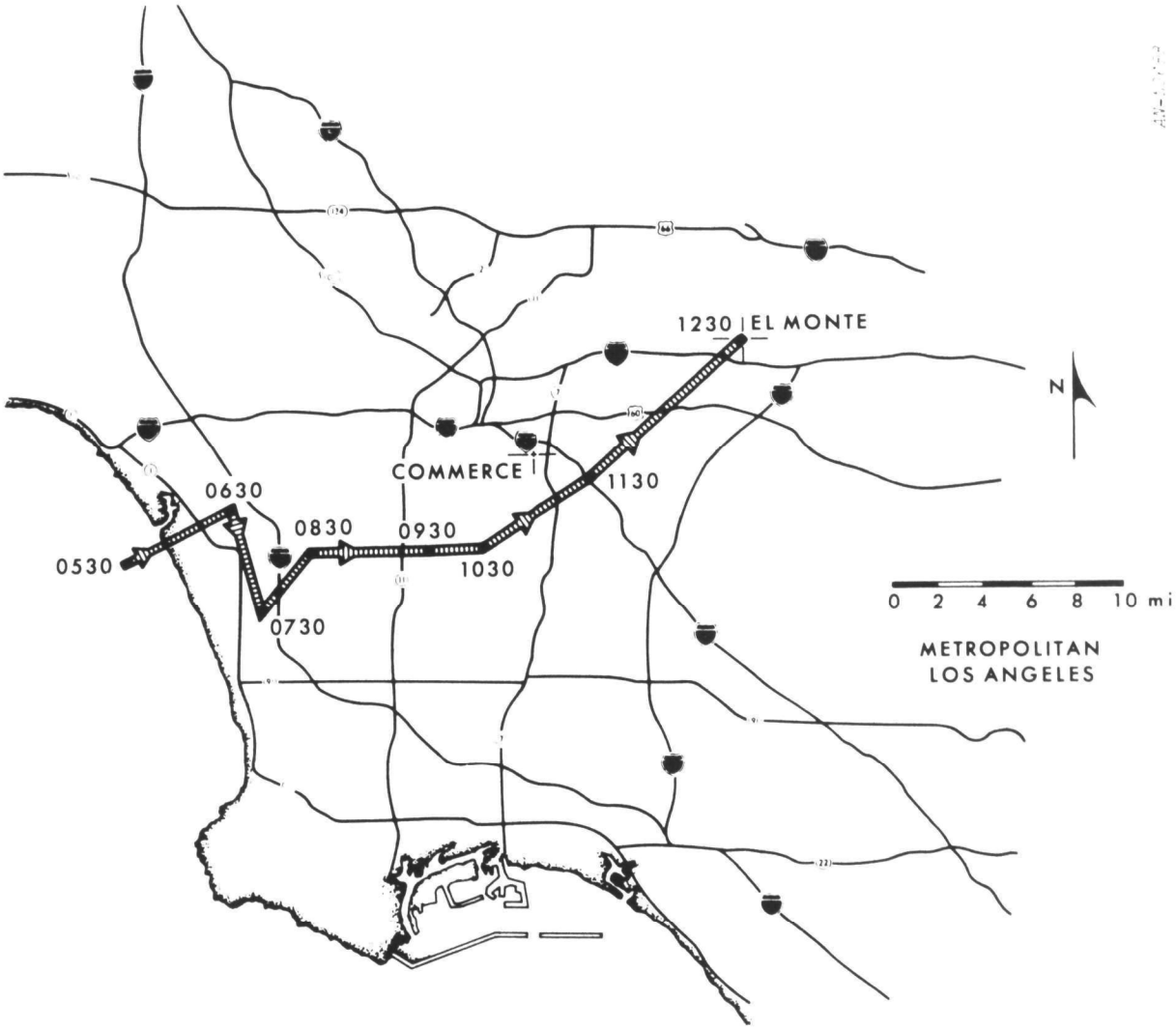

Figure 17. Estimated Trajectory of Air Mass Arriving at El Monte, 1230 hours, 29 Sept. 1969

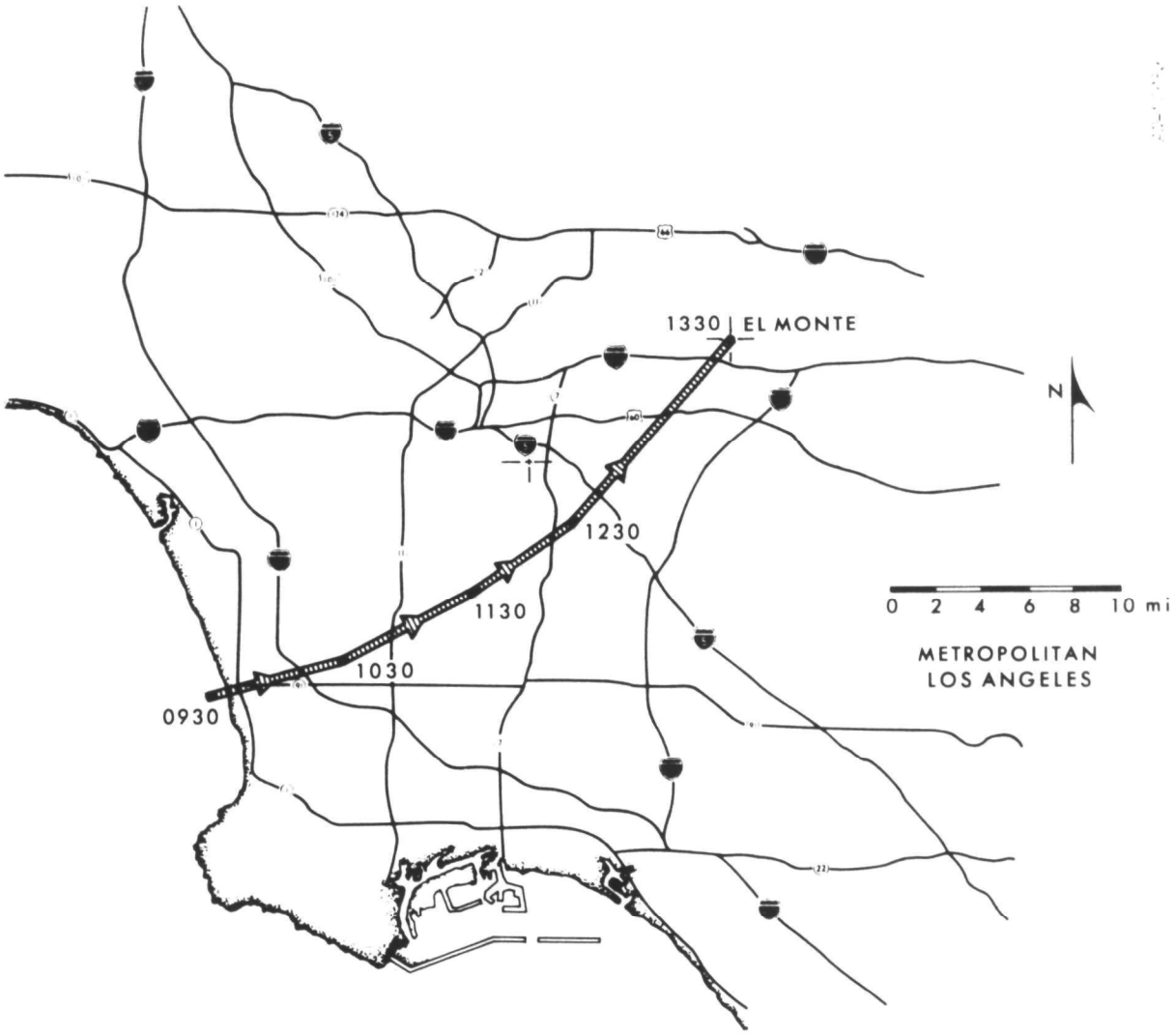

Figure 18. Estimated Trajectory of Air Mass Arriving at El Monte, 1330 hours, 29 Sept. 1969

variety of data that we have available for that day. Note that the earlier morning meandering patterns give way to the dominant onshore flows for all trajectories after 0800 to 0900 hours Pacific Standard Time. The meteorological formulation that we have adopted takes the time and location information from these trajectories to establish the initial conditions and the boundary conditions. Initial conditions are specified as vertical profiles of concentration and boundary conditions as time histories of surface-based pollutant emissions. Of course, these trajectories are not used in the validation tests of the slab model. They are employed to test the moving air parcel model.

Using this approach with data from the two monitoring sites, we are able to match the computing requirements to the data base. Little justification exists at this time to apply complicated grid methods to these validation studies because we only have measurements in great detail from Commerce and El Monte. Just as overly-elaborate chemical models cannot be adequately tested in the atmosphere, neither can highly complex diffusional and atmospheric formulations be checked out with our present store of field observations. Certainly, the day will come when frequent high-resolution readings are made and some of the more detailed theories can be tested.

Even more difficult than the meteorological inputs are those for surface emission fluxes of hydrocarbon, nitric oxide and carbon monoxide species. Originally we did a simple statistical estimate on moving sources based on the California Driving Cycle for a velocity distribution

function and a packing density based on a car length spacing for every ten miles per hour speed for all the arterials and freeways in the basin. Although we arrived at surprisingly realistic values for tonnages of emission and total cars on the road, we switched to LAAPCD inventory estimates (80) when they became available. Table 6 summarizes some of the totals from this official publication. Since tons per day are given, one can compute average surface fluxes, knowing that the basin comprises some 1250 mi^2 according to the same publication.

TABLE 6

CONTAMINANTS IN TONS PER DAY
FROM MAJOR SOURCES WITHIN LOS ANGELES COUNTY IN 1968 (80)

Major Source	Organic Gases			Particulates	NO_x	SO_2	CO	Total
	Reactivity							
	High	Low	Total					
Motor Vehicle	1255	475	1730	45	645	30	9470	11,920
Non-Motor Vehicle	200	620	820	55	305	195	225	1,610
Total	1455	1095	2550	110	950	225	9695	13,530

Additional adjustments must be made for the fact that the source emission strengths are not uniformly distributed in either time or space.

To approximate the automotive sources we used the data reported for the geographical (see Fig. 19) and the temporal (see Fig. 20) distributions. For nonautomotive sources, averages were employed as constant background emissions. The tonnage partitioning between high-reactivity and low-reactivity hydrocarbons from automotive sources roughly represents the ratio of compounds having nonzero reactivity index to those having a zero value in automotive emissions.

Although the source distribution data in Figs. 19 and 20 are nearly twenty years old, they were the best available at the time of the early validation studies. Of course, the tonnages used were from 1968 and they were distributed according to Figs. 19 and 20. For the more recent validation runs involving air trajectories, we used the source distributions developed by the group at Systems Applications, Inc. under the direction of Dr. P. M. Roth. Figures 21 and 22 were adapted from their report (82). Maps for surface street traffic and for stationary sources were also given, but Fig. 21 (for freeways) typifies the data as displayed on a two-mile grid. To get emissions from mileages, we used emission factors based on weighted averages of various model years according to the method of Ref. 83. The weighting factors come from vehicle age distributions.

2. Validation Information

With the atmospheric and emission source inputs, we test the model by predicting time histories of the concentration field in the marine layer. The predictions are then evaluated against a background of validation data. The primary sources of these data are the SRL reports (51, 52) for the 1968-1969 smog seasons.

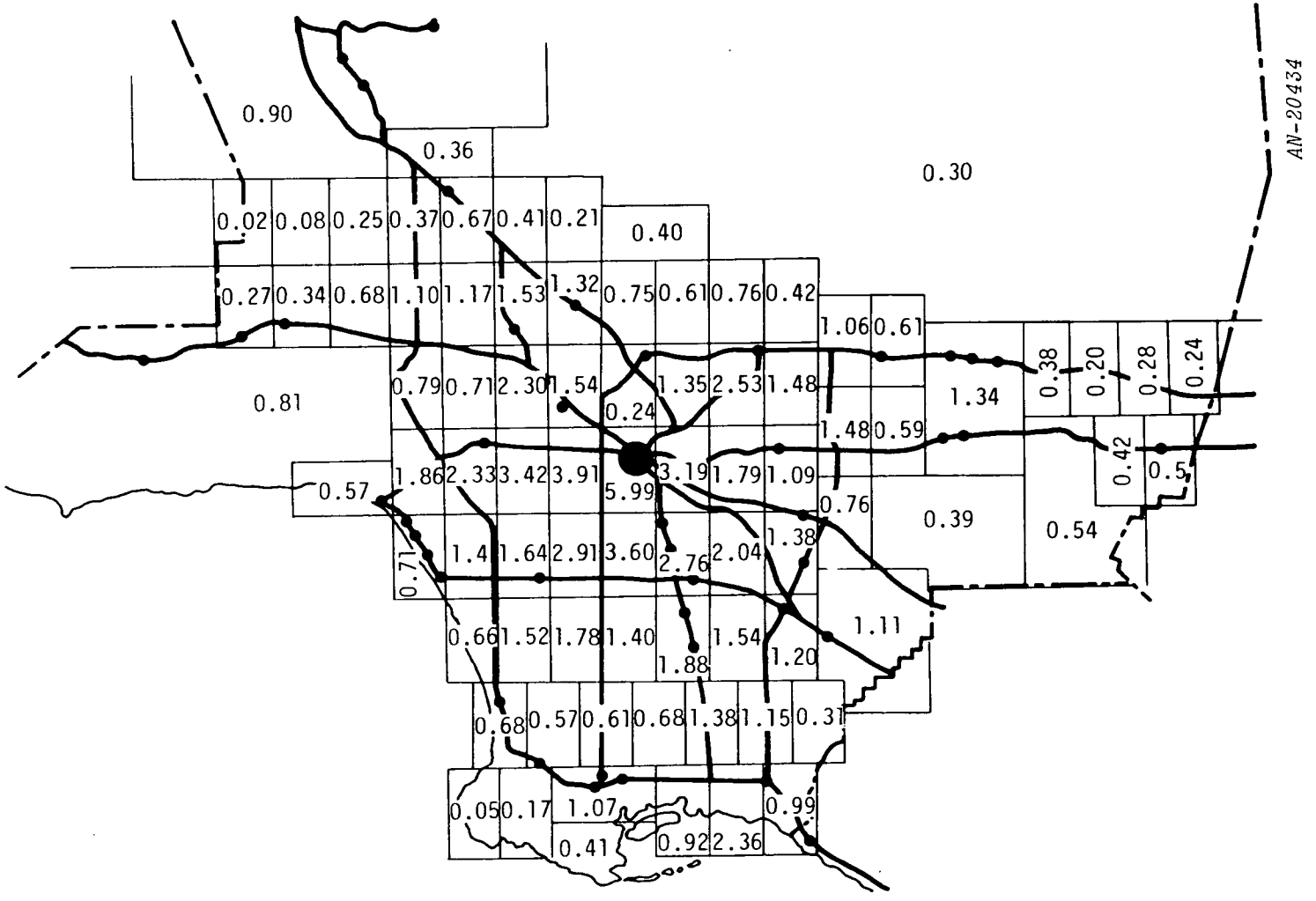

Figure 19. Geographical Traffic Distribution in Los Angeles County, ca. 1951. Numbers Shown Represent Percentage of County's Daily Traffic, in car miles, Occurring in Area (81)

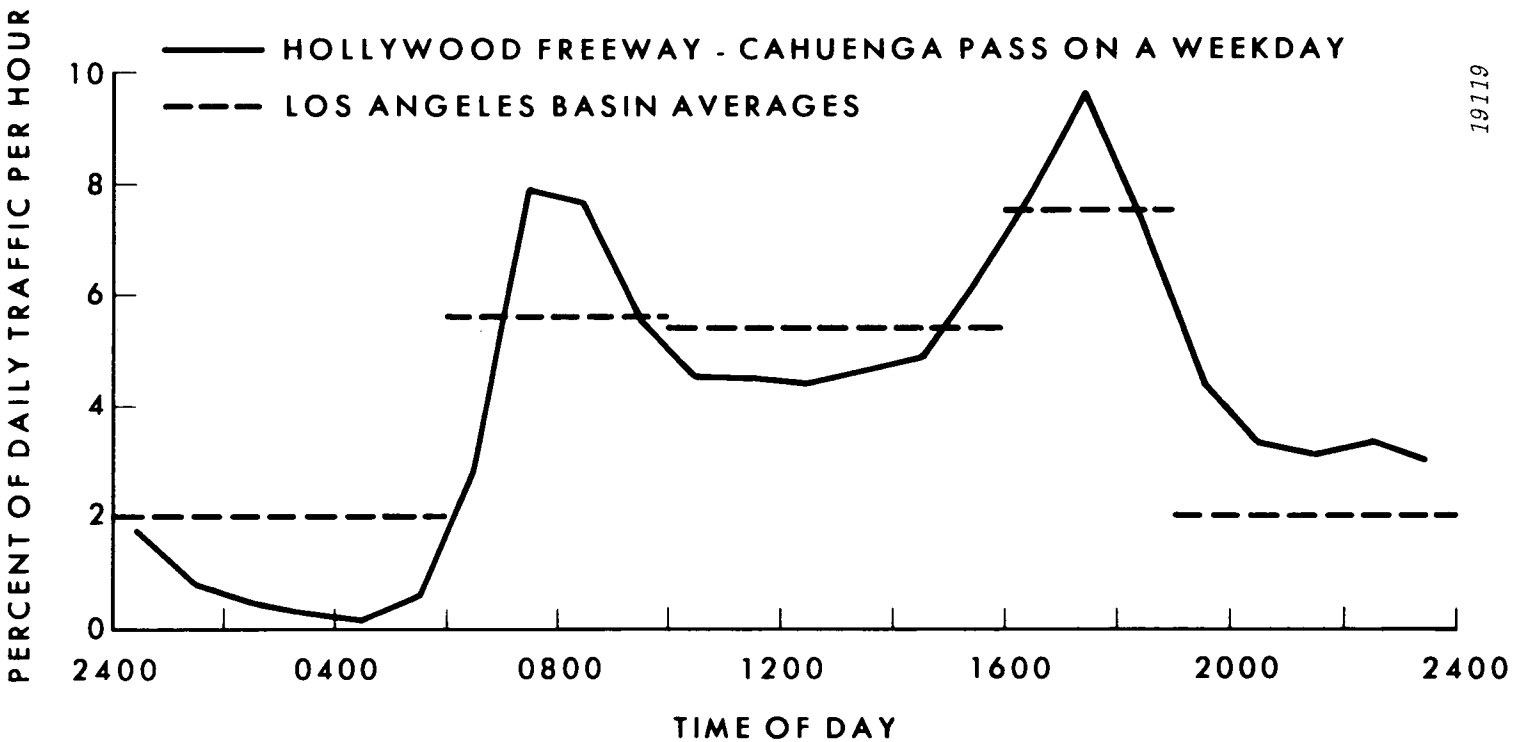

Figure 20. Los Angeles Traffic/Time Distributions ca. 1951 (81)

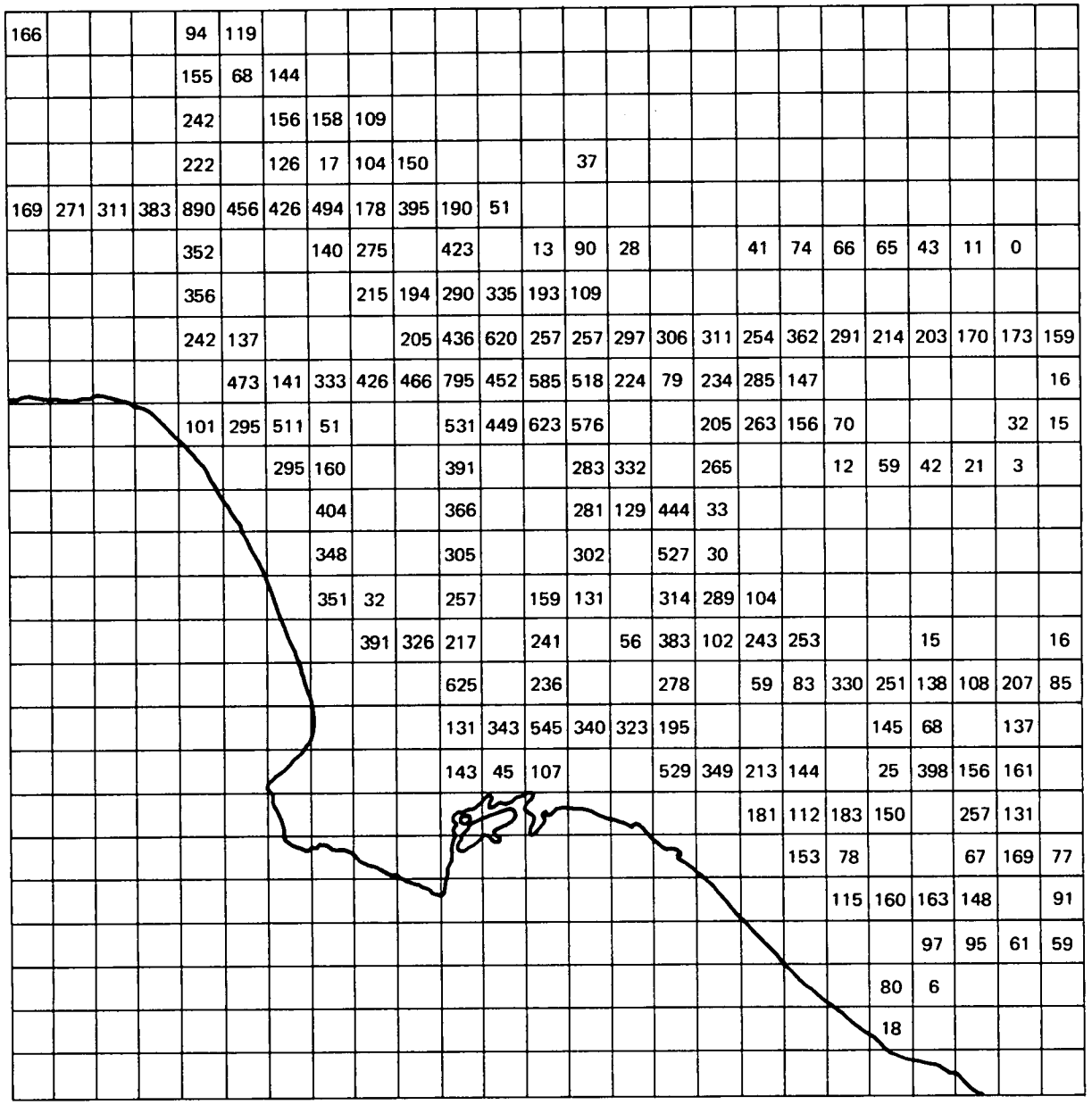

AN-29982

Figure 21. Geographical Distribution of Freeway Traffic in the Los Angeles Basin Area ca. 1970 (thousand vehicle miles per day) (Adapated from Roberts, Roth and Nelson, Ref. 82)

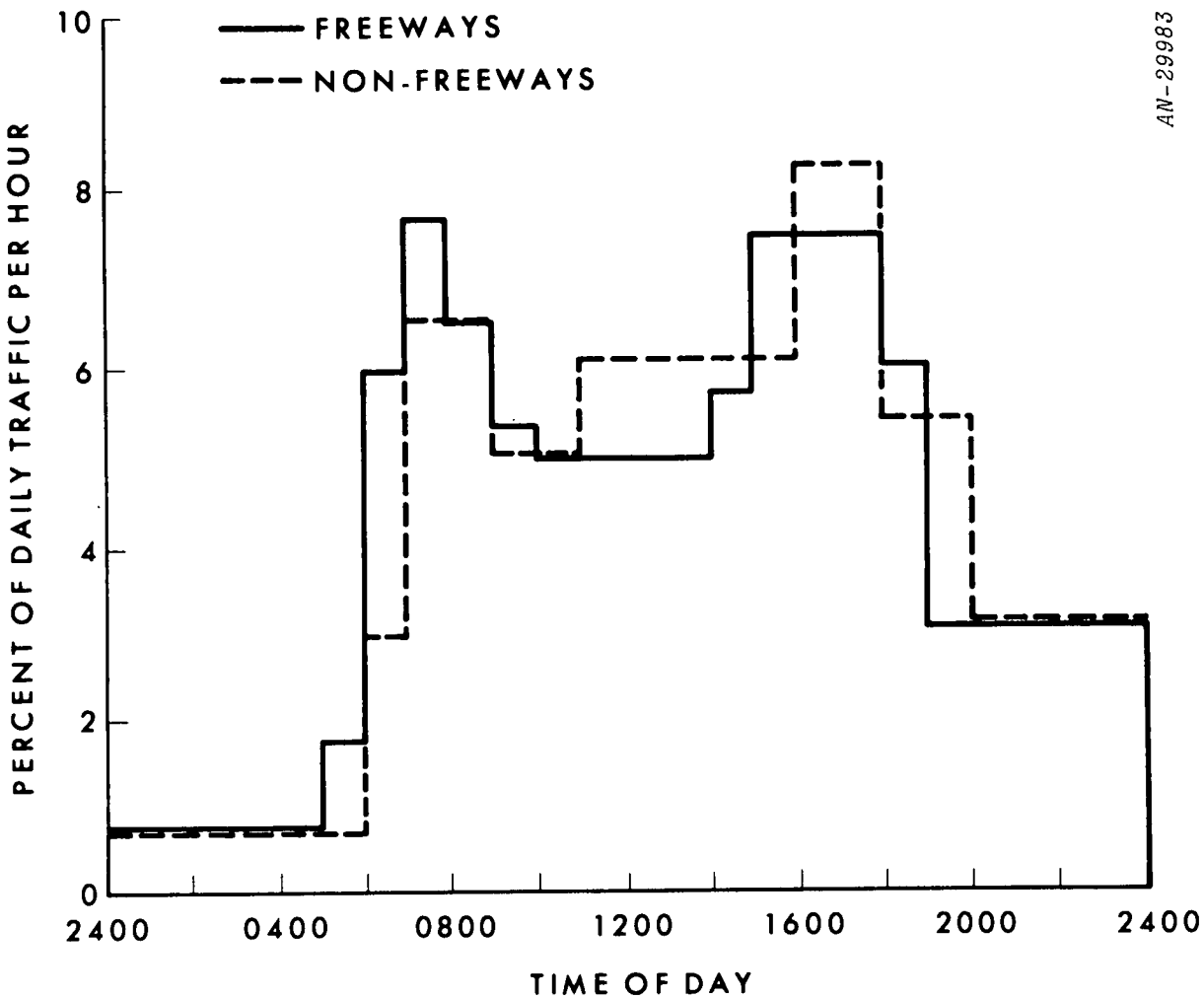

Figure 22. Los Angeles Traffic/Time Distributions ca. 1970 (Adapted from Roberts, Roth, and Nelson, Ref. 82)

Because Volume I of Ref. 51 contains detailed descriptions of the measurements program, it will be reviewed here only briefly. Two fixed sites, Huntington Park and El Monte, California had instrumented trailers which monitored pollutant concentrations, meteorological data and ultraviolet radiation. The sites are 12.7 miles apart and lie along a prevailing air trajectory. The great step forward in this program was the resolution of hydrocarbon concentrations into more than 100 individual species up to C_{10} with a sensitivity to levels below one part per billion using highly refined gas chromatography techniques.

Reference 52 gives descriptions and reports data for a similar program conducted in the 1969 season. The central basin station was located at Commerce and the northeastern basin station remained at El Monte. These sites are separated by 10 miles. Great improvements in data frequency and reliability were made in the 1969 measurement program.

Limited use of other data has been made to supplement the SRL measurements. In 1967 a joint study was made by the National Center for Air Pollution Control, the California Air Resources Board Laboratory, and the Los Angeles County Air Pollution Control District. The objective of the study was directed toward improvement in detailed chemical measurement. It involved air sampling at two sites, Downtown Los Angeles and Azusa. Some of the reduced data (84) have been used in the validation studies. The LAAPCD monitors concentrations over a nine-station network. We have used some of this information from 1968 to augment the SRL data.

The large volume of field data must be assimilated by some form of preprocessing before it is useful for validation tests. Two states of reduction which we have employed are sorting days by type characterized by peak oxidant* and then averaging data over all days of each given type. Consistent with the lumped parameter approach, we reduce the hydrocarbon ensemble by grouping compounds into brackets on a reactivity scale. For a beginning, only two reactivity classes have been employed in accordance with the source inventories shown in Table 6. Low reactivity hydrocarbons include methane, ethane, propane, acetylene, methylacetylene, and benzene. All others are considered to be high reactivity.

C. VALIDATION TESTS OF AN EARLY VERSION OF THE MODEL

In addition to studying the chemistry using chamber data, we studied atmospheric transport of inert and low reactivity species to concentrate on diffusion effects. For initial validation tests, Huntington Park is superior to El Monte because of the symmetry in surrounding source distribution, the remoteness from any mountain interferences, and the regularity in the data. Our search for type 3 days turned up October 23, 1968 as the only one with sufficient data for validation. This was used for the initial DIFKIN tests because the low wind speeds minimize the error in omitting the horizontal advection term. The simplest form of the chemical model (the one diagrammed in Fig. 2) was used in these validation tests.

---

* Days are typed by peak oxidant as follows: type 0, both stations < 20 pphm; type 1, either station 20-30 pphm; type 2, either station > 30 pphm; type 3, either station > 30 pphm <u>and</u> western station peak ≥ eastern station peak (pphm = parts per hundred million). Western and eastern stations are taken to be Huntington Park and El Monte for SRL data, or Downtown Los Angeles and Azusa for LAAPCD data.

Figure 23 shows results for ground level carbon monoxide concentrations at Huntington Park. This species is practically inert so that the results are a test of the transport formulation and the chemical source term for carbon monoxide is neglected. Using measured values to start at 0600,* we computed the solid curve from DIFKIN (no advection) and the dashed curve from TADKIN (input wind observations). Comparison of SRL data with output from the models shows that advection only becomes significant after the first three hours. Good agreement is exhibited by the models (using input data described above) with the validation data. The ventilation behavior is consistent with the local wind speeds displayed on an auxiliary graph on Fig. 23. This approach has been applied on a small-scale grid to study the carbon monoxide pollution in the nearby vicinity of a freeway (85).

Test results with photochemistry have been obtained for type 2 and 3 days using the DIFKIN code. Prior to discussing these results, it is necessary to digress briefly and examine some special features of the data. First, consider the ratio of acetylene (C_2H_2) to total oxides of nitrogen (NO_x). In morning samples, C_2H_2 is essentially unreacted and the NO_x has not been depleted much by the chain breaking reactions. Hence we should expect a plateau of the C_2H_2/NO_x ratio characteristic of motor vehicle exhaust. Previous investigators (84) have shown this

---

* Using airborne sample measurements with ground measurements for type 2 days, we determined the early morning profiles to be well approximated by an exponential decrease with height using a 150-meter scale height.

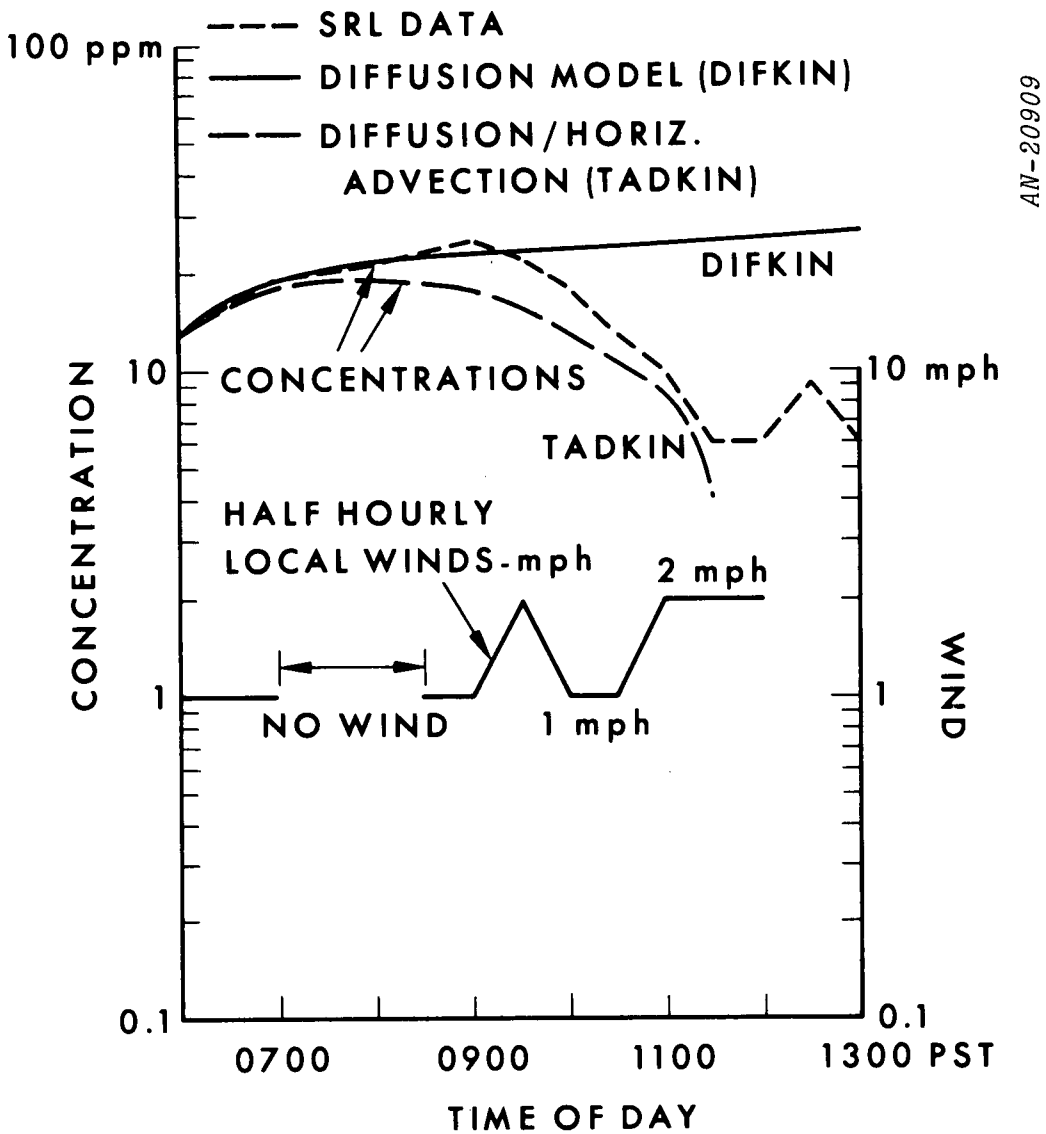

Figure 23. Carbon Monoxide Concentration at Huntington Park on Type 3 Day

ratio to be about four times that typifying automobile exhaust from the California Driving Cycle.* These results are displayed on Fig. 24 suggesting that the estimates from Table 6 may need modification. If we assume that nitric oxide, the emitted pollutant, is depleted in preference to C_2H_2 (say by heterogeneous reactions), then we should lower the NO_x estimates. This hypothesis is tested below by reducing the source strengths for NO in the calculation. Another bit of evidence leading to suspicions of the nitrogen balance is found in the ratios of CO to NO_x (86). Carbon monoxide has long atmospheric reaction times, and since it is nearly exclusively of vehicular origin, it too can be considered as a tracer.

Figures 25 and 26 are plots of the CO/NO_x ratios as they vary throughout an average day of each type. Figure 25 shows the anomaly occurring on high oxidant days in 1968. Morning peaks of CO/NO_x ratio appear to follow traffic curves. They exceed the vehicular ratio of 24 and the all-sources ratio of 16 by large amounts. At its extremum, the average for high-oxidant days exceeds the all-sources value by a factor of four. This is the basis of the inconsistency between air levels and source inventories discovered in the modeling study. The physical explanation for this inconsistency is not yet available. Further diagnostic measurements will be needed to isolate the phenomenology. Even the low-oxidant curve exceeds the source ratios in the morning. It seems to follow the high-oxidant curve at a fixed interval below it until mid-morning. Then both curves begin to merge.

* This is observed for high-oxidant days in 1967.

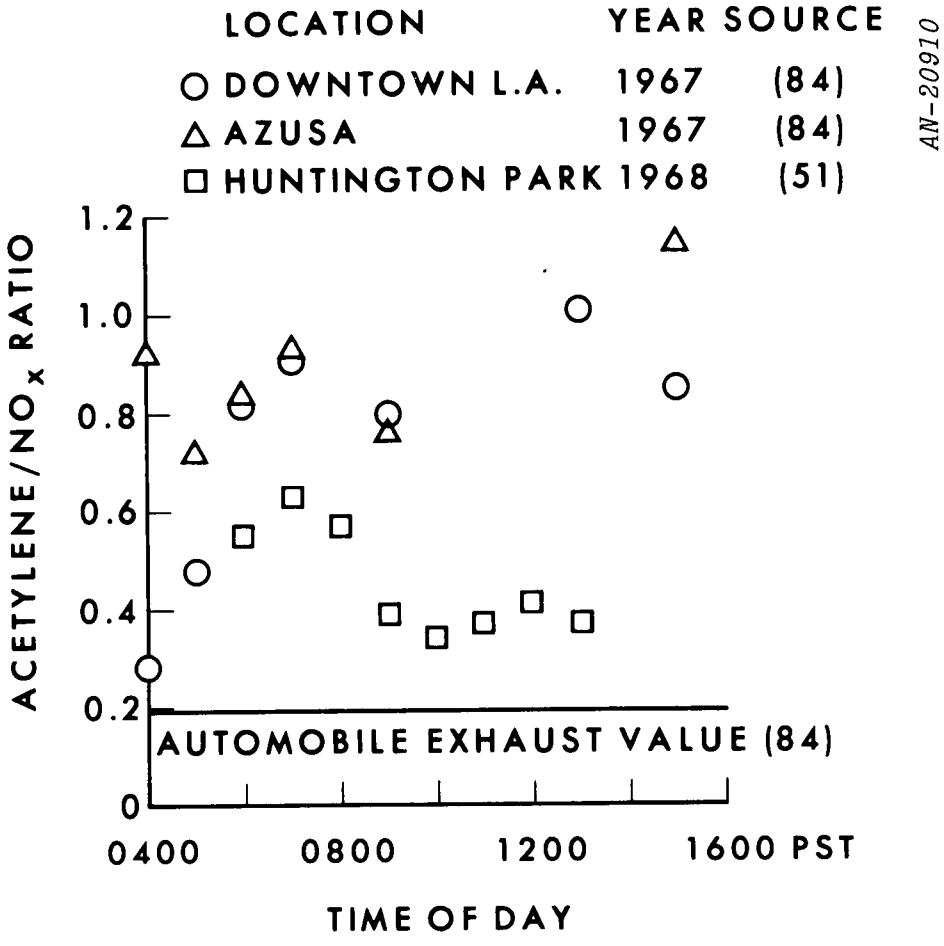

Figure 24. C_2H_2/NO_x Ratios for High Oxidant Days

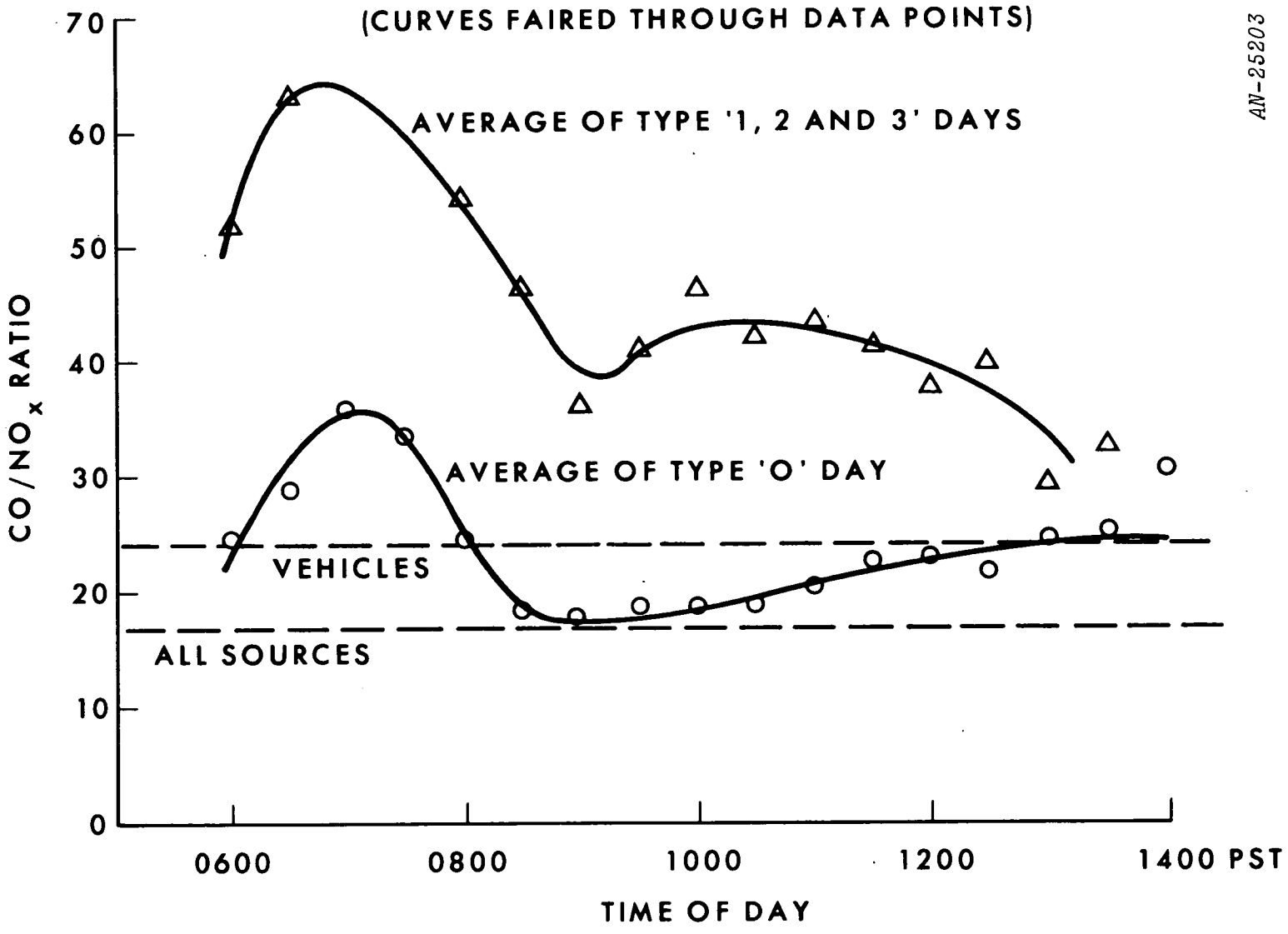

Figure 25. CO/NO$_x$ Ratios for Huntington Park 1968

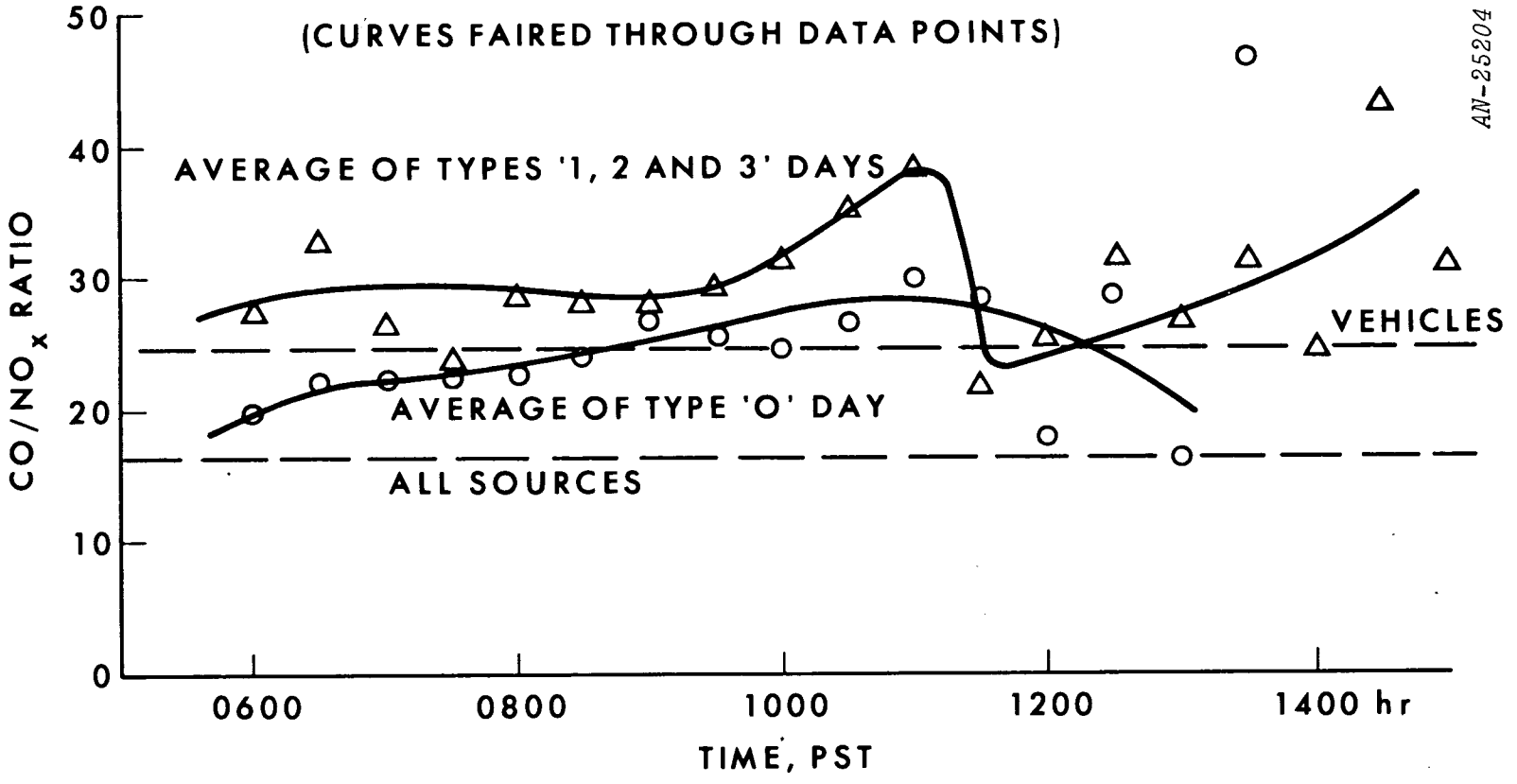

Figure 26. CO/NO$_x$ Ratios for Commerce 1969

It seems plausible to suspect that there are lower morning NO_x levels some days and that this raises peak oxidant. We will see from the model studies that the morning buildups of hydrocarbon and carbon monoxide agreed well with predictions derived directly from inventory statistics. Hence, higher HC/NO_x ratios are associated with higher peak oxidant as shown by the chamber experiments reported in Ref. 47.

The 1969 CO/NO_x ratios do not show the strong association with peak oxidant that the 1968 data exhibit. Figure 26 for Commerce indicates that both high- and low-oxidant days have ratios only slightly higher than the emission source values. The high-oxidant days are likely to have an NO_x deficit rather than a superabundance of CO .

The lack of similarity between 1968 and 1969 nitrogen oxide balances underscores the need to select a wide sample of days for model validation. Conclusions drawn from a single smog episode cannot be relied upon for establishing a general abatement strategy. One suspects that sampling for a particulate nitrate may be a significant step toward resolving the problems of nitrogen-oxide balances. Nitrogen dioxide oxidation processes and interaction with water vapor may form nitric acid which then leads to nitrates in solution or other condensed phases.

The initial tests of the model (DIFKIN) combining diffusion with kinetics were conducted for the type 3 day. Both the rate ratio and NO_x source strength ratio hypotheses were tested, as shown in Figs. 27, 28, and 29. The first set of graphs illustrates most clearly the need for a

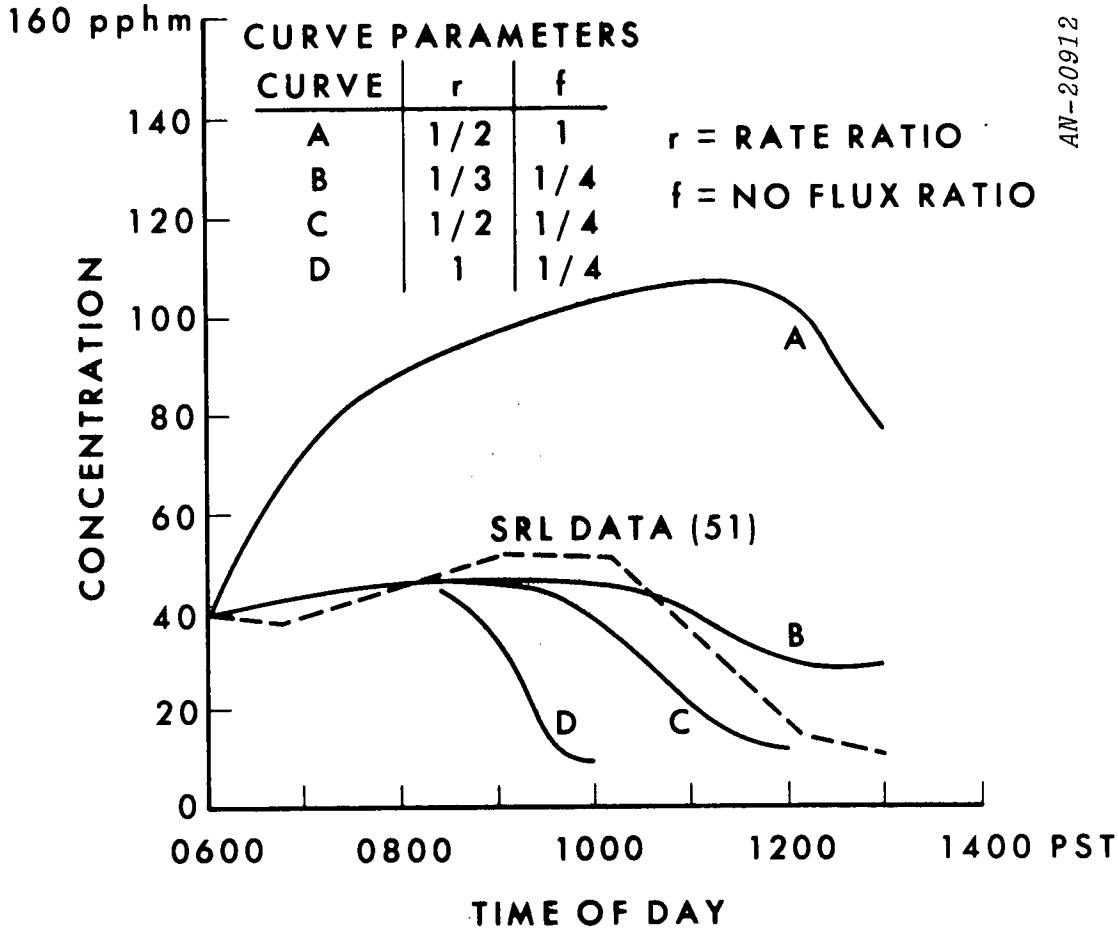

Figure 27. $(NO + NO_2)$ - Concentration Ground Level Huntington Park on Type 3 Day

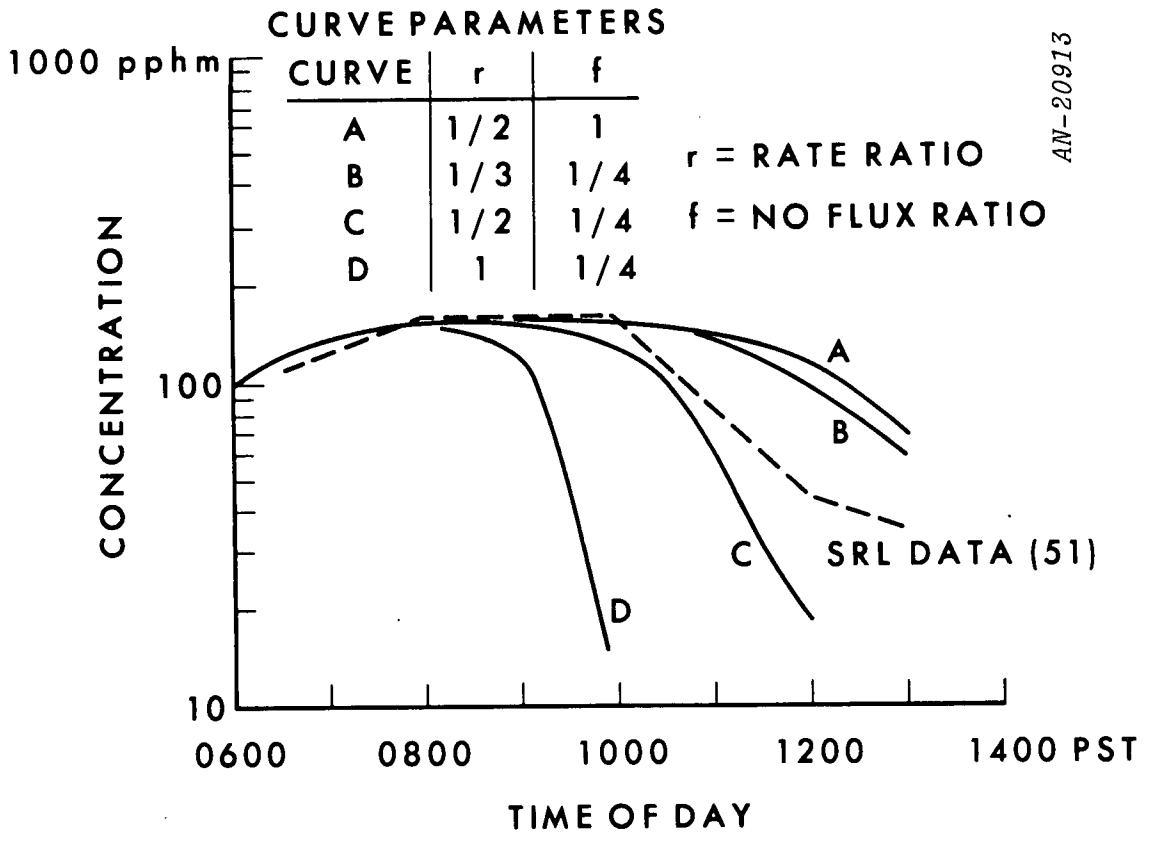

Figure 28. High-Reactivity Hydrocarbons Concentration on the Type 3 Day

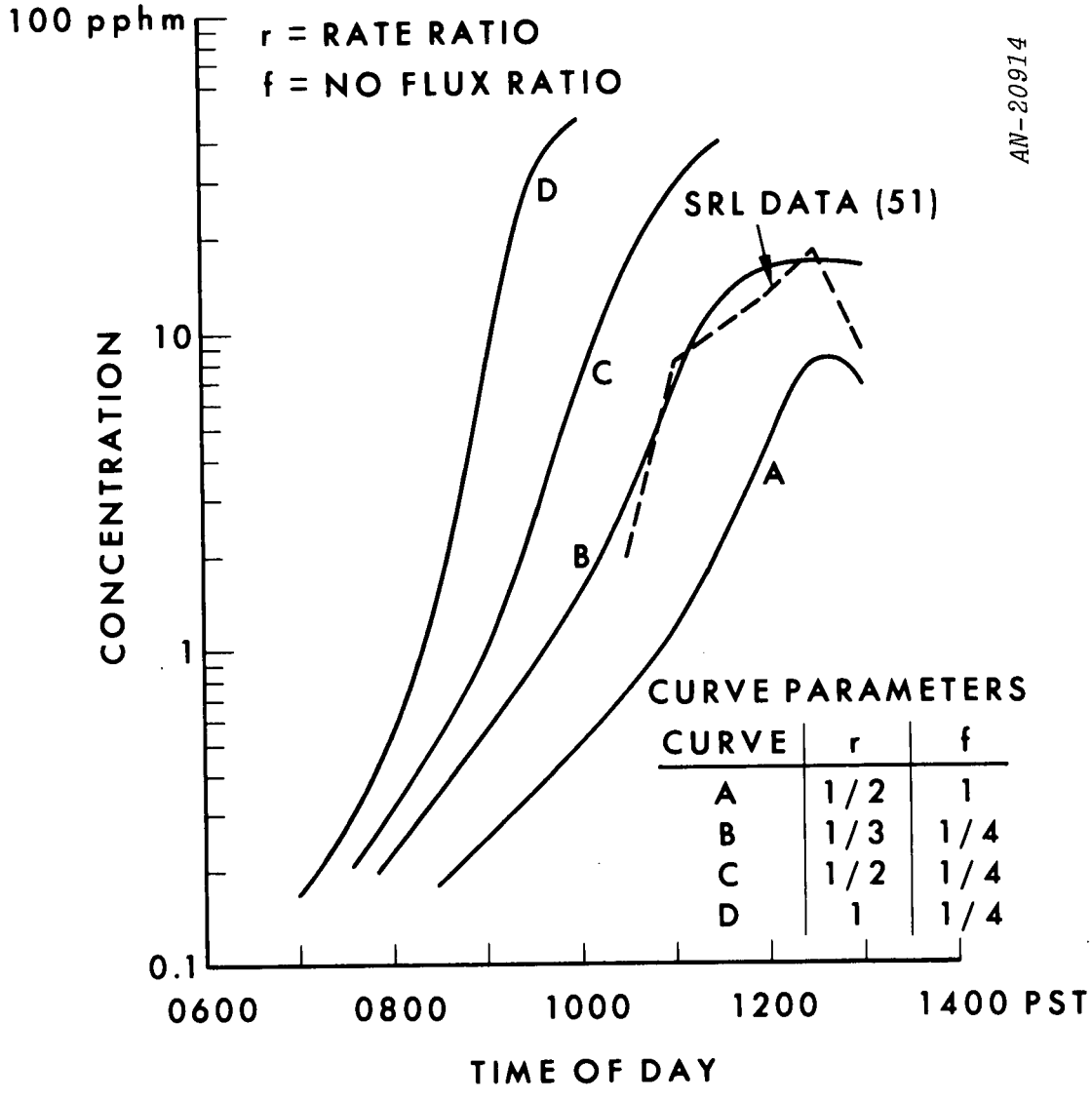

Figure 29. Ozone Concentration at Huntington Park on Type 3 Day

downward adjustment in the nitric oxide source strength (or flux). Consistent with the results of Refs. 84 and 86, Figs. 24, 25, and 26 suggest a reduction. Using $f = 1/4$ (a fourfold strength reduction), we see a great improvement in the model predictions in the NO_x curves in Fig. 27. Because of our present inability to represent the gas-liquid or gas-solid reactions mentioned above, this flux reduction is not merely a curve fitting, but is likely to reflect real physical processes. For these reasons, the $f = 1/4$ adjustment must be regarded as a tentative correction pending the availability of further research data on removal processes for oxides of nitrogen. The ratio of rates is examined in these three figures by comparing curves B, C, and D. Evidently something between 1/2 and 1/3 the propylene oxidation rate constants gives the best agreement with the observed values (51). This tends to support the hypothesis that the reactivity index goes like the oxidation rate constants in the results shown in Fig. 10 and 11.

Expanding the validation data to a larger sample, we selected type 2 days for which data were available during the 1968 smog season. The statistical preprocessing program derived half-hourly means and standard deviations for this sample of days. Hatched areas on Figs. 30, 31, and 32 show the mean values plus or minus one standard deviation. Again, the DIFKIN modeling was tested using five mesh stations including the ground and the inversion base. Moreover, a homogeneous mixing model was demonstrated. This model assumes that anything entering the marine layer from the ground is vertically mixed instantaneously. Reactions proceed according to the kinetic model derived in Sec. II. For all of the results in

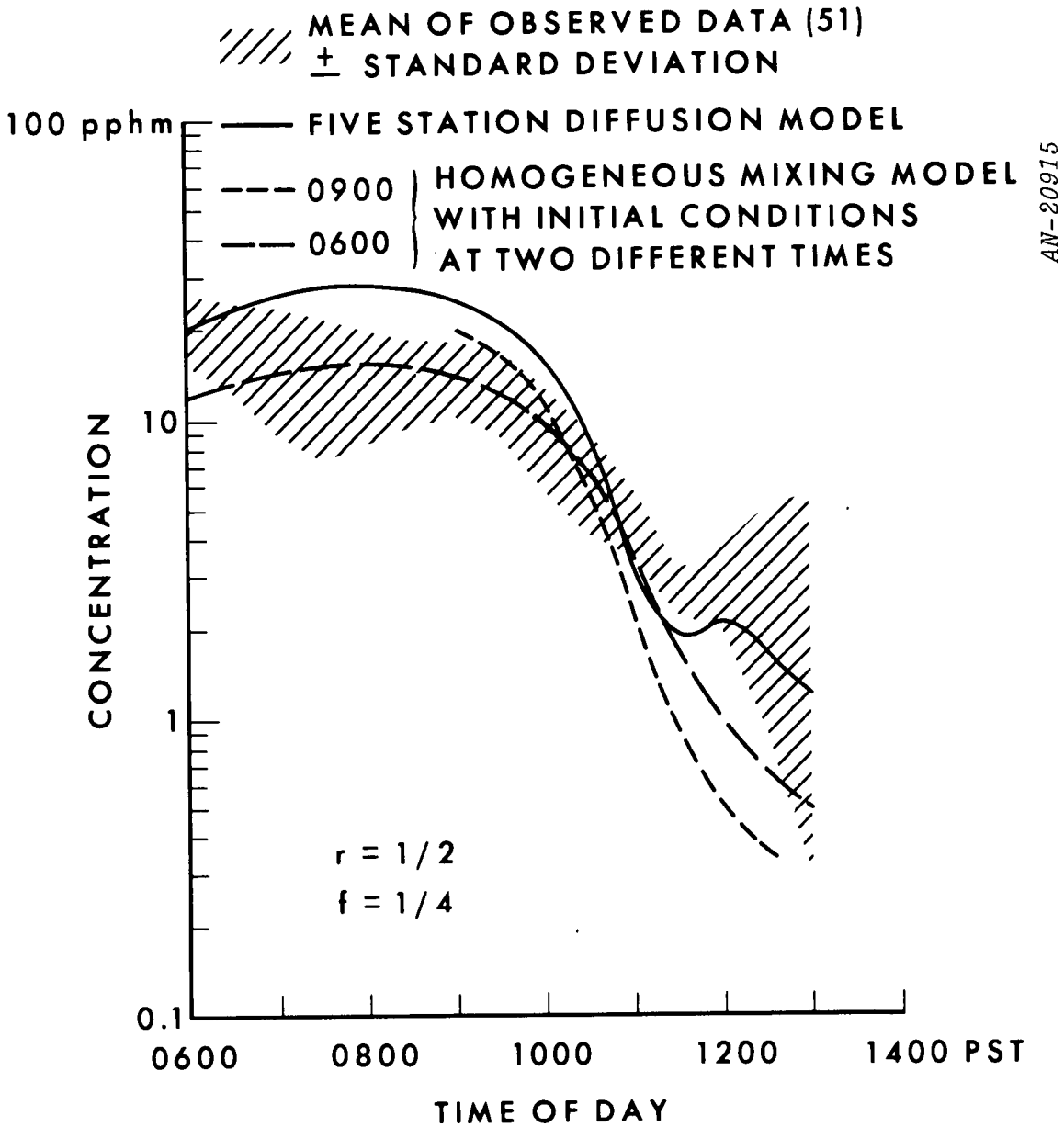

Figure 30. Nitric Oxide Concentration at Huntington Park on Type 2 Day 1968. f = 1/4; r = 1/2

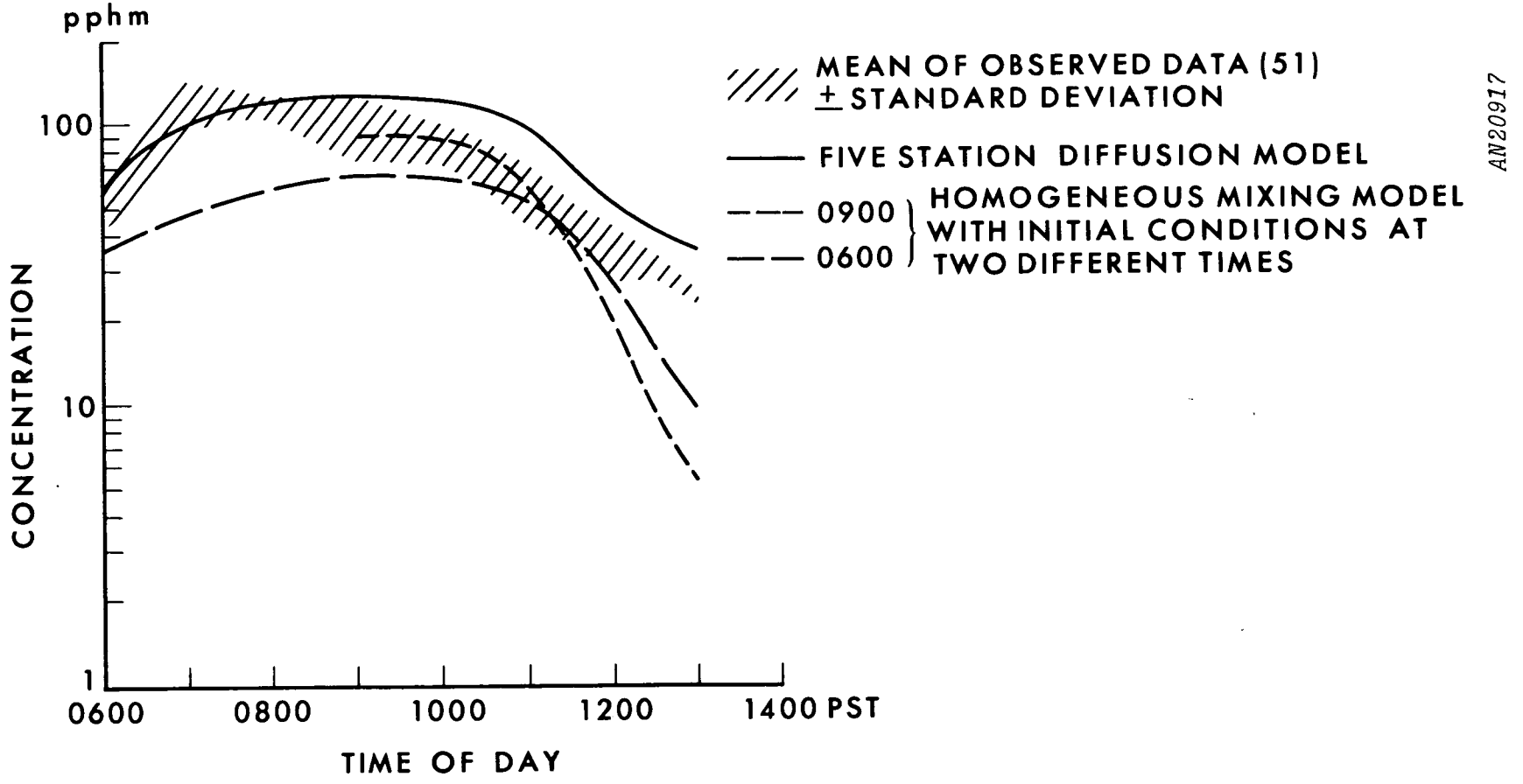

Figure 31. High Reactivity Hydrocarbon Concentration at Huntington Park on Type 2 Days 1968. f = 1/4; r = 1/2

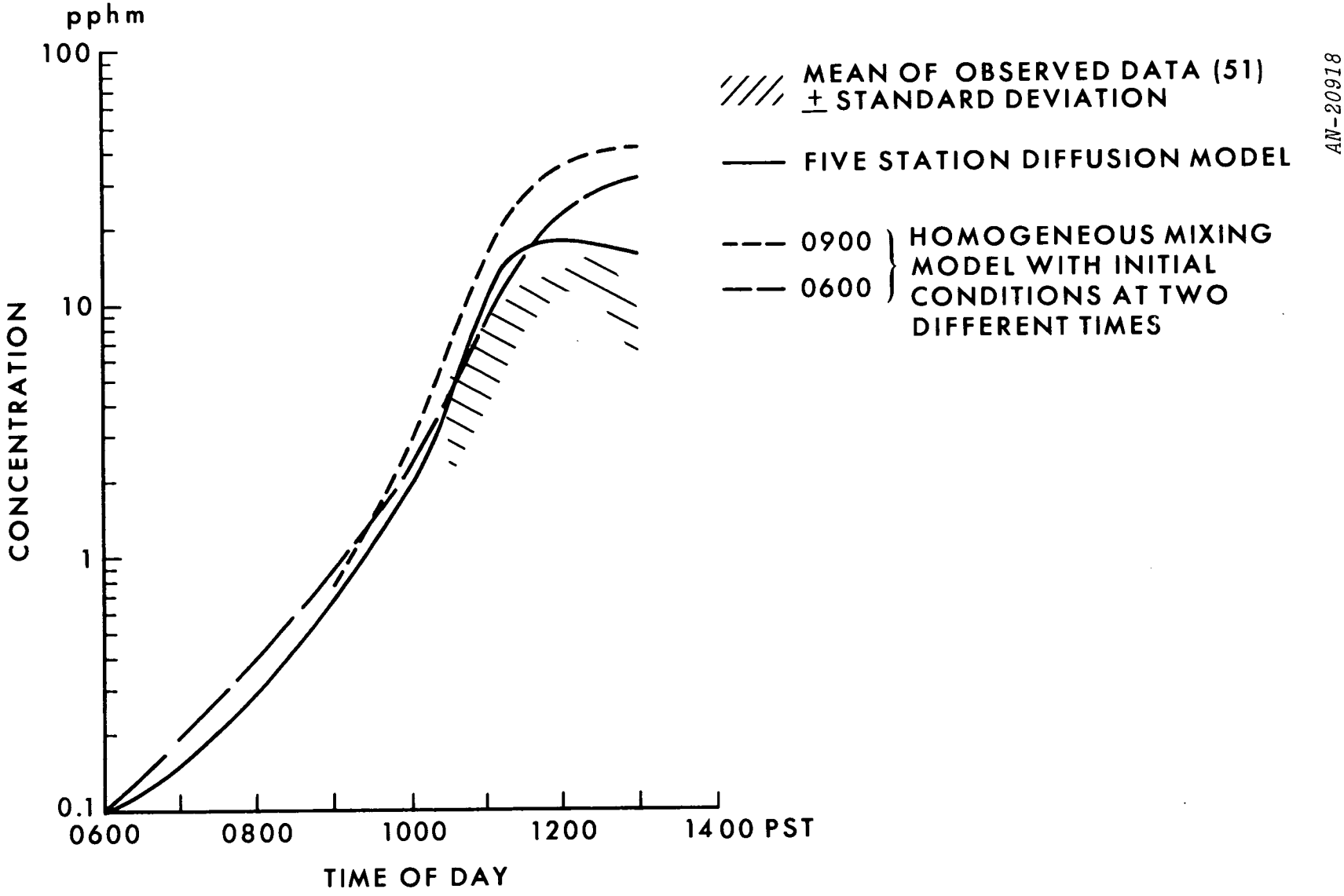

Figure 32. Ozone Concentration at Huntington Park on Type 2 Days 1968.
f = 1/4; r = 1/2

Figs. 30-32, the curve parameters are $f = 1/4$ and $r = 1/2$. The symbol r refers to the ratio of the atmospheric-hydrocarbon oxidation rate constants to those of propylene. Average profile values at 0600 PST and at 0900 PST are used to initiate homogeneous mixing runs. Some of the precision of detail is lost in this approximation. Considering that homogeneous mixing calculations only require 5 to 10 percent of the central processor time needed by the five-station diffusion runs, they may well be useful for cases where parametric effects are studied for many different conditions.

D. SENSITIVITY STUDIES ON 1969 TRAJECTORIES WITH THE EXPANDED MODEL

Based on the semi-Lagrangian formulation of the photochemical/diffusion model, the computed end-point composition of the air masses depends on initial conditions, flux from the ground along the trajectories, and on reaction rates. For our tests, we concentrate on El Monte data because much of the polluted air there comes from somewhere else. This is believed to be a more severe test of the model than that at Huntington Park. The initial conditions are based on measurements insofar as possible. The principal initial values for the 1030 trajectory are as follows for 0730 hours (PST).

c_{HC} = 51 pphm* (6 ppm C total HC)

c_{NO_2} = 24.5 pphm

c_{NO} = 3.5 pphm

---

* pphm = parts per hundred million.

These were interpolated from the Azusa station data (87) from the Los Angeles County Air Pollution Control District. Reference to Fig. 15 shows the basis of this choice. The reactive hydrocarbon value is derived from the assumptions of 34 percent reactive fraction and an average carbon number of 4 for the reactive family of compounds. These are seasonal averages over the 1969 measurement months (52) at El Monte. The analysis that generated the values from gas chromatographic data is discussed elsewhere (86). Similarly the 0730 initial values for the 1130 trajectory are obtained from the Commerce data log (52). They are:

c_{HC} = 94.5 pphm (9.7 ppm C)

c_{NO} = 43.9 pphm

c_{NO_2} = 17.4 pphm

The hydrocarbon conversion factors here are 41 percent reactive fraction and an average carbon number of 4.2.

Since the 1230 trajectory begins near the coast, we employ station 76 (La Cienega Boulevard) measurements for 0630 hours (PST) initial values of nitrogen oxides. No hydrocarbon data are available from that station and an HC/NO_x-ratio of 2 was chosen. Although this is not representative of the inventory ratio, it is representative of many morning air samples. Such an observation further reinforces the suspicion of an NO_x-deficiency on high oxidant days (86). Thus, the values are:

c_{HC} = 54 pphm

c_{NO} = 18 pphm

c_{NO_2} = 9 pphm

The location of the 1330 trajectory origin is near no station and the data indicate that the initial pollution cannot be neglected. Consequently, results were not obtained for the 1330 trajectory.

Ultraviolet data from Ref. 52 were employed to get photodissociation rates for NO_2 by means of calibration functions developed in the data analysis study (86). Inversion base altitudes were averaged from the airborne temperature measurements provided by Scott Research Laboratories (52).

To examine parametrically the influence of inventory levels, we altered the rate of emission for ground level. Halving the nominal NO-fluxes is suggested by the departures of the CO/NO_x-ratios and the C_2H_2/NO_x-ratios obtained for high oxidant days (86). Subsequent halving of both reactive hydrocarbon and nitric oxide fluxes brings us down to the adjustment represented by $f = 1/4$ in Figs. 30, 31, and 32 but preserves the HC/NO_x-ratio. In both cases, the full propylene oxidation rates were employed.

Table 7 summarizes the results for trajectory end points. Advancing down the table we note an ever-growing sensitivity of the results to the flux adjustments. This occurs because the increasing wind speed lengthens the trajectories and there is larger relative exposure of the air mass to high pollutant fluxes.

In the 1030 case, both hydrocarbon and nitric oxide are low, but NO_2 and ozone are high. Changes in the fluxes have marked effects on

TABLE 7

RESULTS OF MODEL SENSITIVITY STUDY
USING 1969 EL MONTE DATA

Concentrations at El Monte in pphm

El Monte Trajectory Arrival Time (PST)	NO			HC			NO_2			O_3		
	Measured Values	$(1/2)\phi_{NO}$ Full ϕ_{HC}	$(1/4)\phi_{NO}$ $(1/2)\phi_{HC}$	Measured Values	$(1/2)\phi_{NO}$ Full ϕ_{HC}	$(1/4)\phi_{NO}$ $(1/2)\phi_{HC}$	Measured Values	$(1/2)\phi_{NO}$ Full ϕ_{HC}	$(1/4)\phi_{NO}$ $(1/2)\phi_{HC}$	Measured Values	$(1/2)\phi_{NO}$ Full ϕ_{HC}	$(1/4)\phi_{NO}$ $(1/2)\phi_{HC}$
1030	3.4	0.5	0.3	43	34.3	24	16.4	20.5	14.5	13.4	32.6	35.3
1130	3.2	1.5	1.5	64	87.4	70.1	21.3	58.5	48.6	23.6	28.4	24.2
1230	1.5	1.1	1.0	38	67.5	48.1	10.3	49.2	34.6	24.5	30.9	24.8

NOTE: Nominal values of emission fluxes are denoted by ϕ . Hence, $(1/2)\phi$ means that we halved the fluxes derived from inventories.

everything but the ozone. Comparing these end-point compositions with the initial values cited above, we note a strong dependence on initial conditions accuracy for this short time scale. Fortunately, the Azusa data are available as an aid in this respect.

For the 1130 results, the ozone and nitric oxide come in closer to the data, but NO_2 is extremely high. This is symptomatic of the large departures from the radiation-supported quasi-equilibrium that we noted in analyzing the El Monte data (86). Although the model does not assume quasi-equilibrium among the three reactions

$$h\nu + NO_2 \rightarrow NO + O$$

$$O + O_2 + M \rightarrow O_3 + M$$

$$O_3 + NO \rightarrow NO_2 + O_2$$

the differential equation solutions nearly always approximate it rather well.

Again, with the 1230 trajectory, the ozone and nitric oxide levels match observations reasonably well, but hydrocarbon and NO_2 are both high. Despite the passage of this air from the seashore and then over extensive regions of the central basin, we note that the initial values of the primary pollutants still influence the final concentrations in a dominant manner.

E. HISTORY ANALYSIS OF THE 1030 EL MONTE TRAJECTORY

Because of the relative completeness of initial conditions that we can relate to the Azusa station, we have chosen the 1030 trajectory to discuss in some detail. Examining Table 7, we note an overabundance of ozone at 1030 and a correspondingly rapid completion of $NO \rightarrow NO_2$ conversion. Reactivity analyses (Sec. II D) and our early modeling studies suggest reduction of the oxidation rate constants. To achieve some level of comparative assessment with the previous work, we assign one-fourth the nominal NO flux and one-half the oxidation rate; hence $f = 1/4$ and $r = 1/2$ describe the conditions as before. This time, however, we preserve the HC/NO_x-ratio as in the entries in Table 7 and reduce hydrocarbon fluxes by a factor of two. This means that the difference in end-point concentrations between this case and the $1/4\phi_{NO}$, $1/2\phi_{HC}$ entries is solely due to the rate constant reduction. This differs from the earlier work in which hydrocarbon fluxes were not reduced.

Figure 33 shows the reactive hydrocarbon history starting at Azusa at 0730 and ending at El Monte at 1030 on September 29, 1969. Despite the sharp reduction in hydrocarbon fluxes, the calculated curve stays above the Azusa levels until 1000 hours when it begins to slope-off in the observed manner. The model output clearly bears a closer relationship to the Azusa measurements than it does to the El Monte observations. This problem is typical of the difficulties we encountered in attempting to model conditions at the eastern portion of the basin at El Monte.

On Fig. 34 we note a sharp drop from the interpolated NO-level between 0730 and 0740 hours. This is reflective of the previously noted failure of the data to approach quasi-equilibrium between NO, NO_2, O_3, and sunlight intensity under high-oxidant conditions. The NO-conversion seems to proceed at roughly the observed rate after the transient is absorbed in the system; however, the level ends up closer to Azusa values than to El Monte values. Note that if we were to employ 0830 El Monte concentrations as initial values, we would have a lower HC/NO-ratio and could expect still slower nitric oxide conversion rates. Thus, both nitric oxide and hydrocarbon decay more like the Azusa data than the El Monte data.

The NO_2 behavior on Fig. 35 exhibits more nearly what one would expect than do either the reactive HC or the NO . Proceeding from the end of its transient adjustment to observed sunlight intensity, the air mass gradually undergoes NO_2-transition from Azusa levels to El Monte levels as it meanders about in the northeastern area of the

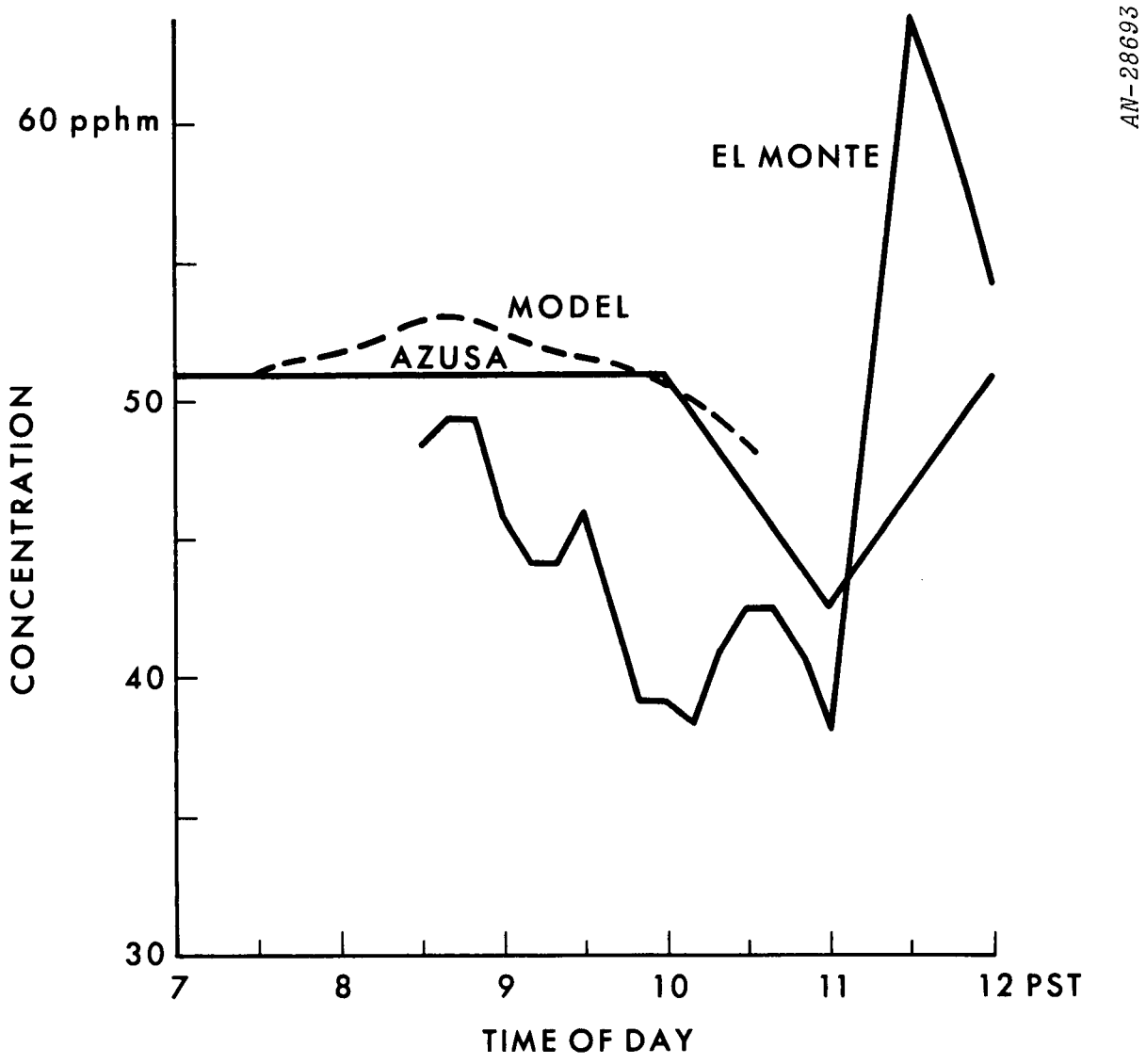

Figure 33. Reactive Hydrocarbon History Along the 1030 Trajectory. f = 1/4; r = 1/2 (Ground level concentrations)

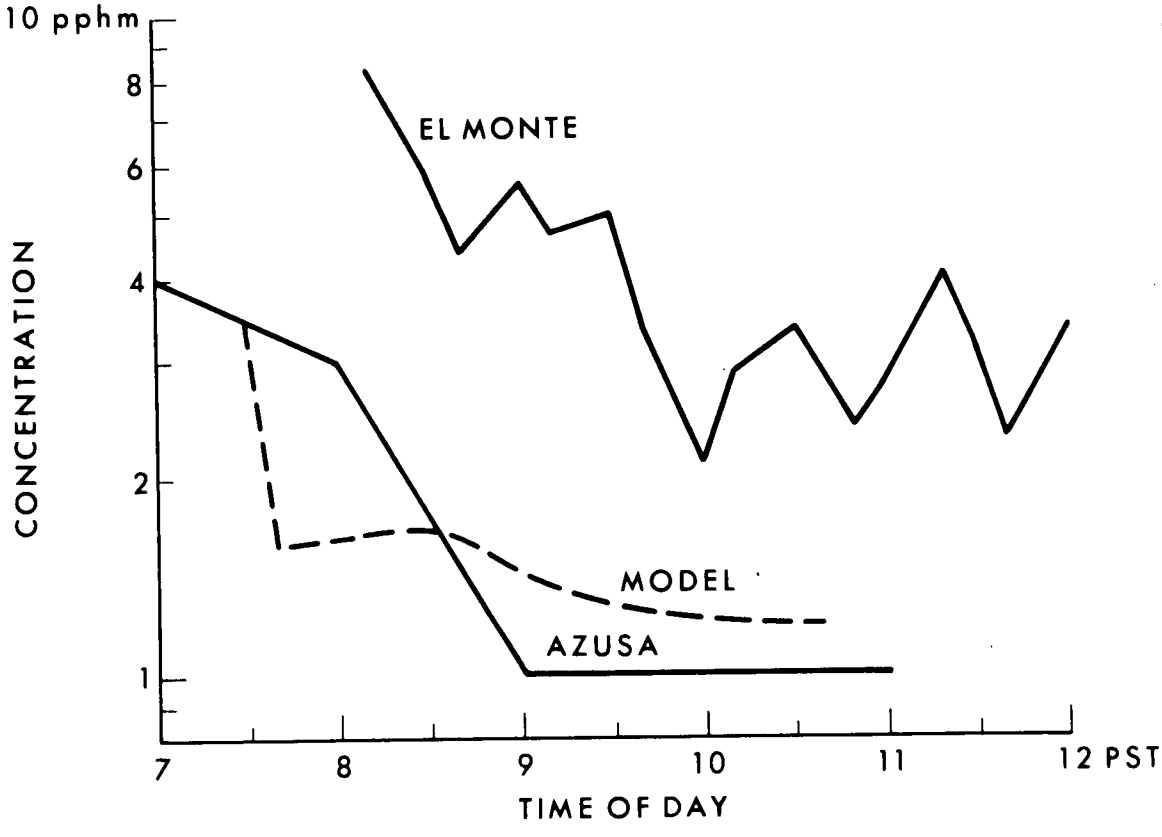

Figure 34. Nitric Oxide History Along the 1030 Trajectory. f = 1/4; r = 1/2 (Ground level concentrations)

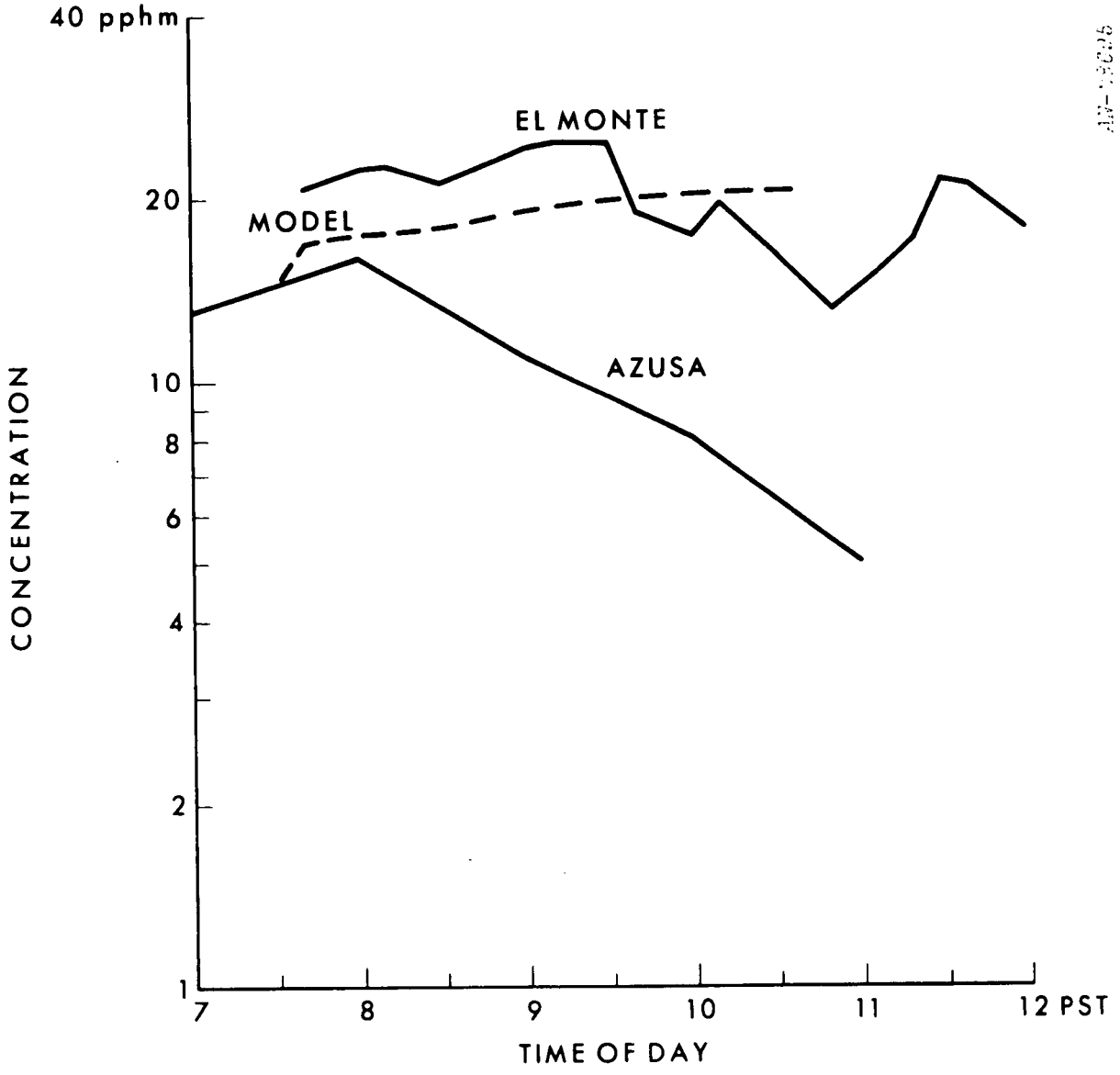

Figure 35. Nitrogen Dioxide History Along the 1030 Trajectory. f = 1/4; r = 1/2 (Ground level concentrations)

basin. Nitric oxide conversion supported by increasing sunlight intensities drives the NO_2 upward. The ground-based sources continue to feed in NO as it reacts and diffuses upward.

Summing over NO and NO_2, we get excellent total balance behavior for these oxides of nitrogen. Figure 36 indicates that not only slopes, but also magnitudes are represented rather well in the gradual change of composition moving from initial to final conditions over the three-hour period. Apparently the dominant effect of the good behavior of the NO_2 brings the balance into favorable agreement with the data. It will be recalled that this was a key test in the choice of $f = 1/4$ after conducting our original modeling study.

Finally, the history of ozone concentration may be seen on Fig. 37. The measurements of both Azusa and El Monte show a remarkable degree of smoothness and regularity compared with the jagged curves of the species displayed in the previous figures. Again, due to the rapid transient response of the $O_3/NO/NO_2$-system to the sunlight ultraviolet intensity, there is a sharp change in the first ten minutes of the model curve. As in the case of NO_2, however, the ozone undergoes a smooth transition from its origin to its destination. Considering the usual sensitivity of ozone to competing rate determining factors, this degree of realism is gratifying.

If we applied this same set of assumptions to the other trajectories, we would get too little ozone at the end points. Table 7 indicates fair agreement with $f = 1/4$ and $r = 1$ as shown in one of the

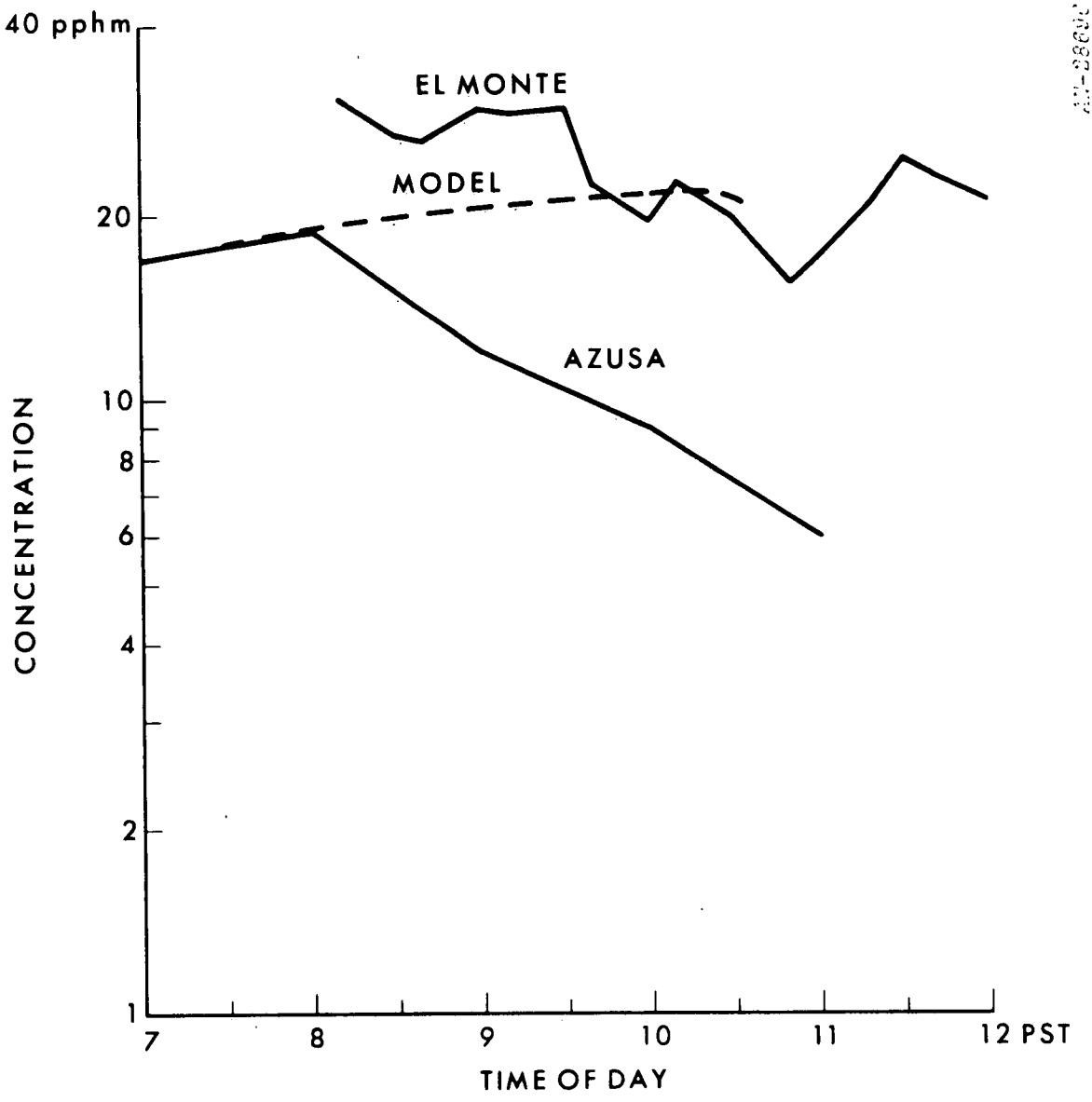

Figure 36. Oxides of Nitrogen ($NO + NO_2$) History Along the 1030 Trajectory. f = 1/4; r - 1/2 (Ground level concentrations)

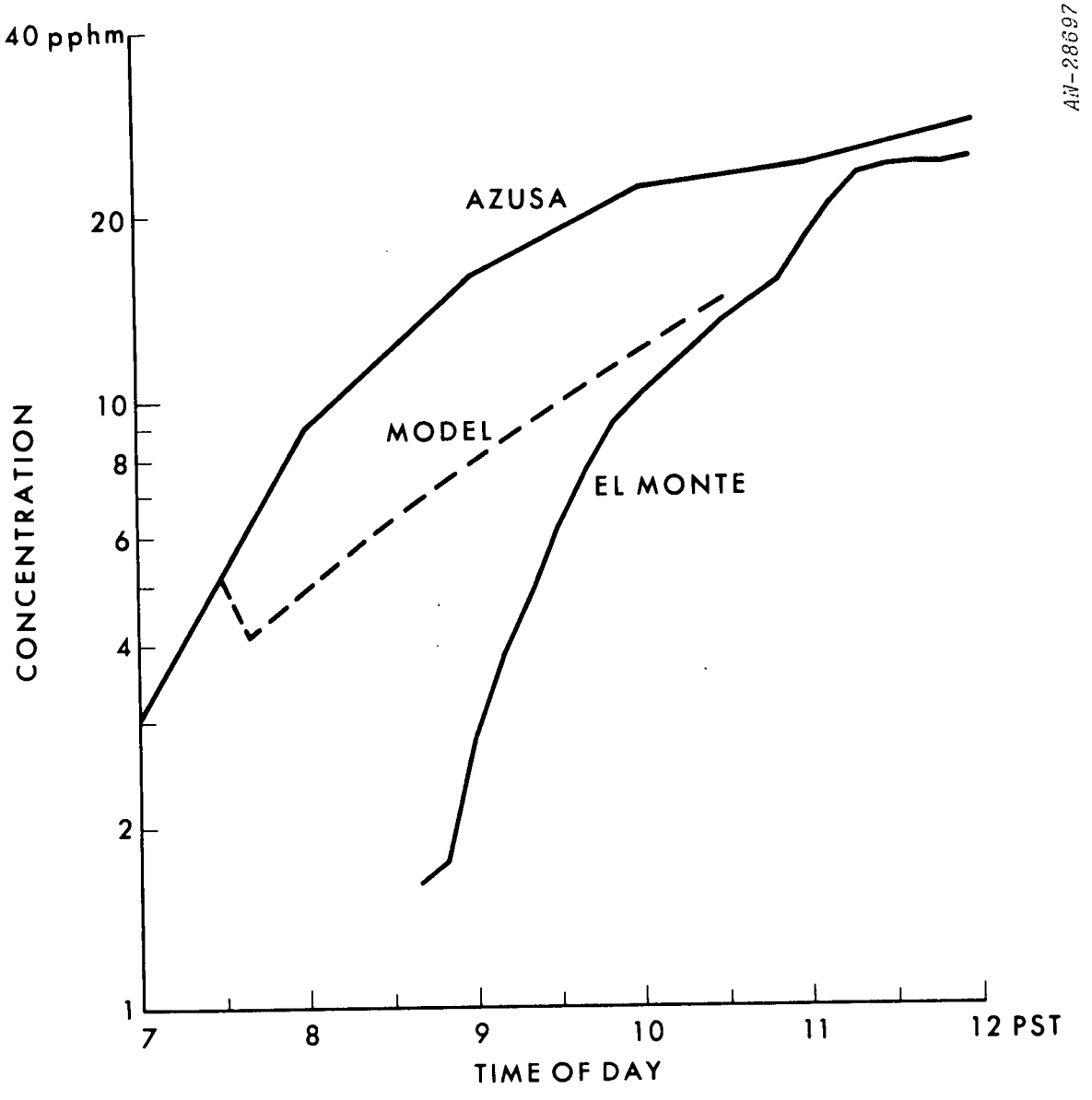

Figure 37. Ozone History Along the 1030 Trajectory. f = 1/4; r = 1/2 (Ground level concentrations)

columns. The hydrocarbon agreement for these other cases would be even worse than it stands if r were decreased to 1/2. Because of low confidence in the initial values that apparently dominate, the other trajectories would likely be less than satisfactory as tests of the model.

V. CONCLUDING REMARKS

An overview of these further developments of the GRC photochemical/diffusion model holds answers to many questions and points the way to future research needs. Before detailing the accomplishments and recommending new directions, we might make the general observation that applying and adapting the modeling tools that we possess now appears preferable to initiating effort on far more detailed chemical dispersion formulations. We have maintained a balanced posture in which the model advances and the improvements in measurements have kept pace with one another.

The chemical descriptions offered here hold the main features of the NO_x-chain termination that controls composition effects on secondary pollutant production. In concert with this, the addition of hydroxyl radical chemistry is a first step in explaining the "excess rate" of hydrocarbon oxidation (over that attributable to O-atom attack). Probably one of the most uncertain aspects of the system is our inclusion of HONO formation (from NO + NO_2) and opposed by photodissociation. If this is an important feature of the free radical balance, we really need to know the photodissociation absorption coefficients for HONO as well as some of the radical-molecule collisional reaction rates. In his task force report (88) for Project Clean Air, H. S. Johnston stresses the need to consider nitrous and nitric acids in the photochemical mechanism. This suggests a very real need to monitor these compounds in the laboratory experiments and in the atmosphere. Their involvement in aerosols and surface reactions may well hold the key to the apparent anomalies in

the nitrogen balance. The identification of chemo-mutagenic effects of HONO is yet another reason that it should be investigated. The brief examination of hydrocarbon synergism shows at least one way that the radical chains are cross-linked to influence combined reaction rates. Experimental data on mixed hydrocarbons will help sort out the most likely mechanisms. Likewise, our small study on possible CO interactions indicates that suggested values of these rate constants indicate a very strong influence on the propylene/nitric oxide system at concentration levels as high as 100 ppm. It may be that atmospheric hydrocarbons that are not involved in the OH-cycle are far less affected. In any event, atmospheric levels of CO are much lower than 100 ppm except in the vicinity of traffic arteries.

Reacting to the need for extended chemical representations, we have applied Padé approximant techniques to the numerical integration algorithms. Speed increases of at least four or fivefold are obtained in the computation comparing the Padé method for the more complex chemical system with previous methods for the simpler system. For equal-sized chemical matrices, the improvements would most likely be even better. In the interest of making these advances available to the community at large, we show the mathematical steps in some detail.

Besides the mathematical improvements, the atmospheric model has been adapted to a semi-Lagrangian formulation. By following selected air masses, we avoid commitments of large quantities of memory and the incursions of artificial diffusion errors. Most important, we do not

end up with stacks of computer printout that relate to regions where there are no measurements. It should be added that predictive calculations will become ever more useful, but our present levels of resources and sophistication demand that effort be concentrated on validation. Only in this way can the confidence be built that is needed for applying modeling techniques to implementation planning.

Validation tests of the model for 1969 Los Angeles basin data turned up several useful findings. For time intervals within a diurnal scale, we must use extreme care in selecting initial conditions. A way to overcome this need is to compute for several days of real time on a continuous basis. Increasing the time scale makes sense because episodes tend to cycle through several days. The cost in computing will go up more than proportionately, however, because as time scales increase so must the spatial domain. Perhaps 100 kilometers of urban/rural influence zone might be needed in lateral expansion. Correspondingly, a larger vertical field will have to be included to account for slow transport within the inversion layer, if there is one. Models that require artificial image flows above the marine layer or that assume artificially inflated "background" levels at the edge of the net will no longer be useful. What used to be boundaries will now be included in the computational field.

The sensitivity tests in the validation studies confirmed some of the suspicions that we expressed earlier (86), namely, that the quasi-equilibrium relationship between ozone and the oxides of nitrogen does

not seem to be recovered in the data. The largest departures are for the highest ozone levels. Attempting to represent the physical setting in a consistent manner, we find it difficult to use the measured ultraviolet intensity to account for the observed ozone buildup and NO-conversion simultaneously. The inconsistency even appears in the initial behavior of a modeling run as a transient "induction" process that rapidly adjusts concentrations to satisfy the rate equations. Unlike some models, ours does not impose the quasi-equilibrium, but rather solves for time history of species with O-atom, RO_2-radicals, and OH in the stationary state.

Because of the extreme dependence on initial conditions, our history analysis concentrates on an air mass with relatively well-defined concentrations at the beginning and the end of its travel. Giving it the initial values, we see the concentrations unfold as the air parcel moves through the computed simulation procedure. In view of the sensitivities discovered, the transition of oxidant species O_3 and NO_2 proceeds better than one might expect. The previously adopted biases on the NO-flux and the propylene oxidation rates were confirmed in this run having very different conditions than those in Huntington Park represented by 1968 data.

Much more work remains to be done. We have so many uncertainties in both the data and the model assumptions, that systematic tests must be devised to isolate the individual influences of the various parameters. Our very limited sensitivity study illuminates some of these very serious

questions that need to be answered. The anomalous pattern of NO-flux followed from our original work, through the data analysis project, and into this work. Either some very serious deficiency exists in the transport formulation, or there are some rapid loss mechanisms for oxides of nitrogen that reduce the apparent emission strengths. In view of the extensive efforts directed toward NO_x-controls, high priority must be given to measuring the terms of the nitrogen balance equation in an urban area. Nitric acid vapor, nitrous acid vapors, and particulate nitrates could hold the key to this question. The modeling is not precise enough to pin down the deficit, but the CO/NO_x and C_2H_2/NO_x analyses of the Los Angeles data (86) showed significant deviations on high-oxidant days. Since the same types of questions have appeared in laboratory experiments, it seems that a greater latitude of nitrogen-bearing compounds should be sought in future atmospheric studies.

The plans announced for a regional air pollution study should hold many of the solutions to the problems identified here. Conversely, application of the model should provide valuable feedback to such programs. Clarifications in the chemical mechanism should take the form of better values of rate constants for the controlling reactions. Perhaps the very selection of which reactions to include might be altered for the air contaminant hydrocarbon mix. Mathematical techniques seem well enough advanced to match the simpler formulations of photochemical modeling schemes to the computing machinery available. The more complex schemes proposed recently will continue to shed light on questions of dispersion parameters and inventory accuracy.

The future of the mathematical modeling techniques is linked to cooperative activity between the theoretical and experimental arts in the field of air pollution. Phenomena of importance are yet to be added to any of the mathematical schemes. The formation of aerosol and its extinction of ultraviolet radiation has not been explicitly treated in the computations. Moreover, the whole area of heterogeneous reactions on either particulate surfaces or urban surfaces remains obscure. The reacting flow problem of mixedness and its influence on kinetics has not been reduced to an engineering procedure for calculational purposes.

Urgent needs for improved air quality management demand renewed vigor in our attack on many of the fluid dynamic and chemical kinetic areas plagued by chronic difficulties. Turbulent mixing and free radical processes play significant roles here as in many previous technical problems. Pragmatic perspective must guide us, however, in the development of mathematical modeling lest it become a prophecy which fulfills itself in totally abstract research activity.

LITERATURE CITED

1. Barth, D. S., "Federal Motor Vehicle Emission Goals for CO, HC, and NO_x Based on Desired Air Quality Levels," Journal of the Air Pollution Control Association, August 1970, Vol. 20, No. 8, pp. 519-523.

2. Callaghan, D. J. and M. Feldstein, Meeting Air Quality Standards. The Pragmatic Approach, Second International Clean Air Congress Paper AD-36H, Washington, D.C., December 6-11, 1970.

3. Sutton, O. G., "A Theory of Eddy Diffusion in the Atmosphere," Proc. Roy. Soc., 1932, Vol. A135, pp. 143-165.

4. Sutton, O. G., Micrometeorology, McGraw Hill, New York, 1953, p. 34 et seq.

5. Frenkiel, F. N., "Atmospheric Pollution in Growing Communities," Smithsonian Institute Annual Report, 1956, pp. 269-299.

6. Pooler, F. Jr., "A Prediction Model of Mean Urban Pollution for Use with Standard Wind Roses," Int. J. Air and Water Poll., 1961, Vol. 4, Nos. 2/4, pp. 199-211.

7. Turner, D. B., "A Diffusion Model for an Urban Area," J. of Appl. Met., February 1964, Vol. 3, pp. 83-91.

8. Clarke, J. F., "A Simple Diffusion Model for Calculating Point Concentrations for Multiple Sources," J. of the Air Pollution Control Assn., Sept. 1964, Vol. 14, No. 9, pp. 347-352.

9. Koogler, J. B., R. S. Sholtes, A. L. Danis, and C. I. Harding, "A Multivariable Model for Atmospheric Dispersion Predictions," J. of the Air Pollution Control Assn., 1967, Vol. 17, pp. 211-214.

10. Miller, M. E. and George C. Holzworth, "An Atmospheric Diffusion Model for Metropolitan Areas," J. of the Air Pollution Control Assn., January 1967, Vol. 17, No. 1, pp. 46-50.

11. Martin, D. O. and J. A. Tikvart, A General Atmospheric Diffusion Model for Estimating the Effects of One or More Sources on Air Quality, US DHEW Public Health Service, National Air Pollution Control Administration, 1968.

12. McElroy, J. L. and F. Pooler, Jr., St. Louis Dispersion Study, Volume II-Analysis, USDHEW Public Health Service, National Air Pollution Control Administration, December 1968.

13. Turner, D. B., Workbook of Atmospheric Dispersion Estimates, US DHEW Public Health Service, National Center for Air Pollution Control, 1967.

14. Smith, M. E., "The Concentrations and Residence Times of Pollutants in the Atmosphere," Chemical Reactions in the Lower and Upper Atmosphere, Stanford Research Institute, April 1961, pp. 273-286.

15. Wanta, R. C., "Meteorology and Air Pollution," Air Pollution, 1968, Vol. 1 2d ed, A. C. Stern Ed., Academic Press, New York, Ch. 7.

16. Lamb, R. G., An Air Pollution Model of Los Angeles, University of California Los Angeles, M. S. Thesis, 1968.

17. Ludwig, F. L., W. B. Johnson, A. E. Moon, and R. L. Mancuso, A Practical, Multipurpose Urban Diffusion Model for Carbon Monoxide, Stanford Research Institute Report, September 1970.

18. Roberts, J. J., E. J. Croke, A. S. Kennedy, J. E. Norco, and L. A. Conley, A Multiple-Source Urban Atmospheric Dispersion Model, Argonne National Laboratory Report ANL/ES-CC-007, May 1970.

19. Karplus, W. J., G. A. Bekey, P. J. Pekrul, "Atmospheric Diffusion of Air Pollutants," Ind. and Eng. Chem., 1958, Vol. 50, pp. 1657-1660.

20. Friedlander, S. K. and J. H. Seinfeld, "A Dynamic Model of Photochemical Smog," Environmental Science and Technology, November 1969, Vol. 3, No. 11, pp. 1175-1182.

21. Calvert, S., "A Simulation Model for Photochemical Smog," California Air Environment, July-September 1969, Vol. 1, No. 3, p. 1.

22. Wayne, L., R. Danchick, M. Weisburd, A. Kokin, and A. Stein, Modeling Photochemical Smog on a Computer for Decision-Making, Paper #7-018 at the 63rd Annual Meeting of the Air Pollution Control Association, St. Louis, Mo., June 14-18, 1970.

23. Westburg, K. and N. Cohen, The Chemical Kinetics of Photochemical Smog as Analyzed by Computer, Paper No. 70-753, American Institute of Aeronautics and Astronautics 3rd Fluid and Plasma Dynamics Conference, Los Angeles, California, June 29-July 1, 1970.

24. Sklarew, R. C., A New Approach: The Grid Model of Urban Air Pollution, Air Pollution Control Association Paper 70-79, 63rd Annual Meeting, St. Louis, Missouri, June 14-18, 1970.

25. Seinfeld, J. H., P. Roth, S. D. Raynolds, and T. A. Hecht, Simulation of the Los Angeles Basin, 161st National Meeting of the American Chemical Society, Los Angeles, California, March 28-April 2, 1971.

26. Eschenroeder, A. Q., Validation of Simplified Kinetics for Photochemical Smog Modeling, General Research Corporation IMR-1096, September 1969.

27. Leighton, P. A., Photochemistry of Air Pollution, Academic Press, New York, 1961.

28. Saltzman, B. E., "Kinetic Studies of Formation of Atmospheric Oxidants," Industrial and Engineering Chemistry, April 1958, Vol. 50, No. 4, pp. 677-682.

29. Wayne, L. G., "On the Mechanism of Photo-Oxidation in Smog," Archives of Environmental Health, August 1963, Vol. 7, No. 8, pp. 113-123.

30. Altshuller, A. P., and J. J. Bufalini, "Photochemical Aspects of Air Pollution: A Review," Photochemistry and Photobiology, 1965, Vol. 4, pp. 97-146.

31. Haagen-Smit, A. J., and L. G. Wayne, "Atmospheric Reactions and Scavenging," Air Pollution, Vol. I, ed. A. C. Stern, Academic Press, New York, 2nd ed., 1968, pp. 149-186.

32. Stephens, E. R., "Chemistry of Atmospheric Oxidants," J. Air Poll. Control Assn., March 1969, Vol. 19, pp. 181-185.

33. Tuesday, C. S., The Atmospheric Photo-oxidation of Trans-Butene-2 and Nitric Oxide, General Motors Research Laboratories GMR-332, 1961.

34. Bufalini, J. J. and K. L. Brubaker, Photo-oxidation of Formaldehyde at Low Partial Pressures, Symposium for Chemical Reactions in Urban Atmospheres, GM Research Laboratories, Warren, Michigan, October 6-7, 1969.

35. Altshuller, A. P., DHEW, private communication, September 1969.

36. Westberg, K., Aerospace Corporation, private communication.

37. DASA Reaction Rate Handbook, DASA 1948, October 1967.

38. Caplan, J. D., "Smog Chemistry Points the Way to Rational Vehicle Emission Control," Vehicle Emissions II: SAE Progress in Technology, 1966, Vol. 12, New York, pp. 20-31.

39. Altshuller, A. P., S. L. Kopczynski, W. A. Lonneman, F. L. Becker, and R. Slater, "Chemical Aspects of the Photo-oxidation of the Propylene-Nitrogen Oxide System," Environmental Science and Technology, November 1967, Vol. 1, pp. 899-914.

40. Kopczynski, S. L., unpublished data, transmitted October 1969.

41. Schuck, E. A. and G. J. Doyle, Photooxidation of Hydrocarbons in Mixtures Containing Oxides of Nitrogen and Sulfur Dioxide, Air Pollution Foundation Report No. 29, San Marino, California, October 1959.

42. Stedman, D. H., E. D. Morris, Jr., E. E. Daby, H. Niki, and B. Weinstock, The Role of OH Radicals in Photochemical Smog, American Chemical Society Division of Water Air and Waste Chemistry, Chicago, Illinois, September 13-18, 1970.

43. Holmes, J. R., A. D. Sanchez, and A. H. Bockian, Atmospheric Photochemistry: Some Factors Affecting the Conversion of NO to NO_2, Pacific Conference on Chemistry and Spectroscopy, San Francisco, October 6-9, 1970.

44. Altshuller, A. P. and J. J. Bufalini, "Photochemical Aspects of Air Pollution: A Review," Environmental Science and Technology, January 1971, Vol. 5, No. 5, pp. 39-64.

45. Seinfeld, J. H., private communication, letter dated June 2, 1970.

46. Altshuller, A. P., S. L. Kopczynski, D. Wilson, W. Lonneman, and F. D. Sutterfield, "Photochemical Reactivities of n-Butane and Other Paraffinic Hydrocarbons," Journal of the Air Pollution Control Assn., October 1969, Vol. 19, No. 10, pp. 787-790.

47. Korth, M. W., A. H. Rose, Jr., and R. C. Stahman, "Effects of Hydrocarbon to Oxides of Nitrogen Ratios on Irradiated Auto Exhaust, Part 1," Journal of the Air Pollution Control Assn., May 1964, Vol. 14, No. 5, pp. 168-175.

48. Agnew, W. G., "Automotive Air Pollution Research," Proc. Roy. Soc., 1968, Series A, Vol. 307, pp. 153-181. (Data reproduced from APCA paper by C. S. Tuesday, B. A. D'Alleva, J. M. Heuss, and G. J. Nebel, June 1967).

49. Heicklen, J., K. Westberg, and N. Cohen, The Conversion of NO to NO_2 in Polluted Atmospheres, Pennsylvania State University Center for Air Environment Studies Publication 115-69, July 1969.

50. Westberg, K., N. Cohen, and K. W. Wilson, "Carbon Monoxide: Its Role in Photochemical Smog Formation," Science, March 12, 1971, Vol. 171, pp. 1013-1015.

51. Final Report on Phase I, Atmospheric Reaction Studies in the Los Angeles Basin, Vols. I and II, Scott Research Laboratories, June 30, 1969.

52. Final Report, 1969 Atmospheric Reaction Studies in the Los Angeles Basin, Vols. I-IV, Scott Research Laboratories, February 1970.

53. Stephens, E. R., and W. E. Scott, "Relative Reactivity of Various Hydrocarbons in Polluted Atmospheres," Proceedings of the American Petroleum Institute, 1962, Vol. 42 (III), p. 665.

54. Altshuller, A. P., "An Evaluation of Techniques for the Determination of the Photochemical Reactivity of Organic Emissions," J. APCA, May 1966, Vol. 16, No. 5, pp. 257-260.

55. Bonamassa, F. and H. Wong-Woo, "Composition and Reactivity of Exhaust Hydrocarbons from 1966 California Cars," Division of Water Air and Waste Chemistry 152nd National Meeting American Chemical Society, New York, N. Y., September 11-16, 1966.

56. Neligan, R. E., "Hydrocarbons in the Los Angeles Atmosphere," Archives of Environmental Health, December 1962, Vol. 5, No. 12, pp. 581-591.

57. Stephens, E. R., and Frank R. Burleson, "Analysis of the Atmosphere for Light Hydrocarbons," Journal of the Air Pollution Control Assn., March 1967, Vol. 17, No. 3, pp. 147-153.

58. Gordon, R., H. Mayrsohn, R. Ingels, "C_2-C_5 Hydrocarbons in the Los Angeles Atmosphere," Environmental Science and Technology, December 1968, Vol. 2, pp. 1117-1120.

59. Altshuller, A. P., S. L. Kopczynski, W. A. Lonneman, and F. D. Sutterfield, "A Technique for Measuring Photochemical Reactions in Atmospheric Samples," Environmental Science and Technology, June 1970, Vol. 4, No. 6, pp. 503-506.

60. Stephens, E. R., and F. R. Burleson, "Distribution of Light Hydrocarbons in Ambient Air," Paper 69-122 Air Pollution Control Association 62nd Annual Meeting, 1969.

61. Neiberger, N. and J. Edinger, Meteorology of the Los Angeles Basin with Particular Respect to the "Smog" Problem, Air Pollution Foundation Report No. 1, April 1954.

62. Renzetti, N. (ed.), An Aerometric Survey of the Los Angeles Basin August November 1954, Air Pollution Foundation Report No. 9, July 1955.

63. Eschenroeder, A. Q., and J. R. Martinez, Mathematical Modeling of Photochemical Smog, General Research Corporation IMR-1210, December 1969 (Also AIAA paper 70-116 presented at the 8th Aerospace Sciences Meeting, New York, N. Y., January 19-21, 1970).

64. Ames, W. F., Nonlinear Partial Differential Equations in Engineering, N. Y. Academic Press, 1965, pp. 341-342.

65. Varga, R. S., "On Higher Order Stable Implicit Methods for Solving Parabolic Partial Differential Equations," J. Math and Physics, 1961, Vol. 40, pp. 220-231.

66. Magnus, D. and H. Schecter, Analysis and Application of the Padé Approximation for the Integration of Chemical Kinetic Equations, Technical Report 642, General Applied Science Laboratories, Inc., 1967.

67. Martinez, J. R., Improving the Efficiency in Atmospheric Reaction Modeling Calculations, General Research Corporation IMR-1291, April 1971. (Also Air Pollution Control Association Paper 71-138 at the 64th National Meeting, Atlantic City, New Jersey, June 27-July 1, 1971.)

68. Pasquill, F., Atmospheric Diffusion, Van Nostrand and Co., London, 1962, p. 72.

69. Rossby, C. G., and R. B. Montgomery, "The Layer of Frictional Influence in Wind and Ocean Currents," Physical Oceanography and Meteorology, M.I.T. and Woods Hole Oceanographic Institution, 1935, Vol. 3, No. 3.

70. Priestly, C. H. B., Turbulent Transfer in the Lower Atmosphere, University of Chicago Press, 1969, pp. 33-38.

71. Aleksandrova, A. K., N. L. Byzova, and G. B. Mashkova, "Experiments on the Spreading of Precipitating Admixture from a Point Source in the Bottom Layer of the Atmosphere," Investigation of the Bottom 300-Meter Layer of the Atmosphere, ed. N. L. Byzova, (translated from the Russian by Israel Program for Scientific Translation), Jerusalem, 1965, pp. 1-12.

72. Lettau, H., "A Reexamination of the 'Leipzig Wind Profile' Considering Some Relations Between Wind and Turbulence in the Frictional Layer," Tellus, 1950, Vol. 2, pp. 189-200.

73. Ivanov, V. N., "Statistical Characteristics of Turbulent Diffusion and Their Estimation in the Bottom Layer of the Atmosphere," Investigation of the Bottom 300-Meter Layer of the Atmosphere, ed. N. L. Byzova (translated from the Russian by Israel Program for Scientific Translation), Jerusalem, 1965, pp. 36-42.

74. Hanna, S. R., "A Method for Estimating Vertical Eddy Transport in the Planetary Boundary Layer Using Characteristics of the Vertical Velocity Spectrum," J. of Atmospheric Sciences, November 1968, Vol. 25, No. 6, pp. 1026-1033.

75. Craig, R. A., "Vertical Eddy Transfer of Heat and Water Vapour in Stable Air," J. of Meteorology, 1949, Vol. 6, pp. 122-133.

76. Wu, S. S., "A Study of Heat Transfer Coefficients in the Lowest 400 Meters of the Atmosphere," Journal of Geophysical Research, April 15, 1965, Vol. 70, No. 8, pp. 1801-1807.

77. Hosler, C. R., "Vertical Diffusivity from Radon Profiles," Journal of Geophysical Research, December 20, 1969, Vol. 74, No. 28, pp. 7018-7026.

78. De Zorzo, G., "Applicazione della Equazione di Diffusione allo Studio della Bassa Atmosfera," Rivista di Meteorologica Aeronautica, March 1970, Vol. 30, No. 1, pp. 3-28.

79. Monthly Reports of Meteorology, Air Pollution Effects and Contaminant Maxima, Air Pollution Control District, County of Los Angeles.

80. Lemke, E. E., G. Thomas, W. E. Zwiacher (eds.), "Profile of Air Pollution Control in Los Angeles County," APCS, Los Angeles County, January 1969, p. 3.

81. Larson, G. P., J. C. Chipman, and E. K. Kauper, "Distribution and Effects of Automotive Exhaust Gases in Los Angeles," Vehicle Emissions I. SAE Progress in Technology Series, 1964, Vol. 6, pp. 7-16.

82. Roberts, P. J. W., P. M. Roth, and C. L. Nelson, Contaminant Emissions in the Los Angeles Basin--Their Sources Rates and Distribution, Systems Applications, Inc. Report 71SAI-6, March 1971.

83. Eschenroeder, A. Q., Some Preliminary Air Pollution Estimates for the Santa Barbara Region, 1970-1990, General Research Corporation IMR-1278, March 1970.

84. Gordon, R. J., H. Mayrsohn, and R. M. Ingels, "C_2-C_5 Hydrocarbons in the Los Angeles Atmosphere," Environmental Science and Technology, December 1968, Vol. 2, pp. 1117-1120.

85. Eschenroeder, A. Q., An Approach for Modeling the Effects of Carbon Monoxide on the Urban Freeway User, General Research Corporation IMR-1259, January 1970.

86. Eschenroeder, A. Q., and J. R. Martinez, Analysis of Los Angeles Atmospheric Reaction Data from 1968 and 1969, General Research Corporation CR-1-170, July 1970.

87. Monitoring Data Sheets from Los Angeles County Air Pollution Control District, 1969.

88. Johnston, H., "Reactions in the Atmosphere," Project Clean Air Task Force Assessments, September 1, 1970, Vol. 4, Task Force No. 7, Section 3, University of California, p. 3-1.